

PLANETS ORBITING EVOLVING BINARY STARS

FRAN BARTOLIĆ



Master's thesis

Department of Physics, University of Rijeka

Supervisors: dr. Alexander James Mustill, Prof. dr. Dijana Dominis Prester

September 2017

ABSTRACT

Circumbinary planets have been observed around both main sequence and post common envelope binary stars. It is not clear if a circumbinary system on the main sequence can survive the post main sequence evolution leading to a post common envelope system. In this work we investigate the evolution of circumbinary planets after the binary stars leaves the main sequence and prior to the onset of common envelope evolution. In particular, we focus on the role of divergent mean motion resonance passage which can excite the eccentricity of the planet. We develop a Hamiltonian model of the previously not studied high order 6 : 1 resonance, applicable to circumbinary systems where the mass ratio between the primary and the secondary star can be large. We then integrate the circumbinary system using an N-body code coupled with a stellar evolution code and compare the results with the analytical model. The results show that the resonances have a small effect in most cases with the effect of secular decrease in eccentricity being dominant. In the majority of cases the planets survive the evolution prior to the common envelope.

SAŽETAK

Planeti u orbiti oko binarnih zvijezda su opaženi oko binarnih zvijezda na glavnom nizu te binarnih zvijezda u fazi nakon izbačaja zajedničke ovojnice. Nije jasno da li planeti u orbiti oko binarnih zvijezda na glavnom nizu mogu preživjeti fazu evolucije binarne zvijezde prije formacije zajedničke ovojnica. U ovom radu istražujemo evoluciju planeta oko binarnih zvijezda nakon što binarna zvijezda napusti glavni niz i prije nego što se formira zajednička ovojnice. Fokusiramo se na ulogu pomaka položaja gravitacijskih rezonancija čiji efekt može biti povećanje ekscentriteta orbite planeta. Razvili smo Hamiltonian za modeliranje specifične rezonancije visokog reda $6 : 1$ koji je primjenjiv na planete oko binarnih zvijezda sa usporedivim masama dviju komponenta zvijezde. Napravili smo numeričke simulacije takvih sustava koristeći kod za simulaciju gravitacijskih interakcija između N tijela povezan sa kodom za simulaciju stelarne evolucije binarne zvijezde. Rezultati pokazuju rezonancije u većini slučajeva imaju mali efekt, dominantne su sekularne interakcije. U većini slučajeva planeti prežive evoluciju binarne zvijezde prije početka faze zajedničke ovojnica.

ACKNOWLEDGMENTS

To Jenny, for supporting me throughout this work.

CONTENTS

1	INTRODUCTION	1
1.1	History	1
1.2	Binary stars and types of planetary orbits	1
1.3	Observed circumbinary planets	2
1.4	Binary stellar evolution	5
1.4.1	Evolution on the main sequence	5
1.4.2	Post main sequence evolution and the common envelope	6
1.5	Motivation for the thesis topic	7
2	THEORETICAL BACKGROUND	13
2.1	The two-body problem	13
2.1.1	The orbit equation and its solution	13
2.1.2	The mean and eccentric anomaly	16
2.1.3	Orbit in an inertial frame	17
2.1.4	Orbit in three-dimensional space	18
2.2	A brief review of Hamiltonian mechanics	20
2.2.1	Hamilton's equations	20
2.2.2	Integrable Hamiltonians	21
2.2.3	Fixed points	22
2.2.4	Canonical transformations	23
2.3	The pendulum	24
2.4	The three-body problem	26
2.4.1	The disturbing function	26
2.4.2	Secular dynamics	32
2.4.3	Resonant dynamics	35
2.5	The small divisor problem	38
3	AN ANALYTICAL MODEL OF RESONANT ECCENTRICITY EXCITATION	41
3.1	The 6:1 mean motion resonance	41
3.2	Reduction to a single degree of freedom	46
3.3	The resonance structure	48
3.4	Resonance passage	53
4	N-BODY SIMULATIONS OF CIRCUMBINARY SYSTEMS UP TO THE COMMON ENVELOPE PHASE	59
4.1	The N-body problem	59
4.2	REBOUND - an open source N-body integrator	60
4.3	binary_c - a binary stellar evolution code	62
4.4	Stability of circumbinary systems on the main sequence	66
4.5	Coupling between binary_c and REBOUND	71
4.6	Initial conditions	75
5	RESULTS	77
5.1	Eccentricity kick predicted by the analytical model	77

5.2 N-body simulations	79
6 CONCLUSIONS	85
6.1 Future work	86
BIBLIOGRAPHY	87

LIST OF FIGURES

Figure 1	Types of orbits in binaries.	3
Figure 2	Orbital parameters of main-sequence CB planets.	4
Figure 3	Roche lobe surface.	7
Figure 4	Evolution of a binary system.	8
Figure 5	Elliptical orbit.	15
Figure 6	Eccentric anomaly.	17
Figure 7	Barycentric orbit.	18
Figure 8	Orbit in 3D space.	19
Figure 9	Pendulum phase space portrait.	25
Figure 10	Jacobi coordinates.	26
Figure 11	Free and forced elements.	34
Figure 12	Geometry of a mean-motion resonance.	35
Figure 13	Approximation of Hansen coefficients.	45
Figure 14	Parameters of the Hamiltonian.	48
Figure 15	Graphical solution for the fixed points.	50
Figure 16	Phase space portraits of the Hamiltonian.	51
Figure 17	Bifurcation diagram	53
Figure 18	Adiabatic invariant evolution.	55
Figure 19	Example stellar evolution trajectories.	64
Figure 20	MMR crossings.	65
Figure 21	Outcomes of binary stellar evolution.	67
Figure 22	MEGNO maps for different integration times.	69
Figure 23	MEGNO maps of circumbinary systems.	72
Figure 24	Coupling between REBOUND and binary_c	74
Figure 25	The kick in eccentricity during resonant passage.	77
Figure 26	N-body results example with a small eccentricity kick	81
Figure 27	N-body results example with a large eccentricity kick	82
Figure 28	Same as fig. 27 except with a higher initial planet eccentricity of $e_0 = 0.2$.	83
Figure 29	A close up view on the secular interactions for the system in fig. 27. The integration time is 1000 years, a fraction of the red giant branch timescale.	84

LIST OF TABLES

Table 1	Observed circumbinary planets orbiting MS stars.	11
Table 2	Observed circumbinary planets orbiting post common envelope stars.	12
Table 3	Different kinds of generating functions.	24
Table 4	6 : 1 MMR harmonic angles.	42
Table 5	Initial parameters for the stellar evolution code <code>binary_c</code> .	63
Table 6	Initial conditions for N-body simulations.	76
Table 7	N-body simulation results for $m_1 = 1.2$.	79
Table 8	N-body simulation results for $m_1 = 1.2$.	79

INTRODUCTION

In this chapter, I introduce the main topic of the thesis, review the observational evidence for planets around binary stars and the basic theory of binary stellar evolution in order to motivate the problem at hand.

1.1 HISTORY

In the past decade the number of detected exoplanets has skyrocketed to thousands of confirmed detections from both space and ground facilities (Winn and Fabrycky, 2015). The vast majority of these planets have been detected around single stars. Interestingly, the very first proposed exoplanet (Campbell, Walker, and Yang, 1988) is located in a binary star system γ Cephei (orbiting around one of the stars), though it was not confirmed until 2003 (Hatzes et al., 2003). First confirmed exoplanet, orbiting a single neutron star pulsar star, was discovered in 1992 (Wolszczan and Frail, 1992) and a year later Thorsett, Arzoumanian, and Taylor (1993) proposed the existence of a circumbinary planet around a binary star system PSR B1620-26 consisting of a neutron star pulsar and a white dwarf (confirmed in 2000). The earliest confirmed exoplanet detection around a main sequence (MS) star came in 1995 when Mayor and Queloz (1995) detected a planet around a single star 51 Pegasi.

Since the first confirmed exoplanet, thousands more have been discovered, mainly by the Kepler space mission. The number of known circumbinary planets (planets orbiting around two stars) is much lower with less than 20 confirmed so far. The interest in these systems is significant because their dynamics is more interesting than that of planets in single star systems, they also provide a test bed for planet formation theories.

1.2 BINARY STARS AND TYPES OF PLANETARY ORBITS

There are two main types of planetary orbits in binary star systems, shown in fig. 1. *S-type* or *circumprimary* planets orbit around one of the two stars in the stellar binary, *P-type* or *circumbinary* (CB) planets orbit around both of the stars. Most S-type systems are similar to single star systems except with the addition of an outside perturber (the second star). The stability of such systems depends primarily on the separation of the stellar binary, if the binary is on a wide orbit ($\gtrsim 50$ au) the effect of the outside perturber is small and the system

might not behave too differently from a single star planetary systems. If the binary is too close however, there may be no stable S-type orbits.

P-type or circumbinary systems are very different from S-type, in this case the planet orbits around both of the stars. Binary stars in such systems are found on very close orbits of the order of tens of days. Intuitively, the closer a P-type orbit is to the orbit of the binary, the greater the chance of an interaction with one of the stars. Conversely, if the planet is very far away from the binary, it experiences gravitational forces as if the binary was a single star with a small gravitational quadrupole moment.

For both types of systems the most interesting physics happens for planets close to unstable zones, in between the two stars for S-type systems and close to the two stars in P-type systems. Such systems pose significant challenges for planet formation theories. Planets form in protoplanetary disks (Armitage, 2010), in S-type systems if protoplanetary disks form around both of the stars, the effect of the gravitational interaction between the two stars is to truncate the disks at a certain orbital radius (Pichardo, Sparke, and Aguilar, 2005). If the disk is truncated too close to the star where icy dust grains cannot form this might hinder or prevent giant planet formation in the core-accretion scenario Lissauer (1993).

Circumbinary disks present a different kind of challenge, in such systems the protoplanetary disk encompasses both of the stars. The inner regions of the disk are stirred by the two stars, increasing the relative velocity Δv between the dust and gas particles in the disk. This increase in the relative velocity can inhibit planetesimal accretion in the inner regions of the disk (Meschiari, 2012). The picture is not that simple because the circumbinary disks might have so-called 'dead zones' where the relative velocity is actually smaller than in single star disks, thus making planet formation easier (Rafikov, 2013; Martin, Armitage, and Alexander, 2013). The formation of CB planets could also occur in post common-envelope disks which form during late stages of binary evolution billions of years after the binary itself has formed, this case will be discussed further in section 1.5.

Because most binary stars consisting of a solar type primary and a smaller companion have a period distribution which peaks around $P_b = 10^4$ days (Duquennoy and Mayor, 1991), S-type systems are far more common than P-type (planet formation is virtually impossible around such wide binaries).

1.3 OBSERVED CIRCUMBINARY PLANETS

The vast majority of CB planets have been detected with the transit method, either directly (the planet blocks some of the light of the star(s)) or via transit timing variations (TTVs for short) of the eclipsing binary where the presence of the planet is inferred (see Perryman,

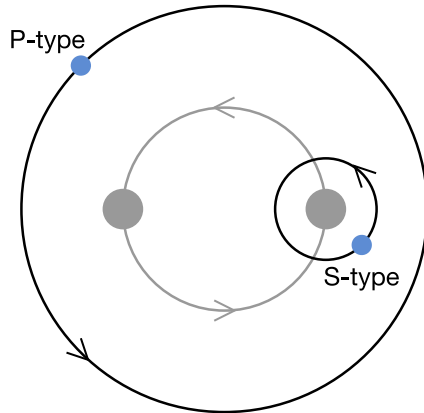


Figure 1: Two types of planetary orbits in binary star systems. S-type or circumprimary orbits encompass one of the stars. P-type or circumbinary orbits encompass both stars.

2011, for explanation of exoplanet detection methods). Recently Bennett et al. (2016) found a circumbinary planet with the gravitational microlensing method.

The observed CB planets can be divided into two categories, those orbiting binary stars on the main-sequence, and those orbiting post main-sequence stars which experienced a common-envelope event (see section 1.4). The first population consists of planets observed mostly with the Kepler satellite, it is listed in table 1. The second population has been detected with TTVs exclusively and is listed in table 2. The data was taken from the open source catalogue of discovered exoplanets called the Open Exoplanet Catalogue (Rein, 2012). The advantage of this catalogue compared to other source is that it is written in a hierarchical way using the XML language which makes it easier to search for all circumbinary planets.

Looking at the two tables, we see that all of the planets in table 2 orbit around binaries with period $P_b < 1$ day, a consequence of common-envelope evolution. The post main-sequence population also has a much higher claimed planet mass. The mass fraction of binary stars appears to be uniformly distributed for the main-sequence population and generally small for the evolved population, as one would expect.

The left panel of fig. 2 shows a scatter plot of the binary properties for the main-sequence population in period–eccentricity space. The binaries have relatively high eccentricities, going all the way up to 0.5 for Kepler-34 and their periods are all less than 50 days. No observed planet hosting main-sequence binaries have a period of less than $\lesssim 7$ days, an unusual fact considering that the Kepler survey is biased towards short period binaries. One possible explanation for the lack of planets around such short-period binaries is the formation mechanism. Short-period binaries are unlikely to form with such a small

period initially, rather, it is thought that they form as a wider binary and shrink their orbit.

The right panel of table 2 shows the planet properties in same space of orbital parameters as the left panel. Looking at the planet period ratio in units of the period of its host binary, no planets can be found within $P = 5 P_b$. Most observed planets pile slightly further away with a single outlier very far away from the binary. The suspected reason for the lack of planets closer to the binary is that the planets pile up near the inner edge of the protoplanetary disk which is truncated due to an unstable inner region where influence of the binary is significant (Pierens and Nelson, 2007). The eccentricities of the planets are generally small and overall smaller than the binary eccentricities. No observed planets are captured in a mean-motion resonance (see chapter 2 for a definition).

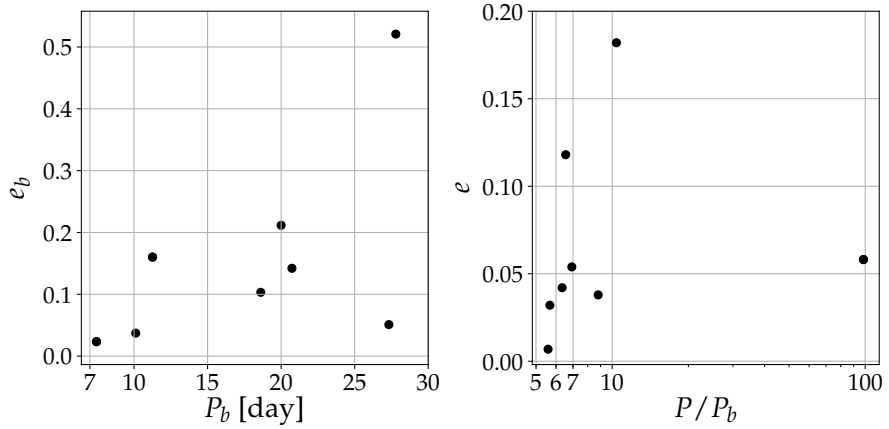


Figure 2: Left panel: the observed orbital parameters of planet hosting main-sequence binary stars with circumbinary planets. Right panel: the same orbital parameters for the circumbinary planets.

All main-sequence CB planets are in nearly co-planar orbits, that is, the mutual inclination of the planet orbit relative to the binary orbit is small ($\lesssim 3^\circ$). The mutual inclinations of binary circumbinary planets with respect to the binary are very important because they influence the observational results from transit surveys. In order for a planet to transit across the binary, from geometry it follows that the mutual inclination has to be very low, near zero. This means that if in general CB planets had near zero mutual inclination, the observed population of planets would be representative of the actual sample since in that case nearly all of the CB planets would transit if the secondary star transits as well. If on the other hand the mutual inclination distribution had some spread around zero, the transit surveys would miss a lot of planets. The latter case is what happens in observations of single star systems with two planets, the outer planet is often missed because its inclination has been in some way excited such that it no longer transits.

There are ways of correcting such survey biases and getting to the true underlying mutual inclination distribution, and as a consequence also the occurrence rate of CB planets. Armstrong et al. (2014) took into account the survey biases of the Kepler mission and derived the occurrence rate of CB planets. They find that if the CB planets are preferentially coplanar with their host binaries, the occurrence rate of planets with radii greater than 6 earth radii and with periods less than 300 days, orbiting around short period main-sequence binaries is around 10%, a value slightly higher than the corresponding occurrence rate for single star systems. They also find that the lack of giant planets in the MS sample is a real effect, it appears that CB planets are generally smaller than their single star cousins.

1.4 BINARY STELLAR EVOLUTION

The subject of this thesis is the influence of stellar evolution on the orbits of CB planets. In this section I will provide a very brief overview of the stellar evolution of binary star systems. For more details see for example Prialnik (2009).

1.4.1 *Evolution on the main sequence*

Stellar evolution in single star systems is driven by compositional changes in the interiors of stars due to nuclear reactions which in turn affect the physical properties of the star via the stellar structure equations. The stellar structure equations (Prialnik, 2009, see for ex.) are a set of partial differential equations that can be solved numerically for the time evolution of the physical parameters (stellar mass, radius, temperature, pressure and luminosity) if one assumes spherical symmetry. The time evolution of star depends primarily on the initial mass. Red dwarf stars with $M \lesssim 0.7 M_{\odot}$ live much longer than Hubble time (13.7 Gyr) while the very high mass stars can have lifetimes on the order of a few million years.

The evolution of stars with masses similar to that of the Sun proceeds as follows. Starting on the main sequence, the star initially burns Hydrogen into Helium which sinks to the center and starts forming a Helium core. This phase lasts for billions of years for sun-like stars until the pressure in the core becomes sufficient for Helium burning to occur. Prior to the start of Helium burning the stellar radius increases during the red giant branch at reaches its highest point just before the ignition of Helium. The Helium burning phase lasts less than a billion years and in the process the radius again increases followed by significant mass loss. Finally, all that is left is the inert core in the form of a White Dwarf.

The evolution of binary stars is not significantly different from that of single stars. If the two stars in a binary are sufficiently far away

they will evolve independently. Close binaries such as those hosting CB planets significantly interact during late stages of stellar evolution, starting with the red giant branch (RGB). For questions regarding the stability of CB planets, we are most interested in the variation of the parameters of the stellar orbit, namely the semi-major axis a_i and the eccentricity e_i .

1.4.2 Post main sequence evolution and the common envelope

Following the main sequence the evolution of the binary is driven by the more massive star (the primary), which evolves faster and starts ascending the RGB first. As it ascends the RGB its radius starts to increase and tidal interactions (which depend very strongly on the stellar radius) become important. What happens is that the secondary star raises a tidal bulge on the primary which lags behind the secondary in its orbit, with a constant phase angle. The tidal bulge then exerts a negative torque on the secondary, effectively pulling it closer together and decreasing the semi-major axis of the orbit. Another effect of the tidal forces is a decrease in the eccentricity which declines towards zero before the end of the RGB. Tidal evolution is described in Murray and Dermott (1999) and Zahn (1989) and Zahn and Bouchet (1989).

To understand what happens in binary systems at the end of the RGB we need to understand the concept of *Roche Lobes*. Roche Lobes are surfaces in 3D space where the force gravitational force experienced on a test particle from the primary equals the force from the secondary, they are shown in fig. 3 as curves in the $x - y$ plane. The radius of the lobe around the more massive star is given by

$$\frac{R_L}{a} = \frac{0.49q^{2/3}}{0.6q^{2/3} + \ln(1 + q^{1/3})} \quad (1)$$

where q is the binary mass fraction and a is the semi-major axis of the binary orbit. If a test particle is located within that radius it will be bound to the primary, if it is located in the other lobe it will be bound to the secondary. The point at the limit between the lobes is called the *Lagrange point L1*. The binary evolution then depends crucially on the ratio R_1/R_L between the current radius of the primary and its Roche lobe radius. If R_1 grows beyond the Roche Lobe radius the envelope no longer stays bound to the primary and the gas overflows on to the secondary, an event called the *Roche Lobe Overflow* (RLOF). This situation is illustrated in fig. 4.

Once RLOF starts very quickly the thin hydrogen envelope of the primary encompasses both of the stars, this phase is known as the *common envelope* (CE). As a result the dense primary core and the secondary star experience strong gas drag which acts as a negative torque. The stars quickly spiral towards each other, and the orbital

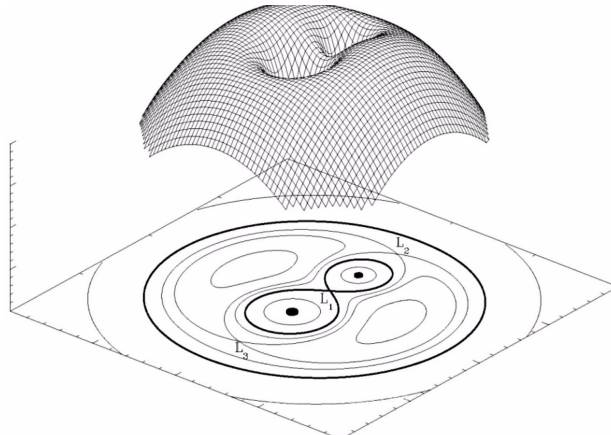


Figure 3: Roche Lobe surface for a binary star. On the level curves the pull of gravity on a test particle from the primary equals the pull from the secondary. Figure taken from https://en.wikipedia.org/wiki/Roche_lobe#/media/File:RochePotential.jpg.

energy released in the process goes into expelling the envelope. The final product depends on just how close the two stars are once the envelope is ejected, the product can either be a tight binary consisting of most often a WD and the secondary which is usually a red dwarf, or it can be a single star created as a result of a merger which happens if the stars spiral into each other.

The CE phase usually lasts on the order of a thousand years and is very poorly understood (Ivanova et al., 2013). It is usually modeled with a single parameter α , the fraction of orbital energy released during the in-spiral phase which goes into expanding and ejecting the envelope.

$$\alpha = \frac{\Delta E_{\text{bind}}}{\Delta E_{\text{orb}}} \quad (2)$$

Higher α means greater probability of envelope ejection while smaller α means that the most likely outcome is a merger between the two stars and partial ejection of the envelope. Observations tell us that usually $\alpha \approx 0.1 - 0.5$. In the process of CE ejection some of the material can stay bound to the star and for a post CE circumbinary (or circumstellar in the case of a merger) disk.

The systems which are most interesting for the subject of this thesis are binaries with primary mass of $1 - 2 M_{\odot}$, those are most likely to host CB planets. We will use a well tested stellar evolution code (see section 4.3) which solves for the time evolution of binary systems.

1.5 MOTIVATION FOR THE THESIS TOPIC

Finally, we move on to the subject of this thesis. We have talked about the CB planets orbiting MS stars (table 1) but have not said much about the ones in table 2 which orbit post CE binaries. All of the

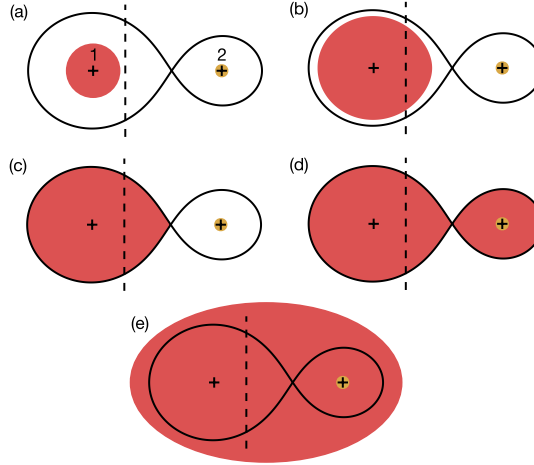


Figure 4: Time evolution of a binary system. a) Initially the primary (star 1) is more massive and fills a larger percentage of its Roche Lobe. b) The primary star evolves first and significantly increases its radius. c) At a certain point, the radius of the primary becomes equal to the Roche Lobe radius and a CE phase starts. d) Mass is transferred from the primary to the secondary. e) A common envelope form around both of the stars, as a result the primary core and the secondary star spiral inwards due to gas drag. The orbital energy released goes into ejecting the envelope with some efficiency.

planets in table 2 have been detected using TTVs which is not as direct of a method as the transit method. In TTV detection one models the *variations* in the times and durations of repeated transits of either a planet or an eclipsing binary which are a result of planet-planet (or planet-star in the case of CB planets) interactions (“[Transit Timing and Duration Variations for the Discovery and Characterization of Exoplanets](#)”). These variations can be used to infer the presence of additional non-transiting bodies in the system.

While the TTVs are generally a reliable and powerful technique for detecting and characterizing exoplanets, the detections of post CB planets presented in table 2 have been cast into serious doubt by Zorotovic and Schreiber (2013). They find the most of the detected planets in table 2 are likely not planets at all, the observed variations could be a result of variations in the shape of a magnetically active secondary star via the so called Applegate mechanism (Applegate, 1992). Other authors (Hinse et al., 2012) find that some of the claimed planets are dynamically unstable on short timescales which means they are less likely to be real.

However, not all of the detections in table 2 are doubtful. In particular, the system NN Ser, a post CE circumbinary system with two giant planets has been observed for 25 years, recent work (Marsh et al., 2013) shows that best fit orbital parameters of the two planets result in a stable system. If the two giant planets are indeed real, the work by Mustill et al. (2013) showed that under standard stellar evo-

lution assumption, the MS progenitors of those planets (orbiting a MS progenitor of the post CE binary star NN Serpentis) are dynamically unstable *on the MS*. Hence, their conclusion is that either the planets formed recently in a post CE disk or they are not real. Tantalizingly, a recent detection of dust around the binary NN Serpentis by ALMA (Atacama Large Millimeter Array) gives credence to the former scenario.

The idea of so called second generation planet formation (where the planets form much later than their host star) has been suggested by several authors recently (Perets, 2010; Schleicher and Dreizler, 2014; Völschow, Banerjee, and Hessman, 2014). If the two planets have indeed recently formed in a post CE disk, they might be some of the youngest planets ever detected. Post CE envelope disks are both predicted to arise in simulations (Ivanova et al., 2013), and have been observed (van Winckel et al., 2009). There is some similarity between these disks and the protoplanetary disks around pre MS binaries (de Ruyter et al., 2006). Perets (2010) points out that there is another possibility, the distinction between second and first generation formation need not be so strict. Lower mass planets could have formed with the binary and if they survived the CE they would have provided initial seeds for second generation formation, potentially making it even more efficient. For NN Serpentis in particular, more observations are needed to confirm the planetary hypothesis and distinguish between the various formation scenarios.

The question remains what exactly happens to CB planets orbiting MS binaries such as those listed in table 1, as the binary evolves first during the RGB phase and then through the CE phase. Kostov et al. (2016) did detailed N-body simulations of planets in table 1 during the CE phase. They find that the planets predominantly survive through the CE phase, migrating further out due to significant mass loss, and potentially gaining significant eccentricities. The surviving planets are roughly consistent with the observed post CE detections (except for the masses which are consistently higher in the post CE population). However, Kostov et al. (2016), and also Mustill et al. (2013) did not take into account the influence of an evolving binary during the RGB phase when significant tidal evolution of the binary's orbit occurs. The subject of this thesis is to look into this phase by means of N-body simulations and analytical models and see if the orbital evolution of the binary prior to CE has a major influence on the stability of CB planets. In particular, during the tidal decay phase the CB experience passing mean motion resonances (see chapter 2) which can potentially have a major influence on the dynamics of CB planets. The work of Kostov et al. (2016) then nicely continues on the subject of this thesis and provides a complete picture of the dynamical evolution of circumbinary systems from the MS phase, all the way past the CE event.

In chapter 2 I review the theory of planetary dynamics needed to understand later chapters. In chapter 3 I develop an analytical model of a high-order mean motion resonance thought to have an influence on the dynamics of close-in CB planets. In chapter 4 I present the numerical codes and techniques used in the N-body simulations and also asses the stability of CB systems on the main sequence. In chapter 5 I present the results of the analytical model and the numerical simulations. Finally, in chapter 6 I summarize what has been done and propose possible improvements to the work.

Name	m_p [M_J]	R [R_J]	a [au]	P [day]	e	I [$^\circ$]	M_1 [M_\odot]	M_2 [M_\odot]	q	a_b	P_b [day]	e_b	P_b/P
Kepler-1647 b	1.52	1.06	2.72	1107.59	0.06	90.10	1.21	0.98	0.81	0.13	11.26	0.16	98.38
Kepler-16 (AB) b	0.33	0.75	0.70	228.78	0.01	90.03	0.69	0.20	0.29	0.22	41.00	-	5.58
Kepler-34 (AB) b	0.22	0.76	1.09	288.82	0.18	90.36	1.05	1.02	0.97	0.12	27.80	0.52	10.39
Kepler-35 (AB) b	0.13	0.73	0.60	131.46	0.04	90.76	0.89	0.81	0.91	0.18	20.73	0.14	6.34
Kepler-38 (AB) b	-	0.40	0.46	105.60	0.03	90.18	0.95	0.25	0.26	0.15	18.62	0.10	5.68
Kepler-413 b	0.21	0.40	-	66.26	0.12	4.07	0.82	0.54	0.66	0.10	10.12	0.04	6.55
Kepler-47 (AB) b	-	0.27	0.30	49.51	-	89.59	1.04	0.36	0.35	0.08	7.45	0.02	6.65
Kepler-47 (AB) c	-	0.42	0.99	303.16	-	89.83	1.04	0.36	0.35	0.08	7.45	0.02	40.70
KIC 9632895 b	0.02	0.56	0.79	240.50	0.04	89.43	0.93	0.19	0.21	0.18	27.32	0.05	8.80
KOI-2939 b	1.52	1.06	2.72	1107.59	0.06	90.10	1.22	0.97	0.79	0.13	11.26	0.16	98.38
PH-1 A(ab) b	-	0.56	0.63	138.51	0.05	90.02	1.38	0.39	0.28	0.17	20.00	0.21	6.93

Table 1: Observed circumbinary planets orbiting around main-sequence stars, excluded is the CB planet OGLE-2007-BLG-349L(AB)c which orbits far away from the star and is not relevant for this study. Planet masses are in units of Jupiter masses and the radius is measured in Jupiter radii, the binary masses are in units of solar masses, e_b and a_b denote the binary eccentricity and semi-major axis respectively. qM_2/M_1 is the binary mass fraction, where $M_1 > M_2$. The inclination is measured with respect to the plane of the sky and the last columns shows the dimensionless period ratio of the planet to the orbital period of the binary. The data was taken from the Open Exoplanet Catalogue (Rein, 2012).

Name	m_p [M_J]	R [R_J]	a [au]	P [day]	e	I [$^\circ$]	M_1 [M_\odot]	M_2 [M_\odot]	q	a_b	P_b [day]	e_b	P_b/P
2M 1938+4603 b	1.90	-	0.92	416.00	-	-	0.48	0.12	0.25	0.0	0.13	-	-
DP Leo b	6.05	-	8.19	10230.00	0.39	-	0.60	0.09	0.15	-	0.06	-	-
FL Lyr b	-	-	-	-	-	-	1.22	0.96	0.79	-	2.18	-	-
HU Aqr (AB) b	4.76	-	3.60	-	0.02	90.0	0.80	0.18	0.22	-	0.87	-	-
HU Aqr (AB) c	20.20	-	6.56	-	0.14	90.0	0.80	0.18	0.22	-	0.87	-	-
HU Aqr (AB) d	80.00	-	12.89	-	0.02	90.0	0.80	0.18	0.22	-	0.87	-	-
HW Vir (AB) b	14.30	-	4.69	4640.00	0.40	-	0.48	0.14	0.29	0.0	0.12	-	-
NN Ser (AB) c	6.96	-	5.39	5654.68	0.14	-	0.54	0.11	0.21	-	0.13	-	-
NN Ser (AB) d	1.74	-	3.36	2793.00	0.22	-	0.54	0.11	0.21	-	0.13	-	-
NSVS 14256825 c	2.80	-	1.90	1276.00	0.00	-	0.42	0.11	0.26	-	0.11	-	-
NSVS 14256825 d	8.00	-	2.90	2506.00	0.52	-	0.42	0.11	0.26	-	0.11	-	-
NY Virginis (AB) b	2.30	-	3.30	2900.00	-	-	0.46	0.14	0.30	-	0.10	-	-
RR Cae (AB) b	4.20	-	5.30	4350.00	0.00	-	0.62	0.18	0.29	-	0.30	-	-
PSR B1620-26 b	1.70	-	20.00	24837.00	0.13	-	1.35	0.34	0.25	-	191.44	0.03	129.8

Table 2: Observed circumbinary planets orbiting around evolve post common-envelope stars. Planet masses are units of Jupiter masses and the radius is measured in Jupiter radii, the binary masses are in units of solar masses, e_b and a_b denote the binary eccentricity and semi-major axis respectively, $q M_2/M_1$ is the binary mass fraction, where $M_1 > M_2$. The inclination is measured with respect to the plane of the sky and the last column shows the dimensionless period ratio of the orbital period of the planet to the orbital period of the binary. The data was taken from the Open Exoplanet Catalogue (Rein, 2012).

2

THEORETICAL BACKGROUND

In this chapter I will review the most important parts of the theory of planetary dynamics. Section 2.1 describes the two–body problem which introduces planet orbits and orbital elements. In section 2.2 I review the basic theory of a different formulation of mechanics called the *Hamiltonian mechanics*. The Hamiltonian formalism and its tools will be necessary for the development of an analytical model of resonance capture in chapter 3. In section 2.3 I describe a useful toy model for studying mean–motion resonances – the pendulum. In section 2.4 I review the theory of the three–body problem which forms the basis for subsequent analysis. Finally, in section 2.5 I talk about the validity of a certain approximation used in chapter 3. For the most part, the derivations in this chapter follow Murray and Dermott (1999) and Mardling (2013).

2.1 THE TWO–BODY PROBLEM

2.1.1 *The orbit equation and its solution*

If we are to attack the problem of three gravitationally interacting bodies in a circumbinary system, we first need to understand a simpler problem – that of two interacting massive bodies. This problem is often called the *Kepler problem* or the *two-body problem*. Consider two bodies with masses m_1 and m_2 and position vectors¹ \mathbf{r}_1 and \mathbf{r}_2 relative to a fixed origin O in inertial space. The forces acting on the two bodies are given by

$$\mathbf{F}_1 = Gm_1m_2 \frac{\hat{\mathbf{r}}}{r^3} = m_1\ddot{\mathbf{r}}_1 \quad (3)$$

$$\mathbf{F}_2 = -Gm_1m_2 \frac{\hat{\mathbf{r}}}{r^3} = m_2\ddot{\mathbf{r}}_2 \quad (4)$$

where $G = 6.672 \text{ m}^3 \text{ kg}^{-1} \text{ s}^{-2}$ is the gravitational constant, $\hat{\mathbf{r}}$ is the unit vector of the relative separation $\mathbf{r} = \mathbf{r}_2 - \mathbf{r}_1$, pointing from \mathbf{r}_1 to \mathbf{r}_2 and r is its magnitude. The double dots denote second time derivatives. From the definition of \mathbf{r} and the equations of motion, it follows that

$$\ddot{\mathbf{r}} = \ddot{\mathbf{r}}_2 - \ddot{\mathbf{r}}_1 = -G(m_1 + m_2) \frac{\hat{\mathbf{r}}}{r^3} \quad (5)$$

which can be rewritten as

$$\ddot{\mathbf{r}} + \mu \frac{\hat{\mathbf{r}}}{r^3} = 0 \quad (6)$$

¹ Throughout the thesis, vector quantities will be written with a bold–face font

where $\mu = G(m_1 + m_2)$. If we take a cross product of eq. (6) with $\mathbf{r} \times$ from the left-hand side and using the fact that $\mathbf{r} \times \mathbf{r} = 0$, we obtain

$$\mathbf{r} \times \ddot{\mathbf{r}} = 0 \quad (7)$$

This can be integrated to get

$$\mathbf{r} \times \dot{\mathbf{r}} = \mathbf{h} \quad (8)$$

where \mathbf{h} is a constant vector perpendicular to the plane spanned by $\mathbf{r} \times \dot{\mathbf{r}}$. \mathbf{h} is in fact the angular momentum per unit mass. Thus, the motion of m_2 relative to m_1 is confined to a plane perpendicular to \mathbf{h} . Since the motion is in a plane, we can simplify the problem further by transferring to polar coordinates (r, θ) centered at m_1 . We then have the following relations between vectors, available in any vector calculus book

$$\mathbf{r} = r\hat{\mathbf{r}} \quad (9)$$

$$\dot{\mathbf{r}} = \dot{r}\hat{\mathbf{r}} + r\dot{\theta}\hat{\theta} \quad (10)$$

$$\ddot{\mathbf{r}} = (\ddot{r} - r\dot{\theta}^2)\hat{\mathbf{r}} + \frac{1}{r} \frac{d}{dt}(r^2\dot{\theta})\hat{\theta} \quad (11)$$

By substituting these transformations into eq. (8) we get

$$\mathbf{h} = r^2\dot{\theta}\hat{z} \quad (12)$$

where \hat{z} is a unit vector perpendicular to the orbital plane.

By inserting the expression for $\ddot{\mathbf{r}}$ (eq. (11)) into eq. (6) and considering only the $\hat{\mathbf{r}}$ component (the $\hat{\theta}$ component simply says that \mathbf{h} is constant which we know already), we have the following scalar equation

$$\ddot{r} - r\dot{\theta}^2 + \frac{\mu}{r^2} = 0 \quad (13)$$

To solve this differential equation, we use the substitution $r = u^{-1}$ and eq. (12). From the chain rule, it follows

$$\dot{r} = -h \frac{du}{d\theta} \quad (14)$$

$$\ddot{r} = -h^2 u^2 \frac{d^2 u}{d\theta^2} \quad (15)$$

And finally, we have

$$\frac{d^2 u}{d\theta^2} + u = \frac{\mu}{h^2} \quad (16)$$

Equation (16) is called the *orbit equation*. This second order differential equation has the solution (after transforming back to r)

$$r = \frac{h^2/\mu}{1 + e \cos(\theta - \omega)} \quad (17)$$

where the *eccentricity* e and the *argument of pericentre* ω are the two constants of integration. Equation (17) defines a *conic section* curve in 2D space. Depending on the eccentricity, it can either be an ellipse for $e < 1$ corresponding to a closed orbit, or a hyperbola for $e > 1$ corresponding to an unbound orbit. The special case $e = 1$ defines a boundary between closed elliptical orbits and open hyperbolic orbits. Any particular orbit is highly unlikely to have an eccentricity of exactly zero. Similarly $e = 0$ defines a circular orbit which is of more interest since most stable planetary orbits are very nearly circular. Figure 5 shows an elliptical orbit in two dimensional space. The mass

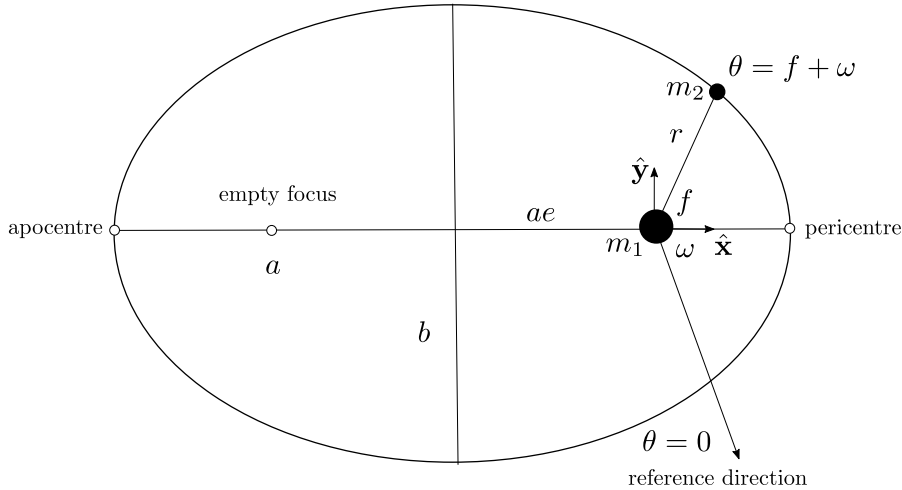


Figure 5: An elliptical orbit. The mass m_1 sits in one focus and m_2 orbits around it. The position of m_2 on the ellipse is specified by two angles, the true anomaly f and the argument of pericentre ω . Only f varies in the two-body problem, ω stays fixed in the absence of an external perturbation.

m_2 orbits around m_1 which is located in one of the foci of the ellipse. The position of m_2 at each moment in time is described by the 2π -periodic angle $f = \theta - \omega$ called the *true anomaly*. The angle ω is specified relative to an arbitrary reference direction and it is constant throughout the motion. $f = 0$ corresponds to the closest approach of m_2 to m_1 which happens at a point in orbit called the *pericentre*. Conversely, the point furthest away from m_2 at $f = \pi$ is called the *apocentre*. The *semi-major axis* of the ellipse a is given by

$$a = \frac{h^2}{\mu} \frac{1+e}{1-e} \quad (18)$$

One can easily derive (ex. Murray and Dermott, 1999) *Kepler's third law*, given by

$$T^2 = \frac{4\pi^2}{\mu} a^3 \quad (19)$$

where T is the orbital period of m_2 around m_1 . We also define the so-called *mean motion* n , as

$$n = \frac{2\pi}{T} \quad (20)$$

The mean motion is the average angular frequency of the periodic motion; it is constant in the two-body problem but in general varies when additional bodies are present.

If we multiply eq. (6) by $\dot{\mathbf{r}}$ and use the expressions for $\dot{\mathbf{r}}$ and $\ddot{\mathbf{r}}$ from eq. (11), we obtain the following constant of motion

$$\frac{1}{2}\mathbf{v}^2 - \frac{\mu}{r} = C \quad (21)$$

where $\mathbf{v}^2 = \dot{\mathbf{r}} \cdot \dot{\mathbf{r}}$ is velocity squared and C is a constant of motion, the energy per unit mass. It can be shown (Murray and Dermott, 1999) that C is given by

$$C = -\frac{\mu}{2a} \quad (22)$$

thus, the energy of a closed orbit in the two-body problem depends only on the semi-major axis.

2.1.2 The mean and eccentric anomaly

By solving the orbit equation, we have established that the mass m_2 orbits around m_1 in an ellipse if $e < 1$. However, it is not immediately clear how to explicitly solve for the time dependence of r and f and thus determine the position of m_2 at any given time, because f and r vary non-linearly with time for $e \neq 0$. For reasons which will become apparent later, we would like to construct an angle which varies linearly with time. One such angle is the *mean anomaly* M defined as

$$M = n(t - \tau) \quad (23)$$

where τ is the *time of pericentre passage* – time elapsed since the orbiting body was at pericentre, and it is constant. M increases linearly with time at a rate equal to the mean motion. At $t = \tau$ we have $M = f = 0$ and at $t = \tau + T/2$ $M = f = \pi$, thus, at the pericentre and apocentre M matches with f . The angle M has no obvious geometrical significance but we can define another angle which does. Figure 6 shows the orbital ellipse with semi-major axis a together with a circumscribed circle of radius a concentric with the ellipse. A line perpendicular to the semi-major axis of the ellipse intersects two points, one on the orbit and one on the circumscribed circle. We define the *eccentric anomaly* E to be the angle between the semi-major axis of the ellipse and the intersected point on the circle. Again, we

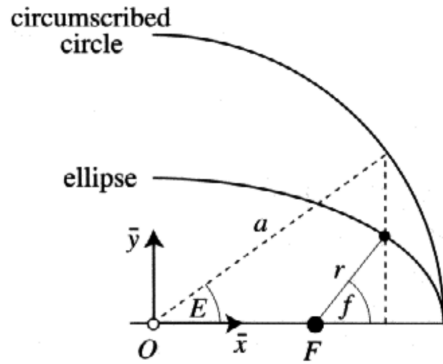


Figure 6: A geometrical description of the eccentric anomaly E . Figure from Murray and Dermott (1999).

have $E = M = 0$ at $f = 0$ and $E = M = \pi$ at $f = \pi$. From geometry one can show that the following relation between the angles f and E is satisfied

$$\cos f = \frac{\cos E - e}{1 - e \cos E} \quad (24)$$

Thus, there is a one-to-one correspondence between f and E as long as both are measured with respect to the positive x axis. To locate the location of the body on its orbit at time t , we need a relationship between E and M . This relationship is called the *Kepler's equation* and is given by (Murray and Dermott, 1999)

$$M = E - e \sin E \quad (25)$$

A solution to this equation enables us to locate the body on its orbit at any given time. The procedure is as follows

1. At a particular time t find M from eq. (23)
2. Solve the Kepler's equation for E
3. Use eq. (24) to find f

Kepler's equation is transcendental in E and therefore it cannot be solved directly.

Finally, we define one last angle λ called the *mean longitude* as

$$\lambda = M + \omega \quad (26)$$

Since it is derived from M , it does not have a geometrical interpretation. All longitudes are defined with respect to a common, arbitrary reference point.

2.1.3 Orbit in an inertial frame

So far we have derived a solution for the *relative motion* of m_2 with respect to m_1 , we now turn to the description of the orbit in a non-accelerating *inertial frame*. It is not difficult to show that the masses m_1

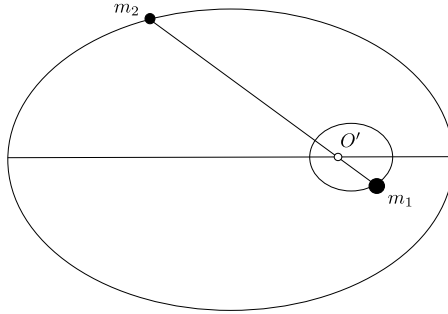


Figure 7: The motion of m_2 and m_1 with respect to their centre of mass O' .

and m_2 again orbit in a conic section around their centre of mass with the same period T as before. Figure 7 shows the orbits with respect to the centre of mass. We need not worry about the motion of the centre of mass itself because of a result from elementary mechanics which says that the centre of mass of a collection of particles always moves at constant velocity in a straight line and is therefore a valid inertial reference frame. The conic sections of the orbits relative to the centre of mass are reduced in scale by mass factors, as follows

$$a_1 = \frac{m_2}{m_1 + m_2} a \quad a_2 = \frac{m_1}{m_1 + m_2} a \quad (27)$$

where a_1 is the semi-major axis of the orbit of m_1 around O' and a_2 is the semi-major axis of the orbit of m_2 around O' .

The *total* angular momentum of the system is given by

$$L = \frac{m_1 m_2}{m_1 + m_2} \sqrt{\mu a (1 - e^2)} \quad (28)$$

and the total orbital energy is

$$E = -G \frac{m_1 m_2}{2a} \quad (29)$$

The energy of a Keplerian orbit depends only on the semi-major axis and the angular momentum depends on both the semi-major axis and the eccentricity. In particular, if the semi-major axis is constant the only way to change the eccentricity is by changing the angular momentum. This simple fact is the essence of so-called secular interactions described in section 2.4. The angular momentum is largest for a circular orbit.

2.1.4 Orbit in three-dimensional space

We have determined that the bodies in the two-body problem move on an ellipse in inertial space. The orientation of that ellipse stays fixed for all time if no external bodies are present. If there are other bodies in the system however, the orbit no longer stays fixed, both its shape and orientation change in three-dimensional space. Because

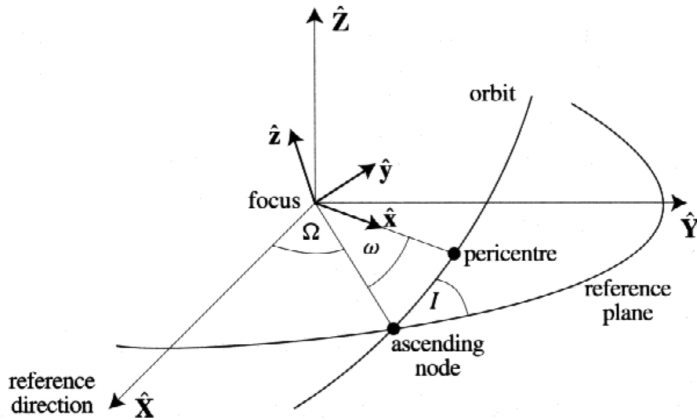


Figure 8: A Keplerian orbit in 3D space, figure from Murray and Dermott (1999).

of that, it is useful to define the orientation of the orbit in 3D space relative to a fixed reference plane. Figure 8 shows the orbit in 3D Cartesian coordinate system, the reference plane is taken to be the $X - Y$ plane. The orbital ellipse intersects the reference plane in two points, in order to define its orientation relative to fixed axes we have to choose one. Independent on whether the orbiting body is moving around the ellipse in a clockwise or counter-clockwise direction, the body will pass through the reference plane *from below* (where below means the $-Z$ direction) at one of the two points. We call this point the *ascending node* and choose it as a reference. The angle from the ascending node to the X axis is then called the *longitude of the ascending node* and is denoted by Ω . The angle between the plane of the ellipse and the reference plane is called the *inclination* of the orbit and is defined in the range $0 \leq I \leq \pi$.

Thus, we have completely described the orbit in 3D space. However, it is useful to define another angle ω called the *longitude of pericentre*. ω is not really a true angle since it is defined as a sum of angles in two separate planes. When the inclination is zero (the orbit is co-planar with the reference plane) we have $\omega = \Omega$.

It can be shown that there is a one-to-one correspondence between a set of Cartesian positions and velocities (x, y, z, v_x, v_y, v_z) of a given massive particle and an *instantaneous* Keplerian orbit defined by $(a, e, I, \Omega, \omega, f)$ with respect to another massive particle. This is why it is still useful to talk about orbits even when we are dealing with a system of multiple bodies. Although those bodies won't stay on a fixed Keplerian orbit for all time, at any given time we can still define an instantaneous Keplerian orbit. Most bodies in stable systems change their orbital elements slowly when exchanging energy and angular momentum with other bodies and it is often more useful to use the orbital elements as a set of coordinates instead of the Cartesian coordinates.

2.2 A BRIEF REVIEW OF HAMILTONIAN MECHANICS

2.2.1 Hamilton's equations

The two-body problem could have been solved equally well using a different formulation of mechanics called *Hamiltonian mechanics*, named after William Rowan Hamilton (1805–1865). Hamiltonian mechanics is equivalent to Newtonian mechanics but is often more suitable for certain types of problems, and the concept of a Hamiltonian function is a lot more general than Newton's second law of mechanics.

In Newtonian mechanics the full description of a dynamical system consisting of N particles is obtained by solving a system of second order differential equations of the form

$$\dot{\mathbf{p}}_i = \mathbf{F}_i \quad (30)$$

where $\dot{\mathbf{p}}_i = m_i \dot{\mathbf{r}}_i$ is the momentum of the i -th particle, m_i is its mass and \mathbf{r}_i its position vector relative to an origin of an inertial reference system. This constitutes a system of $3N$ second order differential equations for the positions vectors \mathbf{r}_i .

In the Hamiltonian formalism a dynamical system is described by a function of *generalized coordinates* \mathbf{q} and *momenta* \mathbf{p} called the *Hamiltonian* $\mathcal{H}(\mathbf{q}, \mathbf{p})$. Each pair (q_i, p_i) constitutes a single *degree of freedom*, it is said to be *conjugate*. The time evolution of these coordinates and momenta (\mathbf{q}, \mathbf{p}) , collectively known as the *phase space*, is given by *Hamilton's equations*

$$\dot{q}_i = \frac{\partial \mathcal{H}}{\partial p_i} \quad \dot{p}_i = -\frac{\partial \mathcal{H}}{\partial q_i} \quad (31)$$

Instead of $3N$ second order differential equations for a system of N particles, this is a system of $6N$ *coupled first-ordered* equations. Once the initial conditions $(\mathbf{q}_0, \mathbf{p}_0)$ are specified, the solution of Hamilton's equations defines a *unique* trajectory in a $6N$ dimensional phase space. The coordinate pair (\mathbf{q}, \mathbf{p}) is said to be *canonical* if the coordinates satisfy Hamilton's equations. The main advantage of the Hamiltonian formalism compared to other formalisms of mechanics is the ability to easily transform to different choices of (\mathbf{q}, \mathbf{p}) , as long as the new set of coordinates is also canonical. There are no other strict requirements on the new coordinates, the momentum p_i coincides with the real momentum $m_i \dot{q}_i$ only in Cartesian coordinates.

We can arbitrarily scale the momentum and the coordinate by a constant factor, for example $p \rightarrow \eta p$ $q \rightarrow \nu q$, as long as we also rescale the time. This can be seen from the form of eq. (31) because

$$\frac{\partial \mathcal{H}}{\partial (\eta p)} = \frac{d\mathbf{q}}{d(\eta t)} \quad (32)$$

and similarly for the coordinate scaling. Transformations of this type are known as *scale transformations* and they are simply a reflection of the fact that the equations of motion should be invariant to the changes of units.

2.2.2 Integrable Hamiltonians

The Hamiltonian formalism is useful for finding conserved quantities. If a generalized coordinate q_i does not appear in the Hamiltonian the corresponding momentum conjugate p_i is a conserved quantity

$$\dot{p}_i = \frac{\partial \mathcal{H}}{\partial q_i} = 0 \quad (33)$$

If the motion is in a fixed potential, the Hamiltonian is equal to the total energy of the system E .

If a particular Hamiltonian \mathcal{H} can be reduced to a form where it depends only on the momenta, that is

$$\mathcal{H}(p) \quad (34)$$

then the momenta p are conserved and the system is said to be *integrable*. An integrable system with n degrees of freedom has n constants of motion. From Hamilton's equations, it follows that the time evolution of the coordinates is simply

$$\dot{q}_i = \frac{\partial \mathcal{H}}{\partial p_i} = \omega_i \quad (35)$$

that is, all of the coordinates evolve linearly in time with constant frequencies ω_i which depend only on the momenta

$$q_i(t) = \omega_i t \quad (36)$$

Integrable systems are very rare in the space of all Hamiltonians and it is not immediately clear if a given Hamiltonian can be reduced to an integrable form.

Systems of the form

$$\mathcal{H} = \mathcal{H}_0(p) + \epsilon \mathcal{H}_1(q) \quad (37)$$

where \mathcal{H}_0 is an integrable Hamiltonian, \mathcal{H}_0 is a perturbation and ϵ is a small parameter are said to be nearly integrable and in general they display chaotic behaviour. However, if ϵ is small enough most solutions still lie in the region of phase space allowed by the solutions of \mathcal{H}_0 .

Systems with a single degree of freedom are always integrable and the Hamiltonian itself is a conserved quantity (i.e. the energy is conserved). The trajectory is defined completely by the value of energy.

They are often used as an approximation for a generally more complex system. Obtaining a single degree of freedom Hamiltonian for a resonance is a major goal of chapter 3.

The Keplerian Hamiltonian for the two-body problem is completely integrable and it can be written as

$$\mathcal{H}_k = -\frac{\mu^2 \mu^*}{2\Lambda^2} \quad (38)$$

where $\mu^* = m_1 m_2 / (m_1 + m_2)$ and Λ is the generalized momentum conjugate to the orbital element coordinate λ , the mean anomaly. The original Keplerian Hamiltonian has 6 degrees of freedom. The conservation of *total* linear and total angular momentum vectors and the conservation of total energy give 7 constants of motion. There is also a hidden symmetry in the problem that we haven't mentioned previously. One can show that one of the three components of the *Runge-Lenz* vector is also a constant of motion, which bring the total to 8. The Runge-Lenz vector is a vector pointing in the direction of periastron, defined by

$$\mathbf{e} = \dot{\mathbf{r}} \times (\mathbf{r} \times \ddot{\mathbf{r}}) / (G(m_1 + m_2)) - \hat{\mathbf{r}} \quad (39)$$

Its magnitude is equal to the eccentricity of the orbit. We see that the number of constants of motion over-determines the problem. In fact, the two extra constants of motion are responsible for the fact that that the relative motion is not only restricted to a conic curve, but it is also a conic section in the inertial (centre of mass) frame. Because of this the orbit is also fixed in 3D space.

2.2.3 Fixed points

Given a Hamiltonian $\mathcal{H}(q, p)$ with a single degree of freedom its *fixed points*, points which do not move under time evolution, are solutions of

$$\dot{p} = 0 \quad \dot{q} = 0 \quad (40)$$

From Hamilton's equations, it follows that their location is given by

$$\frac{\partial \mathcal{H}}{\partial p} = \frac{\partial \mathcal{H}}{\partial q} = 0 \quad (41)$$

Given a fixed point (q_0, p_0) , it is useful to derive the equations of motion in its vicinity. If a test particle in its vicinity moves on a trajectory away from the fixed point, the point is said to be *unstable*. Conversely, if it remains near the fixed point for all time, the point is said to be *stable*. We can expand the Hamiltonian near the fixed point in a Taylor series

$$\begin{aligned} \mathcal{H}(\tilde{q}, \tilde{p}) = \mathcal{H}(q_0, p_0) &+ \frac{\partial^2 \mathcal{H}(q_0, p_0)}{\partial q^2} \frac{\tilde{q}^2}{2} + \frac{\partial^2 \mathcal{H}(q_0, p_0)}{\partial p^2} \frac{\tilde{p}^2}{2} \\ &+ \frac{\partial^2 \mathcal{H}(q_0, p_0)}{\partial q \partial p} \tilde{q} \tilde{p} \end{aligned} \quad (42)$$

where $\tilde{q} = q - q_0$ and $\tilde{p} = p - p_0$. We can write this more succinctly in vectorial form as

$$\mathcal{H}(\tilde{q}, \tilde{p}) = \frac{1}{2} \mathbf{x}^\tau \mathbf{M} \mathbf{x} \quad (43)$$

where $\mathbf{x} = (\tilde{q}, \tilde{p})$ and τ denotes the transpose operation. \mathbf{M} is called the *Hessian matrix* and is given by

$$\mathbf{M} = \begin{pmatrix} \frac{\partial^2 \mathcal{H}}{\partial q^2} & \frac{\partial^2 \mathcal{H}}{\partial q \partial p} \\ \frac{\partial^2 \mathcal{H}}{\partial p \partial q} & \frac{\partial^2 \mathcal{H}}{\partial p^2} \end{pmatrix} \quad (44)$$

it is evaluated at the fixed points (q_0, p_0) . It is symmetric and therefore has two real eigenvalues and two eigenvectors. It can be shown that after diagonalizing this matrix, the Hamiltonian assumes the form

$$\mathcal{H}(q, p) = \frac{1}{2} (\lambda_1 q^2 + \lambda_2 p^2) \quad (45)$$

where λ_1 and λ_2 are the eigenvalues. If the eigenvalues are both negative or both positive (i.e. the determinant is positive) the system undergoes harmonic oscillations (librations) about the fixed point with frequency

$$\omega = \sqrt{\lambda_1 \lambda_2} \quad (46)$$

and we say the fixed point is a *center*. If one of the eigenvalues is negative and the other positive (the determinant is negative) the system is diverging exponentially away from the fixed point in the direction of one *eigenvector* and heading towards the fixed point along the direction of the other eigenvector. The fixed point is unstable and we call it a *saddle*.

2.2.4 Canonical transformations

A *canonical transformation* is a coordinate transformation from a set (\mathbf{q}, \mathbf{p}) to $[Q(\mathbf{q}, \mathbf{p}), P(\mathbf{q}, \mathbf{p})]$ which preserves the form of Hamilton's equations. It can be shown that canonical transformations satisfy the Poisson brackets

$$\{P_i, P_j\} = 0 \quad \{Q_i, Q_j\} = 0 \quad \{Q_i, P_j\} = \delta_{ij} \quad (47)$$

where δ_{ij} is the *Kronecker delta* symbol and the Poisson bracket is defined as

$$\{f, g\} = \sum_{i=0}^N \left(\frac{\partial f}{\partial q_i} \frac{\partial g}{\partial p_i} - \frac{\partial f}{\partial p_i} \frac{\partial g}{\partial q_i} \right) \quad (48)$$

where the sum goes over all the degrees of freedom. The question remains how to easily construct transformations which are canonical.

The answer lies in the form of *generating functions*. Consider a function $F_1(q, Q)$ of the old and new coordinates and let

$$p_i = \frac{\partial F_1}{\partial q_i} \quad (49)$$

After inverting, this equation defines a new coordinate $Q_i = Q_i(q, p)$. One can show that the new momentum is then given by

$$P_i = -\frac{\partial F_1}{\partial Q_i} \quad (50)$$

Thus we have found a way to construct a canonical transformation to new coordinates. We can choose the new coordinates Q_i , however, the requirement that the new coordinates form a conjugate pair restricts our freedom to choose the new momentum as well. The function $F_1(q, Q)$ is called the *generating function of first kind*. There are three additional kinds of generating functions, the possibilities are listed in table 3. Which kind of the generating function is the best depends on

Generating function	Derivatives	
$F_1(q, Q)$	$p_i = \frac{\partial F_1}{\partial Q_i}$	$P_i = \frac{\partial F_1}{\partial q_i}$
$F_2(q, P)$	$p_i = \frac{\partial F_2}{\partial q_i}$	$Q_i = \frac{\partial F_2}{\partial P_i}$
$F_3(p, Q)$	$q_i = -\frac{\partial F_3}{\partial p_i}$	$P_i = -\frac{\partial F_3}{\partial Q_i}$
$F_4(p, P)$	$q_i = -\frac{\partial F_4}{\partial p_i}$	$Q_i = \frac{\partial F_4}{\partial P_i}$

Table 3: Different kinds of generating functions.

the problem at hand.

2.3 THE PENDULUM

A simple single degree of freedom Hamiltonian useful for the study of resonance is that of the pendulum. The Hamiltonian has the form

$$\mathcal{H}(\phi, p) = \frac{1}{2}p^2 - \omega_0^2 \cos \phi \quad (51)$$

Where ω_0 has dimensions of frequency. By solving Hamilton's equations, we obtain

$$\dot{\phi} = p \quad (52)$$

$$\dot{p} = -\omega_0^2 \sin \phi \quad (53)$$

Combining the two equations, we obtain a single equation of motion

$$\ddot{\phi} + \omega_0^2 \sin \phi = 0 \quad (54)$$

We see that in the limit of small ϕ the motion is equivalent to that of the harmonic oscillator oscillating with the frequency ω_0 . The fixed

points are located at $(\phi, p) = (\pm k\pi, 0)$ (where k is an integer) and there is a single stable center point located at $(\phi, p) = (\pi, 0)$. It is sufficient to study the two fixed points $(0, 0)$ and $(\pi, 0)$ since the motion is periodic. For the fixed point at $(0, 0)$, we have

$$\mathbf{M} = \begin{pmatrix} 1 & 0 \\ 0 & -\omega_0^2 \end{pmatrix} \quad (55)$$

and we see that this point is a stable center. For the other point at $(\pi, 0)$, we have

$$\mathbf{M} = \begin{pmatrix} \omega_0^2 & 0 \\ 0 & 1 \end{pmatrix} \quad (56)$$

The point is an unstable saddle point. Figure 9 shows the level curves

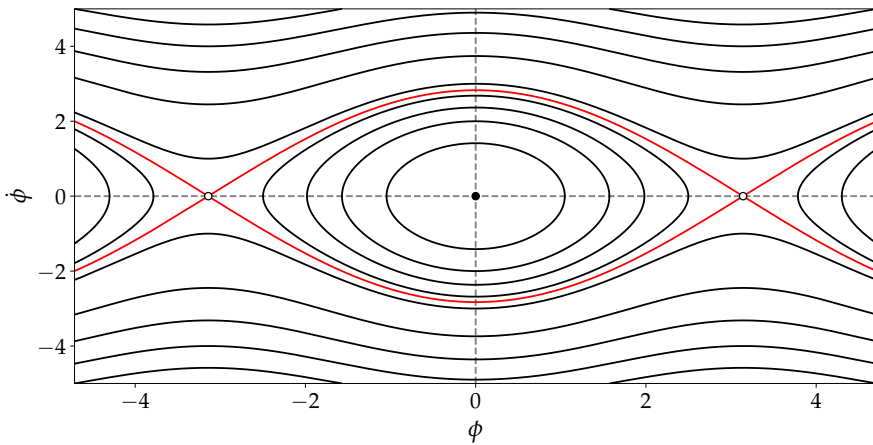


Figure 9: The phase space of a pendulum. The red curve denotes the separatrix filled circles denote stable fixed points, open circles denote unstable fixed points.

(curves of constant \mathcal{H}) of the pendulum. Given a specific value of the energy, the system stays on one of the curves for all time. The motion around the fixed point $(0, 0)$ in between the fixed points at $-\pi$ and π is said to be *libratory*. There is also an entirely different type of motion where ϕ is unbounded, these trajectories are called *circulatory*. The curve which passes through the unstable points separates the two regimes and is called the *separatrix*. As seen from the figure², the oscillation period increases from the initial small amplitude value of $2\pi/\omega_0$ to infinity as the separatrix is approached. Once the separatrix is crossed the motion is unbounded. This steep dependence of the librational period on the distance to the separatrix is responsible for chaos in weakly interacting non-linear systems (see Aarseth, Tout, and Mardling (2008) for a broader discussion of this point). The concepts presented in this section will be important for the study of resonance in the three-body problem.

² This can also be shown rigorously by deriving the expression for ω_{lib} as a function of maximum ϕ .

2.4 THE THREE-BODY PROBLEM

2.4.1 The disturbing function

Finally, we move to the problem of three gravitationally interacting massive bodies, such as the circumbinary system consisting of two stars and an outer planet. The three-body problem is famously not integrable, many great mathematicians such as Newton and Poincaré have tried and failed to find an exact solution. However, it is still possible to do a perturbative analysis in the case when one of the bodies is only weakly interacting with the other two. The following discussion largely follows Mardling2013.

A stable hierarchical system of three bodies naturally divides into two orbits composed of an "inner binary" and an "outer binary". We will work in *Jacobi coordinates* which are defined such that in a hierarchical system consisting of N bodies, the N th body is defined in a coordinate system whose origin is the centre of mass of the previous $N - 1$ bodies. Figure 10 shows a system of three masses m_1 , m_2 and m_3 in Jacobi coordinates. The position vector \mathbf{r} points from m_1 to m_2 and it is the same vector as in our previous analysis of the two-body problem. The position vector \mathbf{R} points from the centre of mass of the inner binary consisting of m_1 and m_2 to the outer mass m_3 . Thus, at any given moment we can define two Keplerian orbits, one for the inner binary and one for the outer binary. Since the three-body problem is not integrable the orbits will in general no longer be fixed and will change their orbital elements with time. This choice of coordinates obviously fails in the case of crossing orbits since the hierarchy loses its meaning, however, a system with crossing orbits is inherently unstable and not the subject of our interest.

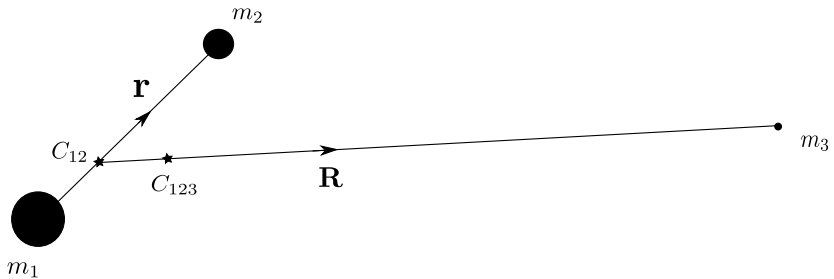


Figure 10: A system of three massive bodies in Jacobi coordinates. The point C_{12} denotes the centre of mass of the inner two bodies and the point C_{123} that of the whole system.

When the system is stable the inner and outer orbits interact only weakly by means of an interacting potential called the *disturbing function*. The disturbing function can be written as an infinite Fourier series of angles called the *harmonic angles* (or sometimes resonance

angles), it is responsible for the exchange of energy and angular momentum between the two orbits. Each resonance angle is a linear superposition of all angles in the system. A resonance angle can either circulate or librate in exactly the same way as the angle in the pendulum model described in the previous section. If a particular resonance angle is librating, we say that the system is in *resonance*. The various resonance angles can mutually interact, under certain conditions a system can exist in two neighbouring resonant states where two resonant angles librate at a similar period. This is known as *resonance overlap* and it leads to chaotic behaviour as the resonance angle approaches the unstable fixed points (Instability and Oscillator, 1969). The resonance overlap criterion is then a good indication of whether the system is chaotic or not.

We can write the equations of motions as

$$\begin{aligned} m_1 \ddot{\mathbf{r}}_1 &= \frac{Gm_1m_2}{r_{12}^2} \hat{\mathbf{r}}_{12} + \frac{Gm_1m_3}{r_{13}^2} \hat{\mathbf{r}}_{13} \\ m_2 \ddot{\mathbf{r}}_2 &= -\frac{Gm_1m_2}{r_{12}^2} \hat{\mathbf{r}}_{12} + \frac{Gm_2m_3}{r_{23}^2} \hat{\mathbf{r}}_{23} \\ m_3 \ddot{\mathbf{r}}_3 &= -\frac{Gm_1m_3}{r_{13}^2} \hat{\mathbf{r}}_{13} - \frac{Gm_2m_3}{r_{23}^2} \hat{\mathbf{r}}_{23} \end{aligned} \quad (57)$$

where the position vectors \mathbf{r}_i point from the centre of mass of system C_{123} to the mass m_i and $\mathbf{r}_{ij} = \mathbf{r}_j - \mathbf{r}_i$. Equation (57) constitutes a system with 9 degrees of freedom. Again we have the 7 conserved quantities due to momentum and energy conservation, however, there is no analogue of the Runge-Lenz vector in the three-body problem. Therefore, the system is not completely integrable, in fact, it admits *chaotic* solutions – solutions which are extremely sensitive to small variations in the initial conditions. There are two kinds of stability, one is called *Lagrange stability* and the other *Hill stability*. The latter happens due to close approaches of two bodies which most often result in an ejection of one of the bodies, and the former does not require close approaches. In this chapter we are primarily interested in Lagrange instability because scattering events are difficult to handle analytically and only become important after the onset of Lagrange instability in circumbinary systems.

We start by rewriting eq. (57) in Jacobi coordinates and define the vectors $\mathbf{r} = \mathbf{r}_2 - \mathbf{r}_1$ and $\mathbf{R} = (m_{123}/m_{12})\mathbf{r}_3$. We can now rewrite eq. (57) as

$$\begin{aligned} \mu_i \ddot{\mathbf{r}} + \frac{Gm_1m_2}{r^2} \hat{\mathbf{r}} &= \frac{\partial \mathcal{R}}{\partial \mathbf{r}} \\ \mu_o \ddot{\mathbf{R}} + \frac{Gm_{12}m_3}{R^2} \hat{\mathbf{R}} &= \frac{\partial \mathcal{R}}{\partial \mathbf{R}} \end{aligned} \quad (58)$$

where $R = |\mathbf{R}|$, $\mu_i = m_1m_2/m_{12}$ and $\mu_o = m_{12}m_3/m_{123}$ and

$$\mathcal{R} = -\frac{Gm_{12}m_3}{R} + \frac{Gm_2m_3}{|\mathbf{R} - \beta_1 \mathbf{r}|} + \frac{Gm_1m_3}{|\mathbf{R} + \beta_2 \mathbf{r}|} \quad (59)$$

is the disturbing function with $\beta_i = m_i/m_{12}$, $i = 1, 2$. We use the subscripts i and o to denote quantities defined with respect to the inner and outer orbits respectively. The notation $\partial/\partial\mathbf{r}$ refers to the gradient with respect to the spherical polar coordinates (r, θ_1, ϕ_1) associated with the position of body 2 relative to the centre of mass C_{12} , similarly, $\partial/\partial\mathbf{R}$ is the gradient associated with the position of body 3 with coordinates (R, θ_o, ϕ_o) relative to the same origin. All information about the mutual interaction of the inner and outer orbits is contained in \mathcal{R}^3 . In the limit when the inner two masses coalesce ($r/R \rightarrow 0$) or the mass ratio between the planet mass m_3 and the total binary mass m_{12} goes to zero ($m_3/m_{12} \rightarrow 0$), \mathcal{R} vanishes and the two orbits no longer interact with each other.

The total energy (or the Hamiltonian) is given by

$$\mathcal{H} = \mathcal{H}_i + \mathcal{H}_o - \mathcal{R} \quad (60)$$

where

$$\mathcal{H}_i = \frac{1}{2}\mu_i \dot{\mathbf{r}} \cdot \dot{\mathbf{r}} - \frac{Gm_1m_2}{r}, \quad \mathcal{H}_o = \frac{1}{2}\mu_o \dot{\mathbf{R}} \cdot \dot{\mathbf{R}} - \frac{Gm_{12}m_3}{R} \quad (61)$$

are the Keplerian Hamiltonians corresponding to the inner and outer orbits and the disturbing function has a role of interaction energy. The two Keplerian Hamiltonians individually are fully integrable as mentioned previously, the complete Hamiltonian is not.

Given eq. (60), one can calculate the Hamilton's equations of motion. Those are equivalent to eq. (58), except that they are first order in time. If those equations are then expressed in terms of the inner and outer orbital elements, they are called *Lagrange's planetary equations*. The derivation is presented in Brouwer and Clemence (for ex. 1961), here we merely state the result for coplanar systems

$$\begin{aligned} \dot{e} &= -\frac{s(1-s)}{\mu n a^2 e} \frac{\partial \mathcal{R}}{\partial \lambda} - \frac{s}{\mu n a^2 e} \frac{\partial \mathcal{R}}{\partial \omega} \\ \dot{\omega} &= \frac{s}{\mu n a^2 e} \frac{\partial \mathcal{R}}{\partial e} \\ \dot{\epsilon} &= -\frac{2}{\mu n a} \frac{\partial \mathcal{R}}{\partial a} + \frac{s(1-s)}{\mu n a^2 e} \frac{\partial \mathcal{R}}{\partial e} \end{aligned} \quad (62)$$

where the subscripts of the orbital elements are either i or o for the inner and outer orbits respectively. $s = \sqrt{1-e^2}$ and ϵ is the mean longitude at $t = t_0$ and is related to the mean longitude by $\int_0^t ndt$ (see. Mardling, 2013, for details). There is no unique general solution for eq. (62), best one can do is to expand \mathcal{R} in a series and consider a few dominant terms in certain cases.

³ Historically, most versions of the expanded disturbing function have units of energy per unit mass. The expansion presented in RM2013 has units of energy

We start by expanding the last two terms in eq. (59) using a well known⁴ expansion in terms of *spherical harmonics*.

$$\frac{1}{|\mathbf{R} - \beta_s \mathbf{r}|} = \frac{1}{R} \sum_{l=0}^{\infty} \frac{4\pi}{2l+1} \left(\frac{\beta_s r}{R} \right)^l \sum_{m=-l}^l Y_{lm}(\theta_i, \phi_i) Y_{lm}^*(\theta_o, \phi_o) \quad (63)$$

Y_{lm} is a spherical harmonic⁵ of *degree l* and *order m* with Y_{lm}^* being its complex conjugate. Using eq. (63) the disturbing function \mathcal{R} becomes

$$\mathcal{R} = G\mu_i m_3 \sum_{l=2}^{\infty} \sum_{m=-l}^l \left(\frac{4\pi}{2l+1} \right) \mathcal{M}_l \left(\frac{r^l}{R^{l+1}} \right) Y_{lm}(\theta_i, \phi_i) Y_{lm}^*(\theta_o, \phi_o) \quad (64)$$

where \mathcal{M}_l is a mass factor given by

$$\mathcal{M}_l = \frac{m_1^{l-1} + (-1)^l m_2^{l-1}}{m_{12}^{l-1}} \quad (65)$$

Equation (64) is a spherical harmonic expansion with coefficients proportional to $(r/R)^l$. In order for this series to converge, we require that r/R be a small number. This is satisfied for all CB planets because, as will be shown later, there is an inner instability region just outside of the stellar binary and the only stable orbits exist further outside the stellar binary's orbit. A spherical harmonic is defined by

$$Y_{lm}(\theta, \phi) = \sqrt{\frac{2l+1}{4\pi} \frac{(l-m)!}{(l+m)!}} P_l^m(\cos \theta) e^{im\phi} \quad (66)$$

where $P_l^m(\theta, \phi)$ is the *associated Legendre function* (Jackson, 2007).

Next, we focus on coplanar systems (mutual inclination between orbits is assumed to be zero) and thus we take $\theta_i = \theta_o = \pi/2$ (the motion is restricted to the $x-y$ plane), $\phi_i = f_i + \omega_i$ and $\phi_o = f_o + \omega_o$ where f_i and f_o are the true anomalies of the outer and inner orbits respectively. We obtain

$$\mathcal{R} = g\mu_i m_3 \sum_{l=2}^{\infty} \sum_{m=-l,2}^l \frac{1}{2} c_{lm}^2 \mathcal{M}_l e^{im(\omega_i - \omega_o)} (r^l e^{imf_i}) \left(\frac{e^{-imf_o}}{R^{l+1}} \right) \quad (67)$$

where

$$c_{lm}^2 = \frac{8\pi}{2l+1} [Y_{lm}(\pi/2, 0)] = c_{l-m}^2 \quad (68)$$

⁴ Expressions involving a difference between two vectors such as $1/|\mathbf{r} - \mathbf{r}'|$ occur in all kinds of problems in physics.

⁵ Spherical harmonics are special functions which form a complete set of orthogonal functions on the sphere, any function defined in terms of spherical polar coordinates can be expanded in an infinite series of spherical harmonics as $f(\theta, \phi) = \sum_{l=0}^{\infty} \sum_{m=-l}^l f_m^l Y_l^m(\theta, \phi)$. The series converges if the coefficients f_m^l decay in l sufficiently rapidly.

and the notation $m = -l, 2$ in the summation over m means that the summation is taken in steps of 2. The first few values for c_{lm} can be found in Mardling (2013). For stable systems the expressions in the last two brackets of eq. (67) are nearly periodic and can therefore be expanded in a *Fourier series* of the inner and outer mean anomalies $M_i = n_i t + M_i(0)$ and $M_o = n_o t + M_o(0)$, where n_i, n_o are the mean motions associated with the inner and outer orbits and $M_i(0), M_o(0)$ are their values at $t = 0$. The result is

$$r^l e^{imf_i} \stackrel{\mathcal{F}}{=} a_i^l \sum_{n=-\infty}^{\infty} X_n^{l,m}(e_i) e^{inM_i} \quad (69)$$

and

$$\frac{r^{-imf_o}}{R^{l+1}} \stackrel{\mathcal{F}}{=} a_o^{-(l+1)} \sum_{n'=-\infty}^{\infty} X_{n'}^{-(l+1),m}(e_o) e^{-in'M_o} \quad (70)$$

where the \mathcal{F} above the equality sign denotes Fourier expansion and the *Fourier coefficients* given by

$$\begin{aligned} X_n^{l,m}(e_i) &= \frac{1}{2\pi} \int_0^{2\pi} \left(\frac{r}{a_i} \right)^l e^{imf_i} e^{inM_i} dM_i \\ &= \frac{1}{2\pi} \int_0^{2\pi} r^{l+1} e^{imf_i} e^{-inM_i} dE_i = \mathcal{O}(e_i^{|m-n|}) \end{aligned} \quad (71)$$

and

$$\begin{aligned} X_{n'}^{-(l+1),m}(e_o) &= \frac{1}{2\pi} \int_0^{2\pi} \left(\frac{R}{a_o} \right)^{-(l+1)} e^{-imf_o} e^{in'M_o} dM_o \\ &= \frac{1}{2\pi} \int_0^{2\pi} R^{-l} e^{-imf_o} e^{in'M_o} dE_o = \mathcal{O}(e_o^{|m-n'|}) \end{aligned} \quad (72)$$

are called the *Hansen coefficients*. The notation $\mathcal{O}()$ refers to the order of the leading terms. Plugging eq. (69) and eq. (70) into eq. (67), we obtain (Mardling, 2013)

$$\mathcal{R} = \sum_{m=0}^{\infty} \sum_{n=-\infty}^{\infty} \sum_{n'=-\infty}^{\infty} \mathcal{R}_{mn} \cos \phi_{mn} \quad (73)$$

where

$$\phi_{mn} = nM_i - n'M_o + m(\varpi_i - \varpi_o) \quad (74)$$

is the *harmonic angle*,

$$\mathcal{R}_{mn} = \frac{G\mu_i m_3}{a_o} \sum_{l=l_{\min}, 2}^{\infty} \zeta_m c_{lm}^2 \mathcal{M}_l \alpha^l X_n^{l,m}(e_i) X_{n'}^{-(l+1),m}(e_o) \quad (75)$$

is the *harmonic coefficient* associated with the harmonic angle $\phi_{mn\bar{n}}$, $\alpha = a_i/a_o$ is the semi-major axis ratio, and the factor ζ_m is defined as

$$\zeta_m = \begin{cases} 1/2 & m = 0 \\ 1 & \text{otherwise} \end{cases} \quad (76)$$

The summation over l stars at

$$l_{\min} = \begin{cases} 2 & m = 0 \\ 3 & m = 1 \\ m & m \geq 2 \end{cases} \quad (77)$$

The series contains three independent indices associated with each harmonic coefficient since there are three independent frequencies in the problem. The indices n and n' are associated with the two mean motions and the index m is associated with the change in the relative orientation of the orbits called the *rate of apsidial advance* $\dot{\omega}_i - \dot{\omega}_o$. The terms corresponding to $l = 2$ are called *quadropole* terms, those with $l = 3$ are *octopole* terms etc. . The harmonic angle can also be written in terms of mean longitudes $\lambda_i = M_i + \omega_i$ and $\lambda_o = M_o + \omega_o$ as

$$\phi_{mn\bar{n}} = n\lambda_i - n'\lambda_o + (m-n)\omega_i - (m-n')\omega_o \quad (78)$$

The harmonic angle has to be invariant to the rotation of the coordinate axes because no direction in space is special. Since such a rotation changes all longitude angles by the same amount, their coefficients should add up to zero. This property is called the *d'Alembert relation* (Murray and Dermott, 1999). A short inspection of eq. (78) shows that this is indeed satisfied for all possible coefficients.

At this point, it is useful to review what has been done. We have started with the equations of motion for the three-body problem and expressed them in terms of the Keplerian motion of masses m_1 and m_2 (the inner orbit), the motion of mass m_3 around the centre of mass of the inner two masses (the outer orbit), and an interaction term between the two orbits called the disturbing function. The disturbing function can be written as an infinite series of spherical harmonics whose coefficients depend on r/R . We then impose the condition of coplanar orbits and rewrite the spherical harmonics in terms of exponentials containing the three angles in the problem. Finally we expand the terms with the exponentials in an infinite Fourier series. We end up with an expression for \mathcal{R} which is a triple infinite Fourier cosine series whose coefficients contain another infinite series in α , the semi-major axis ratio, which reflects the original expansion in r/R . The dependence on the eccentricity is contained only in the Hansen coefficients, which can *in principle* be calculated exactly. We now move to the question of significance of the various terms in eq. (73).

2.4.2 Secular dynamics

There are two different kinds of harmonic angles, those which include the mean longitudes, which necessarily vary on an orbital timescale, and those which don't include the mean longitudes but contain only the angles which vary on a slower timescale, such as $\omega_i - \omega_o$ and the inclination angles in non-coplanar systems. As we will be shown in section 2.5, in many cases one can ignore the disturbing function terms involving the fast-varying mean longitudes and average them over the orbital period, this is due to the fact that for such terms ϕ is slowly varying and therefore $\cos \phi$ becomes significant. In practice, the averaging⁶ is achieved by simply retaining only the terms with $n = n' = 0$ in eq. (73). The resulting disturbing function is called the *secular*⁷ disturbing function and it is given by

$$\tilde{\mathcal{R}} = \sum_{m=0}^{\infty} \tilde{\mathcal{R}}_m \cos[m(\omega_i - \omega_o)] \quad (79)$$

where

$$\tilde{\mathcal{R}}_m = \frac{G\mu_i m_3}{a_o} \sum_{l=l_{\min},2}^{\infty} \zeta_m c_{lm}^2 M_l \alpha^l X_0^{l,m}(e_i) X_0^{-(l+1),m}(e_o) \quad (80)$$

Closed-form expressions exist for Hansen coefficients when $n = n' = 0$. Up the octopole order, the secular disturbing function becomes (Mardling, 2013).

$$\begin{aligned} \tilde{\mathcal{R}} = & \frac{G\mu_i m_3}{a_o} \left[\frac{1}{4} \left(\frac{a_i}{a_o} \right)^2 \frac{1 + \frac{3}{2}e_i^2}{(1 - e_o^2)^{3/2}} \right] \\ & - \frac{15}{16} \left(\frac{a_i}{a_o} \right)^3 \left(\frac{m_1 - m_2}{m_{12}} \right) \frac{e_i e_o (1 + \frac{3}{4}e_i^2)}{(1 - e_o^2)^{5/2}} \cos(\omega_i - \omega_o) \end{aligned} \quad (81)$$

It turns out that a purely secular coplanar three-body problem involving only terms up to octopole order is fully integrable (ex. Murray and Dermott, 1999) and hence does not admit chaotic solutions.

One can show (Murray and Dermott, 1999) that by using the Lagrange planetary equations together with eq. (81) expanded to second order in eccentricity, it is possible to obtain a unique solution. The solution is best expressed in the following coordinates

$$h_i = e_i \sin \omega_i \quad k_i = e_i \cos \omega_i \quad (82)$$

$$h_o = e_o \sin \omega_i \quad k_o = e_o \cos \omega_o \quad (83)$$

⁶ One can show (Murray and Dermott, 1999) that the averaging over the mean longitudes is equivalent to considering the dynamics of rings made up by spreading the orbiting masses around their orbits. The procedure is called *Gauss's averaging method*, it shows us that secular interactions between planets are equivalent to interactions between massive rings because the specific location of given mass along its orbit doesn't matter on long timescales.

⁷ The word secular comes from Latin *seculum* meaning century, or long period.

Lagrange planetary equations in the new coordinates reduce to form

$$\begin{pmatrix} \dot{h}_i \\ \dot{h}_o \end{pmatrix} = \mathbf{A} \begin{pmatrix} k_i \\ k_o \end{pmatrix} \quad \text{and} \quad \begin{pmatrix} \dot{k}_i \\ \dot{k}_o \end{pmatrix} = -\mathbf{A} \begin{pmatrix} h_i \\ h_o \end{pmatrix} \quad (84)$$

where the matrix \mathbf{A} contains constant factors. This system can be solved as an eigenvalue problem, the solutions are

$$\begin{aligned} h_i &= \sum_{l=1}^2 e_{il} \sin(g_l t + \beta_l) & k_i &= \sum_{l=1}^2 e_{il} \cos(g_l t + \beta_l) \\ h_o &= \sum_{l=1}^2 e_{ol} \sin(g_l t + \beta_l) & k_o &= \sum_{l=1}^2 e_{ol} \cos(g_l t + \beta_l) \end{aligned} \quad (85)$$

where the frequencies g are the eigenvalues of the matrix \mathbf{A} with e_{ol} and e_{il} the components of two corresponding eigenvectors. These are determined from the initial conditions together with the phases β_l . Equation (85) is known as the *Laplace-Lagrange secular solution*. As expected, the solution does not depend on the mean longitudes since we are neglecting them in the secular disturbing function. The solution gives the variation of the eccentricities and pericentres⁸ of the two orbits as a function of time and it implies that the orbits are stable for all time within the limits of the secular approximation (terms with mean longitudes can be averaged out) and the eccentricity expansion to second order. The Laplace-Lagrange holds not only in the three body case but also in the N-body case and it successfully reproduces most aspects of the secular dynamics of the Solar System.

Free and Forced elements

In section 2.4.2 we have shown that it is possible to find an exact solution for the evolution of slowly-varying orbital elements in the three-body problem. We can use this solution to study the dynamics of an outer massless particle perturbed by the other three bodies. Let the orbital elements of the massless particle be $(a', \lambda', e', I' = 0, \omega', \Omega' = 0)$. Through a derivation similar to that described in section 2.4.2 (see ch. 7 sec. 4 of Murray and Dermott, 1999) we obtain the following solution for h' and k'

$$h' = e_{\text{free}} \sin(At + \beta) + h_0(t) \quad k' = e_{\text{free}} \cos(At + \beta) + k_0(t) \quad (86)$$

⁸ In fact, the Laplace-Lagrange secular solution is also valid in the case of inclined system in which there are two additional coordinates $p = I \sin \Omega$ and $q = I \cos \Omega$.

where e_{free} , β and A are constants determined by the initial conditions and the functions $h_0(t)$ and $k_0(t)$ are given by

$$h_0(t) = - \sum_{l=1}^2 \frac{v_l}{A - g_l} \sin(g_l t + \beta_l) \quad (87)$$

$$k_0(t) = - \sum_{l=1}^2 \frac{v_l}{A - g_l} \cos(g_l t + \beta_l) \quad (88)$$

where v_l , g_l and β_l are again constants depending on the initial conditions, such as the mass ratios and (fixed) semi-major axes.

The solution is best described by plotting eq. (86) in the plane $(e' \cos \omega', e' \sin \omega')$. Figure 11 shows the geometrical interpretation

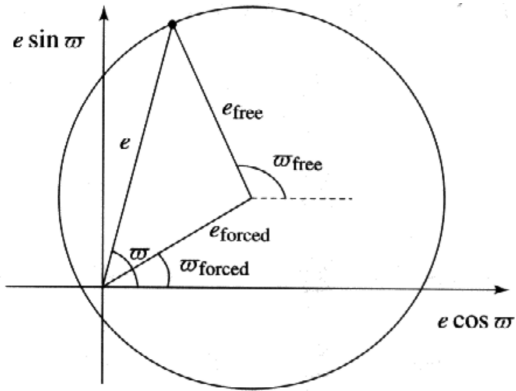


Figure 11: The geometric relationship between the free and forced eccentricities and longitudes. Figure taken from Murray and Dermott (1999).

for the motion of the test particle. The point in the plane represents a certain (h', k') value, which defines a vector pointing from the origin to the point with magnitude e' and closing an angle ω' with the x axis. This vector can be thought of as a vector sum of two vectors. One points from the origin to the point (h_0, k_0) with magnitude e_{forced} called the *forced eccentricity* at an angle ω_{forced} called the *forced longitude of pericentre*, the other pointing from (h_0, k_0) to the point (h, k) with magnitude e_{free} called the *free eccentricity* at an angle $\omega_{\text{free}} = At + \beta$ called the *free longitude of pericentre*.

Thus, the particle's motion can be thought of as a motion around a circle centered at (h_0, k_0) at rate constant rate A where the point (h_0, k_0) itself moves in a complicated path determined by the Laplace-Lagrange solution for the three massive bodies.

2.4.3 Resonant dynamics

Consider the harmonic angle defined in eq. (78), $\cos \phi_{mn\bar{n}}$ becomes large when $\phi_{mn\bar{n}}$ is a slowly varying angle, in other words, $\dot{\phi}_{mn\bar{n}} \approx 0$. Differentiating eq. (78) with respect to time, we have

$$\dot{\phi}_{mn\bar{n}} = n\bar{n}_i - \bar{n}'\bar{n}_o + (m-n)\dot{\omega}_i - (m-\bar{n}')\dot{\omega}_o \approx 0 \quad (89)$$

where $\bar{n}_i = \lambda_i$ and $\bar{n}_o = \lambda_o$ are the two mean motions. We can rewrite eq. (89) as

$$\frac{\bar{n}_i + (\frac{m}{n} - 1)\dot{\omega}_i}{\bar{n}_o + (\frac{m}{n'} - 1)\dot{\omega}_o} = \frac{n'}{n} \quad (90)$$

Since the rates of pericentre precession $\dot{\omega}_i$ and $\dot{\omega}_o$ are small compared to the mean motions, we require approximately

$$\frac{\bar{n}_i}{\bar{n}_o} = \frac{n'}{n} \quad (91)$$

Thus, the harmonic angle is slowly varying if there is an integer ratio (since n and n' are integer coefficients in a Fourier series) between the mean motions of the inner and outer orbits, or equivalently, there is an integer ratio between the periods since $n = 2\pi/P$. If this requirement is satisfied, we say that the mean motions are *commensurate*. If eq. (90) is satisfied we say that the system is in an $n' : n$ *mean motion resonance*. The difference $n' - n$ is called the *resonance order*. The effect of the precession of pericentres is to shift the location of a mean motion resonance (MMR for short) from an exact mean motion commensurability.

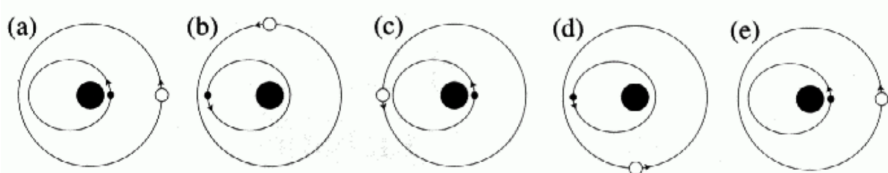


Figure 12: The relative positions of Jupiter (white circle) and an asteroid (small filled circle) in a 2 : 1 mean motion resonance. Figure taken from Murray and Dermott (1999).

An MMR is best understood by considering the geometry of the orbits. Figure 12 shows an example of a 2 : 1 mean motion resonance of Jupiter with an inner asteroid. If both bodies start at $\omega_i = \omega_o = 0$ in *conjunction*⁹ (panel (a) in fig. 12) and we neglect the pericentre precession, they will experience a conjunction again once the asteroid has gone twice around its orbit (panel (d) in fig. 12). Conjunctions happen independently of whether or not there is a resonant relationship

⁹ A conjunction is defined by $\lambda_i = \lambda_o$

between the mean motion, the crucial point is that in the case of an MMR, the conjunctions happen *at the same position on the orbit*. Another aspect of MMRs is visible in fig. 12, if one of the bodies starts at apocentre and the other at pericentre, the conjunctions – points of closest approach, always happen when the bodies are as far away from each other as possible. Thus, the effect of the 2 : 1 MMR in this case is to prevent close encounters and the resonance acts as a stabilizing agent. Conversely, if bodies started at pericentre the conjunctions would happen at a point where the two orbits are closest to each other and the resonance would act to destabilize the system via close encounters between the bodies. We see that capture into MMR can be either beneficial or destructive for a planetary system, the exact outcome depending on the geometry of the orbits at the point of resonant capture.

In the case when the pericentre precession cannot be neglected the picture is somewhat more complicated, the conjunctions occur at the almost same relative position in the two orbits, but not necessarily also at the same position in inertial space.

A consequence of eqs. (71) and (72) defining the Hansen coefficients is that the combined power exponent of the inner and outer eccentricities grows with the resonance order. The eccentricity dependence for a given term in the disturbing function is of the form $\mathcal{O}(e_i^{|m-n|} e_o^{|m-n'|})$. The combined exponent is then

$$|m - n| + |m - n'| = \begin{cases} n' - n, & n \leq m \leq n' \\ |2m - n - n'|, & \text{otherwise} \end{cases} \quad (92)$$

The term in the disturbing function expansion corresponding to a specific $n' : n$ MMR with the lowest combined order in eccentricity is the one with $n \leq m \leq n'$ and its combined exponent is equal to the resonance order. Thus, we have the result that the higher the resonance order of a particular MMR, the ‘stronger’ is the corresponding dominant term in the disturbing function expansion. Mardling, 2013 refers to the resonant terms which satisfy eq. (92) as the *principal resonances* or *principal harmonics* of an $n' : n$ MMR. For example, for the 2 : 1 MMR there are two principal resonances with harmonic angles $\phi_{112} = \lambda_i - 2\lambda_o + \omega_o$ and $\phi_{212} = \lambda_i - 2\lambda_o + \omega_i$.

From eq. (75) it follows that $\mathcal{R}_{mnn'} = \mathcal{O}(\alpha^m)$, $m \geq 2$, $\mathcal{R}_{0nn'} = \mathcal{O}(\alpha^2)$ and $\mathcal{R}_{1nn'} = \mathcal{O}(\alpha^3)$. Thus, unless $e_o \ll e_i$, the principal resonance with $m = n$ provides the largest contribution to the disturbing function, unless $n = 1$, in which case the $m = 2$ harmonic gives the largest contribution.

2.4.3.1 Resonance widths

In general, the harmonic angle $\phi_{mnn'}$ will circulate in a manner similar to that of a pendulum, unless the system is sufficiently close to a

period commensurability in which case it can librate. The harmonic angle can librate even if the system is not at exact resonance because the orbits exchange energy and the period ratio changes slightly after every outer orbit. If $\phi_{mn\bar{n}}$ is librating then $\oint \cos \phi_{mn\bar{n}} d\phi_{mn\bar{n}} \neq 0$ where the integral is taken over one libration cycle. A natural question to ask then is just how close to a period commensurability we have to be in order for a specific harmonic angle to start librating. This is referred to as the *resonance width*. Just as in the case of a pendulum described in section 2.3, the libration period depends on the distance from the border between the libration region and the circulation region, i.e., the separatrix.

In order to calculate the resonance width, Mardling (2013) derives a pendulum like differential equation for the harmonic angle $\phi_{mn\bar{n}}$. Given a pendulum equation it is straightforward to calculate the dimensionless width of the resonance in units of period ratio.

Assuming $\dot{\omega}_i \ll n_o$ and $\dot{\omega}_i \ll n_o$, eq. (89) is approximately

$$\dot{\phi}_{mn\bar{n}} = nn_i - n'n_o \quad (93)$$

Consider the case of an $N : 1$ resonant term with $m = 2$ (the dominant term for an $N : 1$ principal resonance. We want to derive an equation of the form

$$\dot{\phi}_N = -\omega_N^2 \sin \phi_N \quad (94)$$

where $\phi_N \equiv \phi_N$ is determined by the parameters of the system. Once we know ϕ_N we can determine the libration criterion from the equation of the pendulum separatrix

$$\dot{\phi}_N = \pm 2\omega_N \cos \left(\frac{\phi_N}{2} \right) \quad (95)$$

Libration occurs if $\dot{\phi}_N < 2\omega_N$. We start by rewriting eq. (93) as

$$\ddot{\phi}_N = n_o \left(\frac{n_i \dot{n}_o}{n_o n_i} - N \frac{\dot{n}_o}{n_o} \right) = -\frac{3}{2} n_o \left(\frac{n_i \dot{a}_i}{n_o a_i} - N \frac{\dot{a}_o}{a_o} \right) \quad (96)$$

where we have used Kepler's third law to replace the mean motions with semi-major axes. We can then use Lagrange's planetary equations together with the dominant disturbing function term for $N : 1$ resonance to calculate \dot{a}_i and \dot{a}_o . The result is

$$\begin{aligned} \ddot{\phi}_N &= -\omega_N^2 \sin \phi_N \\ &= \frac{9}{4} n_o^2 \left[\frac{m_3}{m_{123}} + N^{2/3} \left(\frac{m_{12}}{m_{123}} \right)^{2/3} \left(\frac{m_1 m_2}{m_{12}^2} \right) \right] X_1^{2,2}(e_i) X_N^{-3,2}(e_o) \sin \phi_N \end{aligned} \quad (97)$$

The harmonic angle ϕ_N librates around 0 because $X_1^{2,2}(e_i) < 0$ and $X_N^{-3,2}(e_o) > 0$ for all e_i and e_o and thus there is a minus sign in

front of ω_N^2 . If it weren't for the minus sign, the angle would librate around π Mardling (2013). The libration condition is then

$$\dot{\phi}_N = n_o \left(\frac{n_i}{n_o} - N \right) < 2\omega_N \quad (98)$$

Thus, the distance from resonance N in units of inner mean motion within which the harmonic angle is librating is given by

$$\begin{aligned} \sigma &= \frac{n_i}{n_o} - N = \frac{2\omega_n}{n_o} \\ &= 3 \left[\frac{m_3}{m_{123}} + N^{2/3} \left(\frac{m_{12}}{m_{123}} \right)^{2/3} \left(\frac{m_1 m_2}{m_{12}^2} \right) \right]^{1/2} \sqrt{x_1^{2,2}(e_i) X_N^{-3,2}(e_o)} \end{aligned} \quad (99)$$

where σ is the dimensionless distance from resonance.

The Hansen coefficients can be calculated to arbitrary order using a series expansion of the integrals 71 and 72. One can show that $\lim_{e_o \rightarrow 0} \sigma = 0$ for $N \geq 3$, that is, the widths of high N resonances are only significant if e_o is not very small. We also have $\lim_{e_i \rightarrow 0} \sigma = 0$ which implies that the resonance widths become infinitely narrow for circular inner orbits. However, the situation when $e_i = 0$ is physically unrealistic since some eccentricity is always induced secularly (see section 2.4.2). We will use eq. (99) in chapter 4 together with numerical techniques to predict the stability of circumbinary systems.

So far, we have managed the disentangle the three body problem by expanding the interaction potential term in a Fourier series and classifying the behaviour of different terms in the expansions. We have defined what it means for a system to be in a mean motion resonance and derived a useful expression which enables us to calculate the location of the regions of instability due to resonance overlap. However, we haven't mentioned how the system got into resonance in the first place.

The main subject of this thesis is what happens during *resonance passage* as n_i/n_o grows due to tidal decay of the stellar binary. In order to describe the physics behind resonant passage, we need to use Hamiltonian mechanics from section 2.2. Ideally, we would like to have a single degree of freedom Hamiltonian which describes the passage of whichever resonance is important for CB planets. In the next section we will show that it is always possible to construct such Hamiltonian by considering a single dominant resonant term in the disturbing function. Considering more than one terms at the time usually leads to a Hamiltonian with more degrees of freedom.

2.5 THE SMALL DIVISOR PROBLEM

We have mentioned that in order to study resonance capture, we have to reduce the Hamiltonian 60 to a single degree of freedom, which can

only be done if we isolate a single resonant term. How do we know that by considering a single dominant term we can still capture the major aspects of the dynamics of resonance passage? Certainly this assumption has to fail if the system is in a region of resonance overlap. We can make this approximation more rigorous in the following way.

Consider a Hamiltonian of the form

$$\mathcal{H}(\mathbf{J}, \boldsymbol{\theta}) = \mathcal{H}_0(\mathbf{J}) + \epsilon \cos(\mathbf{k} \cdot \boldsymbol{\theta}) \quad (100)$$

where ϵ is a small parameter, $(\mathbf{J}, \boldsymbol{\theta})$ for a conjugate pair of variables where \mathbf{J} is the momentum vector and $\boldsymbol{\theta}$ is the coordinate vector, \mathbf{k} is a vector whose elements are integers. This Hamiltonian has the form of eq. (60) where we have isolated a particular term in \mathcal{R} . We transform the coordinates by means of a canonical transformation $(\mathbf{J}, \boldsymbol{\theta}) \rightarrow (\mathbf{I}, \boldsymbol{\theta}')$ generated by

$$F_2(\boldsymbol{\theta}, \mathbf{I}) = \mathbf{I} \cdot \boldsymbol{\theta} - \frac{\epsilon}{\mathbf{k} \cdot \boldsymbol{\omega}} \sin(\mathbf{k} \cdot \boldsymbol{\theta}) \quad (101)$$

Where $\boldsymbol{\omega}$ is just an unknown vector at this point. Table 3 then give the relations between new and old coordinates

$$\frac{\partial F_2}{\partial \mathbf{I}} = \boldsymbol{\theta} = \boldsymbol{\theta}' \quad (102)$$

$$\frac{\partial F_2}{\partial \boldsymbol{\theta}} = \mathbf{I} - \frac{\epsilon \mathbf{k}}{\mathbf{k} \cdot \boldsymbol{\omega}} \cos(\mathbf{k} \cdot \boldsymbol{\theta}) = \mathbf{J} \quad (103)$$

Inserting the new coordinates in eq. (100), we we have

$$\mathcal{H}(\mathbf{I}, \boldsymbol{\theta}') = \mathcal{H}_0 \left(\mathbf{I} - \frac{\epsilon \mathbf{k}}{\mathbf{k} \cdot \boldsymbol{\omega}} \cos(\mathbf{k} \cdot \boldsymbol{\theta}') \right) + \epsilon \cos(\mathbf{k} \cdot \boldsymbol{\theta}') \quad (104)$$

If we expand \mathcal{H}_0 to first order in the small parameter ϵ , we have

$$\mathcal{H}(\mathbf{I}, \boldsymbol{\theta}') = \mathcal{H}_0(\mathbf{I}) - \frac{\epsilon \nabla \mathcal{H}_0(\mathbf{I}) \cdot \mathbf{k}}{\mathbf{k} \cdot \boldsymbol{\omega}} \cos(\mathbf{k} \cdot \boldsymbol{\theta}') + \epsilon \cos(\mathbf{k} \cdot \boldsymbol{\theta}') \quad (105)$$

If we take $\boldsymbol{\omega}$ to be equal to $\nabla \mathcal{H}_0(\mathbf{I})$ the $\epsilon \cos(\mathbf{k} \cdot \boldsymbol{\theta}')$ term is cancelled. Note that if $\nabla \mathcal{H}_0(\mathbf{I})$, it is a function of \mathbf{I} and we should have taken that into account when taking the derivative of F_2 , however, to first order in ϵ , the transformation is correct.

Here we have considered only a cosine term but the procedure is equally valid for any number of terms since their general form is the same. The procedure relies crucially on the last step in which we expand \mathcal{H}_0 around \mathbf{I} which is only allowed if $\mathbf{k} \cdot \boldsymbol{\omega}$ is not small (since ϵ is small). If however $\mathbf{k} \cdot \boldsymbol{\omega}$ is small which happens if the perturbation term is commensurate, the expansion fails because the new momenta are not close to the old ones. This is known as the *small divisor problem*. Thus, any attempt to remove a commensurate term in the disturbing function by means of a canonical transformation fails. Any non-commensurate term however, can be consistently removed.

Therefore, as long a single resonant term in the disturbing function dominates, and all the other terms are non-commensurate, we can consider only a single term in Hamiltonian 6o. It remains to show that such a Hamiltonian can then be reduced to a single degree of freedom.

3

AN ANALYTICAL MODEL OF RESONANT ECCENTRICITY EXCITATION

In this chapter I develop a new analytical model of a 6:1 resonance in the case where the inner two bodies are comparable in mass. The 6:1 MMR is the first important resonance encountered by CB planets similar to the observed MS population once the binary starts evolving off the main-sequence. I use this model to predict the eccentricity kick to a planet orbiting the evolving binary as the stars approach each other due to tidal forces.

3.1 THE 6:1 MEAN MOTION RESONANCE

After reviewing the theory required for studying resonant capture in the framework of a three-body problem with arbitrary mass ratios, we turn to the construction of a one dimensional Hamiltonian for a particular mean motion resonance relevant to CB planets. The question is, which resonances are relevant?

Looking at the CB planets orbiting main-sequence stars, we see that all of them are located outside of the 5 : 1 MMR with the stellar binary. This is due to the fact that the inner regions in period space are mostly unstable because of resonance overlap as will be shown in chapter 4. Thus, as the stellar binary evolves and the period ratio $P_o/P_i = n_i/n_o$ grows, the first major resonance that will be encountered is the 6 : 1 resonance, which is 5th order. More distant resonances such as 7 : 1 and 8 : 1 might be important as well, however, since resonance ‘strength’ drops off with resonance order, their effects will be less important (see eq. (92)).

A 6 : 1 MMR is defined by the labels $n' = 6$, $n = 1$ in the disturbing function expansion in eq. (73). Table 4 lists all of the harmonic angles associated with the principal harmonics of a 6 : 1 MMR together with the leading order of the harmonic coefficient in the semi-major axis ratio α and the inner and outer eccentricities. As expected, the sum of the exponent powers of e_i and e_o is equal to 5 which is the order of the resonance.

In general we would have to consider all of the angles in table 4 because near a 6 : 1 commensurability they will all librate and it is not possible to remove them via a canonical transformation because of the small divisor problem described in section 2.5. There is however a single harmonic angle associated with the dominant term, the one with $m = 2$, its harmonic coefficient is proportional to α^2 while all the other harmonic coefficients are higher order in α . The difference

Harmonic angle $\phi_{mnn'}$	Leading order of $\mathcal{R}_{mnn'}$
$\phi_{116} = \lambda_i - 6\lambda_o + 5\omega_o$	$\mathcal{O}(\alpha^3, e_i^0, e_o^5)$
$\phi_{216} = \lambda_i - 6\lambda_o + \omega_i + 4\omega_o$	$\mathcal{O}(\alpha^2, e_i^1, e_o^4)$
$\phi_{316} = \lambda_i - 6\lambda_o + 2\omega_i + 3\omega_o$	$\mathcal{O}(\alpha^3, e_i^2, e_o^3)$
$\phi_{416} = \lambda_i - 6\lambda_o + 3\omega_i + 2\omega_o$	$\mathcal{O}(\alpha^4, e_i^3, e_o^2)$
$\phi_{516} = \lambda_i - 6\lambda_o + 4\omega_i + \omega_o$	$\mathcal{O}(\alpha^5, e_i^4, e_o^1)$
$\phi_{616} = \lambda_i - 6\lambda_o + 5\omega_i$	$\mathcal{O}(\alpha^6, e_i^5, e_o^0)$

Table 4: Harmonic angles associated with the principal harmonics of a $6 : 1$ mean motion resonance (those with $n \leq m \leq n'$).

between the dominant term and the next one is of order $\mathcal{O}(\alpha)$ in absolute value. For a $6 : 1$ resonance, $\alpha = a_i/a_o \approx 6^{-2/3} = 0.3$, discarding the other terms is thus not an ideal approximation but it is one we have to make in order to obtain an integrable Hamiltonian.

After isolating only the $\mathcal{R} = \mathcal{R}_{216} \cos \phi_{216}$ term in the disturbing function, the Hamiltonian 6o becomes

$$\mathcal{H} = \mathcal{H}_k + \mathcal{R} \quad (106)$$

where

$$\mathcal{H}_k = \mathcal{H}_i + \mathcal{H}_o = -G \frac{m_1 m_2}{a_i} - G \frac{m_{12} m_3}{a_o} \quad (107)$$

is the Keplerian part of the Hamiltonian which depends only on the semi-major axes and

$$\mathcal{R} = \frac{3}{4} \frac{G \mu_i m_3}{a_o} \left(\frac{a_i}{a_o} \right)^2 X_1^{2,2}(e_i) X_6^{-3,2}(e_o) \cos(\lambda_i - 6\lambda_o + \omega_i + 4\omega_o) \quad (108)$$

is the single resonant disturbing function term. The Hamiltonian 106 is written in terms of the orbital elements (λ, a, e, ω) which do not form a canonically conjugate set of variables. We choose to rewrite the Hamiltonian in so called *Poincaré variables* which are often used in Celestial mechanics and do form a canonically conjugate set of variables. The Poincaré variables are defined in terms of the orbital elements as

$$\begin{aligned} \lambda_i &= \lambda_i & \Lambda_i &= \mu_i \sqrt{G m_{12}} a_i \\ \gamma_i &= -\omega_i & \Gamma_i &= \mu_i \sqrt{G m_{12} a_i} \left(1 - \sqrt{1 - e_i^2} \right) \end{aligned} \quad (109)$$

and similarly for the outer orbit with $m_{12} \rightarrow m_{123}$ and the index o for the orbital elements. Remembering eq. (28) for the angular momentum of a Keplerian orbit, we see that the Poincaré Lambdas correspond to the angular momentum for a circular outer and inner orbit respectively. The Gammas are then the differences between two-body

angular momenta for a circular and elliptical orbit¹. We can then solve the system 109 for the orbital elements in terms of Poincaré variables, the result is

$$\begin{aligned} a_i &= \frac{\Lambda_i^2}{G\mu_i^2 m_{12}} \\ e_i &= \frac{1}{\Lambda_i} \sqrt{\Lambda_i^2 - (\Gamma_i - \Lambda_i)^2} \\ \omega_i &= -\gamma_i \end{aligned} \tag{110}$$

and again similarly for the outer orbital elements. We have taken the positive root of e_i since eccentricity is defined to be positive. The Hamiltonian 106 expressed in terms of the new variables is then

$$\begin{aligned} \mathcal{H} = & -G^2 \frac{\mu_i^3 m_{12}^2}{2\Lambda_i^2} - G^2 \frac{\mu_o^3 m_{123}^2}{2\Lambda_o^2} \\ & - \frac{3}{4} G^2 \frac{\mu_o^6}{\mu_i^3} \frac{m_{123}^3 m_3}{m_{12}^2} \frac{1}{\Lambda_o^2} \left(\frac{\Lambda_i}{\Lambda_o} \right)^4 X_1^{2,2}(\Lambda_i) X_6^{-3,2}(\Lambda_o) \cos(\lambda_i - 6\lambda_o - \gamma_i - 4\gamma_o) \end{aligned} \tag{111}$$

We can simplify the Hamiltonian 111 by changing to dimensionless units. This is achieved by scaling all masses, lengths and time by a constant factor, as follows

$$\hat{m} = \frac{m}{m'} \quad \hat{a} = \frac{a}{a'} \quad \hat{t} = \frac{t}{t'} \tag{112}$$

where m stands for any quantity with the dimension of mass in eq. (111) and a stands for any quantity with the dimension of length. Time is not present explicitly in eq. (111). The hats denote the fact that the new variables are dimensionless. Plugging in the rescaled variables in the Hamiltonian (and taking out G , which has dimensions, from the definition of the Poincaré momenta) we obtain a Hamiltonian of the form

$$\mathcal{H} = \frac{Gm'^2}{a'} \hat{\mathcal{H}} \tag{113}$$

where $\hat{\mathcal{H}}$ is now dimensionless and exactly the same as eq. (111) except with G factored out and all variables with a physical dimension given hats. The factor Gm'^2/a' has dimensions of energy (as it should) and we can multiply the Hamiltonian \mathcal{H} by its inverse to obtain a dimensionless Hamiltonian. Multiplying any Hamiltonian by a

¹ In secular interactions the sum of all Γ elements of the system is called the *angular momentum deficit* (AMD). It is a conserved quantity because the semi-major axes are constant and the total angular momentum is conserved. Laskar (1997) has shown that the Solar System is AMD unstable in the sense that if say all planets except, say, Venus attained maximum angular momentum (corresponding to a circular orbit), Venus's eccentricity would increase enough for crossing orbits to occur.

constant factor is equivalent to rescaling the time by that same factor². We then choose the scaling factors which give the simplest Hamiltonian, a natural choice is $m' = m_{12}$ as a unit of mass, \tilde{a}_i (the reason for the use of \sim will become clear in the next paragraph) as a unit of semi-major axis, and $1/n_i$ as a unit of time. Thus we can set everywhere $m_{12} = \tilde{a}_i = \tilde{a}_o = 1$. The dimensionless Hamiltonian is then given by

$$\begin{aligned}\mathcal{H} = & -\frac{\mu_i^3}{2\Lambda_i^2} - \frac{\mu_o^3}{2\Lambda_o^2} \\ & - \frac{3}{4} \frac{\mu_o^6}{\mu_i^3} \frac{m_3}{\Lambda_o^2} \left(\frac{\Lambda_i}{\Lambda_o} \right)^4 X_1^{2,2}(\Gamma_i) X_6^{-3,2}(\Gamma_o) \cos(\lambda_i - 6\lambda_o - \gamma_i - 4\gamma_o)\end{aligned}\quad (114)$$

where we have omitted all the hats for clarity and we have used the approximation $m_{123} \approx m_{12}$, since the most massive planets we will be considering are $m_3 \approx 10^{-3}m_{12}$ which is negligible.

In order to reduce the Hamiltonian 114, to a form which resembles that of the pendulum, we have to expand it in a Taylor series around a location of an exact resonance. Since we are interested in the dynamics in the vicinity of the resonance, this is a valid expansion. We choose to expand the Keplerian part to *second order* and the resonant term to *zeroth order* around $\Lambda_i = \tilde{\Lambda}_i$ and $\Lambda_o = \tilde{\Lambda}_o$, where 'tilde' denotes Poincaré momenta evaluated at exact resonance³

$$\begin{aligned}\tilde{\Lambda}_i &= m_1 m_2 \sqrt{\tilde{a}_i / \tilde{a}_i} = m_1 m_2 = \mu_i \\ \tilde{\Lambda}_o &= \mu_o \sqrt{\tilde{a}_o / \tilde{a}_i} = 6^{1/3} \mu_o\end{aligned}\quad (115)$$

where we have used Kepler's third law to evaluate the outer semi-major axis at the location of 6 : 1 MMR. The Hamiltonian 114 becomes

$$\begin{aligned}\mathcal{H} = & \frac{\mu_i^3}{2\tilde{\Lambda}_i^3} (\Lambda_i - \tilde{\Lambda}_i) - \frac{3}{2} \frac{\mu_i^3}{\tilde{\Lambda}_i^4} (\Lambda_i - \tilde{\Lambda}_i)^2 + \frac{\mu_o^3}{2\tilde{\Lambda}_o^3} (\Lambda_o - \tilde{\Lambda}_o) - \frac{3}{2} \frac{\mu_o^3}{\tilde{\Lambda}_o^4} (\Lambda_o - \tilde{\Lambda}_o)^2 \\ & - \frac{3}{4} \frac{\mu_o^6}{\mu_i^3} \frac{m_3}{\tilde{\Lambda}_o^2} \left(\frac{\tilde{\Lambda}_i}{\tilde{\Lambda}_o} \right)^4 X_1^{2,2}(\Gamma_i) X_6^{-3,2}(\Gamma_o) \cos(\lambda_i - 6\lambda_o - \gamma_i - 4\gamma_o)\end{aligned}\quad (116)$$

where we have ignored constant terms because Hamilton's equations are invariant to an addition of a constant to the Hamiltonian. We

² This follows from Hamilton's equations. Since $\frac{\partial}{\partial p}(a\mathcal{H}) = \frac{dq}{dt}$ where a is some constant, it follows that $\frac{\partial \mathcal{H}}{\partial p} = \frac{dq}{d(at)}$.

³ There is a subtlety here concerning the definition of Γ_i and Γ_o which is worth pointing out. After expanding the resonant term about the resonance location to zeroth order in $\tilde{\Lambda}_i$ and $\tilde{\Lambda}_o$, we also choose to neglect the variation of a_i and a_o in Γ_i and Γ_o because it is negligible in the resonant term. We thus have $\Gamma_i = \tilde{\Lambda}_i \left(1 - \sqrt{1 - e_i^2} \right)$ and $\Gamma_o = \tilde{\Lambda}_o \left(1 - \sqrt{1 - e_o^2} \right)$.

then define new momenta $J_i = \Lambda_i - \tilde{\Lambda}_i$ and $J_o = \Lambda_o - \tilde{\Lambda}_o$ which are shifted from Λ_i and Λ_o by a constant (it is easy to check that the canonical form is preserved).

Finally, we turn to the Hansen coefficients which we have kept in symbolic form so far. There are no closed-form solutions for the integrals eqs. (71) and (72) which define the coefficients. It is however possible to obtain a series solution in eccentricities using a computer algebra system. Mardling, 2013 provides Wolfram Mathematica (*Mathematica, Version 11.1*) code for a series solution in eccentricities. The integral for the inner Hansen coefficient is given by eq. (71) as

$$X_1^{2,2}(e_i) = \frac{1}{2\pi} \int_0^{2\pi} (1 - e_i \cos E_i)^{1+1} [\cos(mf_i) + i \sin(mf_i)] [\cos(nM_i) - i \sin(nM_i)] dE_i \quad (117)$$

where we have used the relation $(r/a_i) = 1 - e_i \cos E_i$ and wrote the exponentials in complex number form by using the Euler's identity. We do the same with $X_6^{-3,2}(e_o)$. Next, we replace the trigonometric terms and the mean anomaly by using eqs. (24) and (25). Finally, we expand the integrand in the inner coefficient in a Taylor series around e_i , and similarly around e_o for the outer coefficient.

We can only use the lowest order approximation for the Hansen coefficients accurate to order $\mathcal{O}(e_i^3, e_o^6)$, otherwise the Hamiltonian becomes too complicated later on. In order to establish the domain of validity of this approximation, we plot the Hansen coefficients as functions of eccentricity. Figure 13 shows that the first order approximation is valid up to about $e_i \leq 3$ for the inner eccentricity, and $e_o \leq 0.4$ for the outer. This is a fairly limiting assumption, however, the majority of the observe circumbinary systems are comfortably in the low eccentricity regime so it remains justified. Finally, after con-

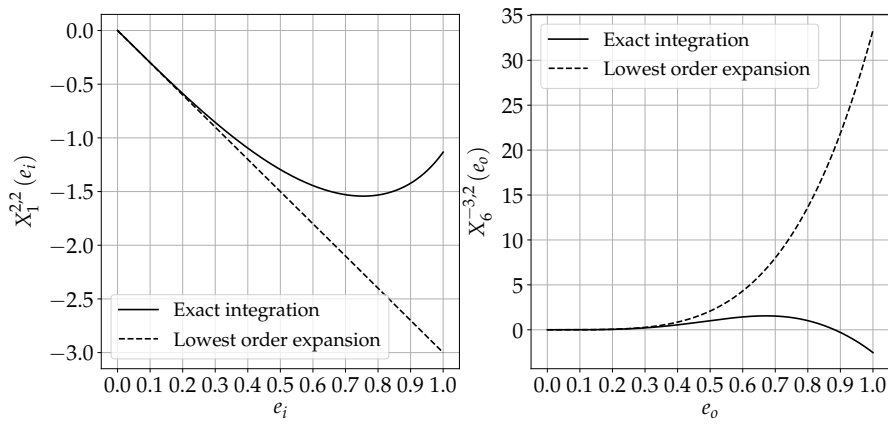


Figure 13: Lowest order expansion term for the Hansen coefficients (dashed curves) compared to exact integration.

verting the series approximation to Poincaré momenta, the Hamiltonian 114 becomes

$$\begin{aligned}\mathcal{H} = & \frac{\mu_i^3}{2\tilde{\lambda}_i^3}J_i - \frac{3}{2}\frac{\mu_i^3}{\tilde{\lambda}_i^4}J_i^2 + \frac{\mu_o^3}{2\tilde{\lambda}_o^3} + J_o - \frac{3}{2}\frac{\mu_o^3}{\tilde{\lambda}_o^4}J_o^2 \\ & + \frac{4797\sqrt{2}}{16}m_3\frac{\mu_o^6}{\mu_i^3}\frac{\tilde{\lambda}_i^{\frac{7}{2}}}{\tilde{\lambda}_o^8}\sqrt{\Gamma_i\Gamma_o^2}\cos(\lambda_i - 6\lambda_o + -\gamma_i - 4\gamma_o)\end{aligned}\quad (118)$$

3.2 REDUCTION TO A SINGLE DEGREE OF FREEDOM

The Hamiltonian 116 has four degrees of freedom. We would like to find a canonical transformation which reduces the number of degrees of freedom to one. It is known from one of the first Hamiltonian models of resonance (Henrard and Lemaître, 1983) that a suitable canonical transformation has the harmonic angle as a position coordinate. Inspired by this fact, we choose a canonical transformation to coordinates $(\theta_1, \theta_2, \theta_3, \theta_4; \Theta_1, \Theta_2, \Theta_3, \Theta_4)$ generated by

$$F_2 = -(\lambda_i - 6\lambda_o - \gamma_i - 4\gamma_o)\Theta_1 + \lambda_i\Theta_2 + \lambda_o\Theta_3 + \gamma_i\Theta_4 \quad (119)$$

From table 3, it follows that

$$\begin{aligned}J_1 &= \frac{\partial F_2}{\partial \lambda_i} = -\Theta_1 + \Theta_2 & \theta_1 &= \frac{\partial F_2}{\partial \Theta_1} = -(\lambda_i - 6\lambda_o - \gamma_i - 4\gamma_o) \\ J_2 &= \frac{\partial F_2}{\partial \lambda_o} = 6\Theta_1 + \Theta_3 & \theta_2 &= \frac{\partial F_2}{\partial \Theta_2} = \lambda_i \\ \Gamma_i &= \frac{\partial F_2}{\partial \gamma_i} = \Theta_1 + \Theta_4 & \theta_3 &= \frac{\partial F_2}{\partial \Theta_3} = \lambda_o \\ \Gamma_o &= \frac{\partial F_2}{\partial \gamma_o} = 4\Theta_1 & \theta_4 &= \frac{\partial F_2}{\partial \Theta_4} = \gamma_i\end{aligned}\quad (120)$$

We can then easily solve for the new momenta in terms of old momenta

$$\begin{aligned}\Theta_1 &= \frac{1}{4}\Gamma_o \\ \Theta_2 &= J_1 + \frac{1}{4}\Gamma_o \\ \Theta_3 &= J_2 - \frac{3}{2}\Gamma_o \\ \Theta_4 &= \Gamma_i - \frac{1}{4}\Gamma_o\end{aligned}\quad (121)$$

and the Hamiltonian expressed in terms of the new coordinates is

$$\begin{aligned}\mathcal{H} = & \left(-\frac{3 \cdot 6^{2/3}}{2m_3} - \frac{3}{2\mu_i}\right)\Theta^2 + \left(\frac{3\Theta_2}{\mu_i} - \sqrt[3]{\frac{9}{2}\frac{\Theta_3}{m_3}}\right)\Theta \\ & + \frac{533 \cdot 2^{5/6}\sqrt[3]{3}}{24}\frac{\sqrt{\mu_i}}{m_3}\Theta^2\sqrt{\Theta + \Theta_4}\cos(\theta)\end{aligned}\quad (122)$$

Where we have taken $\theta_1 \equiv \theta$ and $\Theta_1 \equiv \Theta$. The resulting Hamiltonian depends only on one coordinate θ with Θ its momentum conjugate and is therefore a fully integrable single degree of freedom Hamiltonian. From Hamilton's equations, it follows that $\dot{\Theta}_2 = \dot{\Theta}_3 = \dot{\Theta}_4 = 0$, that is, Θ_1, Θ_2 and Θ_3 are constants of motion.

The Hamiltonian 122 depends on many parameters which are constants, we wish to reduce the number of parameters to a smallest set of linearly independent parameters. We proceed by rewriting eq. (122) as

$$\mathcal{H} = \alpha\Theta^2 + \beta\Theta + \epsilon\Theta^2\sqrt{\Theta + \Theta_4}\cos\theta \quad (123)$$

where

$$\begin{aligned} \alpha &= -\frac{3 \cdot 6^{2/3}}{2m_3} - \frac{3}{2\mu_i} \\ \beta &= \frac{3\Theta_2}{\mu_i} - \sqrt[3]{\frac{9}{2}\frac{\Theta_3}{m_3}} \\ \epsilon &= \frac{533 \cdot 2^{5/6} \sqrt[3]{3}}{24} \frac{\sqrt{\mu_i}}{m_3} \end{aligned} \quad (124)$$

α and ϵ depend purely on the mass ratios $\mu_i = m_1 m_2$ and m_3 , the ϵ parameter depends on Θ_2 and Θ_3 which in turn depend on the distance to the resonance. In order to further reduce the number of parameters, we scale the momentum Θ by means of a simple scale transformation $\Theta \rightarrow \eta\Theta$, where η is a constant factor to be determined; remembering that we also have to scale time by the same factor. Hamiltonian 123 becomes

$$\mathcal{H} = \eta^2\alpha\Theta^2 + \eta\beta\Theta + \eta^{5/2}\epsilon\Theta^2\sqrt{\Theta + \frac{\Theta_4}{\eta}}\cos\theta \quad (125)$$

We then choose the scaling parameter η such that the coefficients in front of the first and the last term become equal, that is, we require that

$$\eta^2\alpha = \eta^{5/2}\epsilon \quad (126)$$

It follows that

$$\eta = \left(\frac{\alpha}{\epsilon}\right)^2 \quad (127)$$

and the Hamiltonian is

$$\mathcal{H} = \frac{\alpha^5}{\epsilon^4}\Theta^2 + \beta\frac{\alpha^2}{\epsilon^2}\Theta + \frac{\alpha^5}{\epsilon^4}\Theta^2\sqrt{\Theta + \frac{\Theta_4}{\eta}}\cos\theta \quad (128)$$

We can now multiply the Hamiltonian by the dimensionless factor $\frac{\epsilon^4}{\alpha^5}$ which corresponds to rescaling the time again. The final Hamiltonian then has the form

$$\mathcal{H} = \Theta^2 - \delta\Theta + \Theta^2\sqrt{\Theta + c}\cos\theta \quad (129)$$

where the two constants δ and c are given by

$$\delta = -\frac{\beta \epsilon^2}{\alpha^3} \quad (130)$$

$$c = \left(\frac{\epsilon}{\alpha}\right)^2 \Theta_4 = \left(\frac{\epsilon}{\alpha}\right)^2 \left(\Gamma_i - \frac{1}{4}\Gamma_o\right) \quad (131)$$

We have thus managed to reduce the $6 : 1$ resonant Hamiltonian to the simplest possible form, a one degree of freedom Hamiltonian with two parameters. We now turn to studying its structure.

3.3 THE RESONANCE STRUCTURE

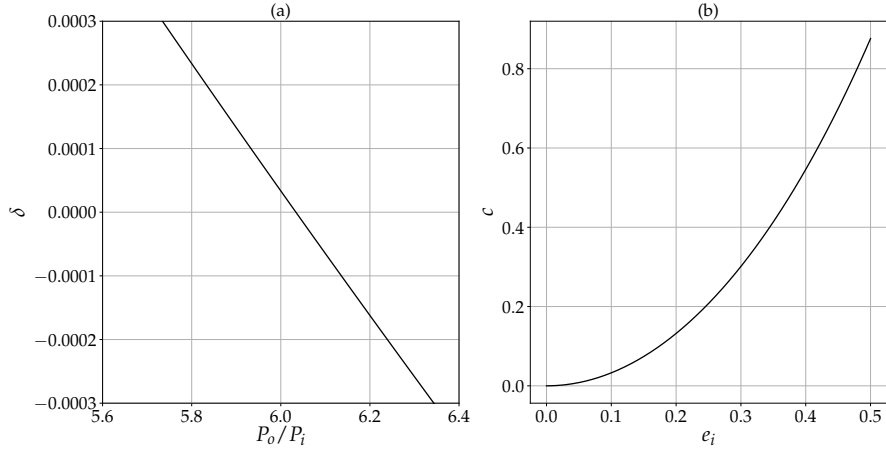


Figure 14: (a) Hamiltonian parameter δ as a function of the period ratio $\mu_i = 0.5$, $m_3 = 10^{-3}$, $e_i = 0.2$, $e_o = 0.05$. (b) Hamiltonian parameter c as a function of the inner eccentricity for $\mu_i = 0.5$, $m_3 = 10^{-3}$, $e_o = 0.05$.

In order to gain insight into the dependence of the two parameters δ and c , we plot them in fig. 14. We see that δ is a measure of proximity to the exact commensurability since it reaches zero at $P_o/P_i \approx 6$. In the case of an evolving circumbinary system, δ monotonically decreases from a positive value to a negative value or equivalently, a changing period ratio can be seen as varying δ . Thus, we can model the passage through the resonance by varying δ .

The c parameter stays constant by definition as the period ratio varies, because the Poincaré momenta Γ_i and Γ_o in eq. (131) are evaluated at exact resonance. More interesting is the dependence of c on the inner eccentricity, shown in panel (b) of fig. 14. We see that $c > 0$ for all e_i and a particular value of e_o . In fact, the plot shown in (b) stays almost exactly the same for all reasonable values of e_o . Negative values of c occur only for extremely small eccentricities which never really occur because some eccentricity is always induced due to secu-

lar interactions. In what follows, we therefore consider only the case $c > 0$ ⁴.

The fixed points of the Hamiltonian are given by Hamilton's equations as

$$\frac{\partial \mathcal{H}}{\partial \Theta} = \frac{\partial \mathcal{H}}{\partial \theta} = 0 \quad (132)$$

We obtain

$$-\Theta^2 \sqrt{\Theta + c} \sin \theta = 0 \quad (133)$$

$$\frac{\Theta^2}{2\sqrt{\Theta + c}} \cos \theta + 2\Theta \sqrt{\Theta + c} + 2\Theta - \delta = 0 \quad (134)$$

The only non trivial solution for the first equation is $\theta = \{0, \pi\}$ for $\theta \in \{0, 2\pi\}$. The second equation then becomes

$$(-1)^s \frac{\Theta^2}{2\sqrt{\Theta + c}} + 2\Theta \sqrt{\Theta + c} 2\Theta - \delta = 0 \quad (135)$$

where $s = \{0, 1\}$. There is no analytic solution for eq. (135), we can gain insight into the possible solution by searching for the roots graphically. We define $R = \sqrt{2\Theta}$ and rewrite eq. (135) as

$$f(\delta, R) = g(R, c) \quad (136)$$

where

$$f(\delta, R) = -\delta + R^2 \quad (137)$$

and

$$g(R, c) = (-1)^s \frac{R^4}{8\sqrt{\frac{1}{2}R^2 + c}} + R^2 \sqrt{\frac{1}{2}R^2 + c} \quad (138)$$

Figure 15 shows a plot of $f(\delta, R)$ and $g(R, c)$ for a fixed value of c . Each solid line corresponds to a different value of delta. The intersections of f and g are the roots of eq. (135). There are two solutions for $\delta > 0$ and no solutions for $\delta < 0$. At $\delta = 0$ and $\Phi = 0$, a double root of eq. (135) either appears or disappears depending on whether zero is approached from above or below. Thus, we conclude that there are two distinct behaviours of the Hamiltonian depending on the sign of δ , $\delta = 0$ is then called a *bifurcation point* of the Hamiltonian.⁵

The properties of Hamiltonian 129 are most easily seen in phase space plots for different values of δ . Instead of (Θ, θ) coordinates,

⁴ For negative c the bifurcation diagram of the Hamiltonian is different and more difficult to handle.

⁵ In the theory of dynamical systems, a bifurcation occurs when a small change in a certain parameter of a system causes a sudden *topological* change in its behaviour.

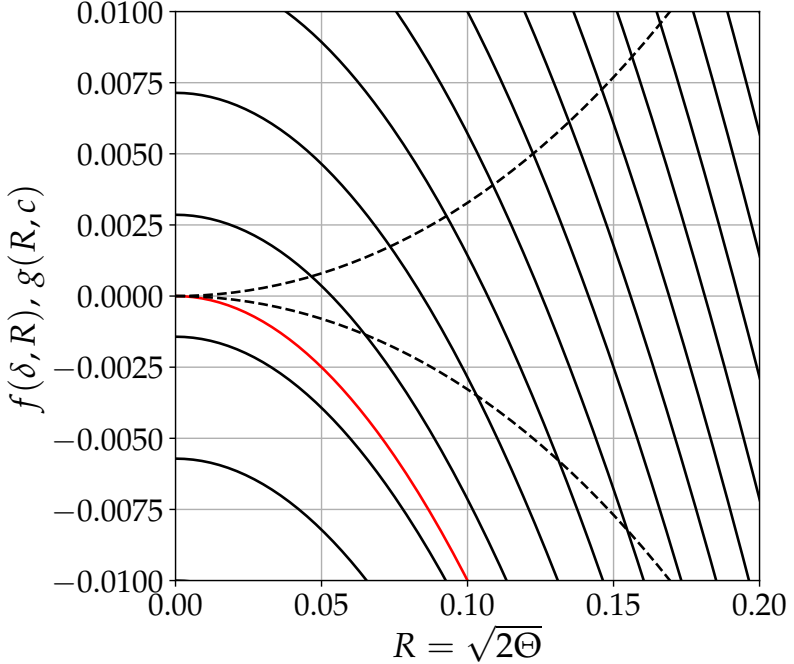


Figure 15: A graphical solution to the equation defining the fixed points of the Hamiltonian 129. The solid lines are plots of $f(\delta, R)$ for various values of δ . The dashed lines are plots of the function $g(R, c)$ for a fixed positive value of $c = 0.1$.

we plot the Hamiltonian in so called Poincaré Cartesian variables, defined as

$$\begin{aligned} x &= \sqrt{2\Theta} \cos \theta \\ y &= \sqrt{2\Theta} \sin \theta \end{aligned} \tag{139}$$

This would be a standard polar to Cartesian transformation were it not for the square roots. The square roots are necessary if the transformation is to be canonical (Ferraz-Mello, 2007), and the factor of 2 is for convenience. The reason we use these coordinates is because the coordinates (θ, Θ) are singular at the origin $\Theta = 0$ since θ becomes ill defined. The Hamiltonian in the new coordinates is then

$$\mathcal{H} = \frac{1}{4} (x^2 + y^2) - \frac{1}{2} \delta (x^2 + y^2) + \frac{1}{8} x (x^2 + y^2)^{3/2} \sqrt{4c + 2x^2 + 2y^2} \tag{140}$$

Because the coordinates (θ, Θ) are ill-defined at the origin, when solving eq. (135) for the fixed points, we missed a third fixed point at the origin. It is easy to see by writing down the Hamilton's equations in (x, y) coordinates that the origin $(0, 0)$ is always a fixed point, independent of the value of δ .

The phase space structure is shown in fig. 16 for three different values of δ . Consider for now the first panel which shows the phase

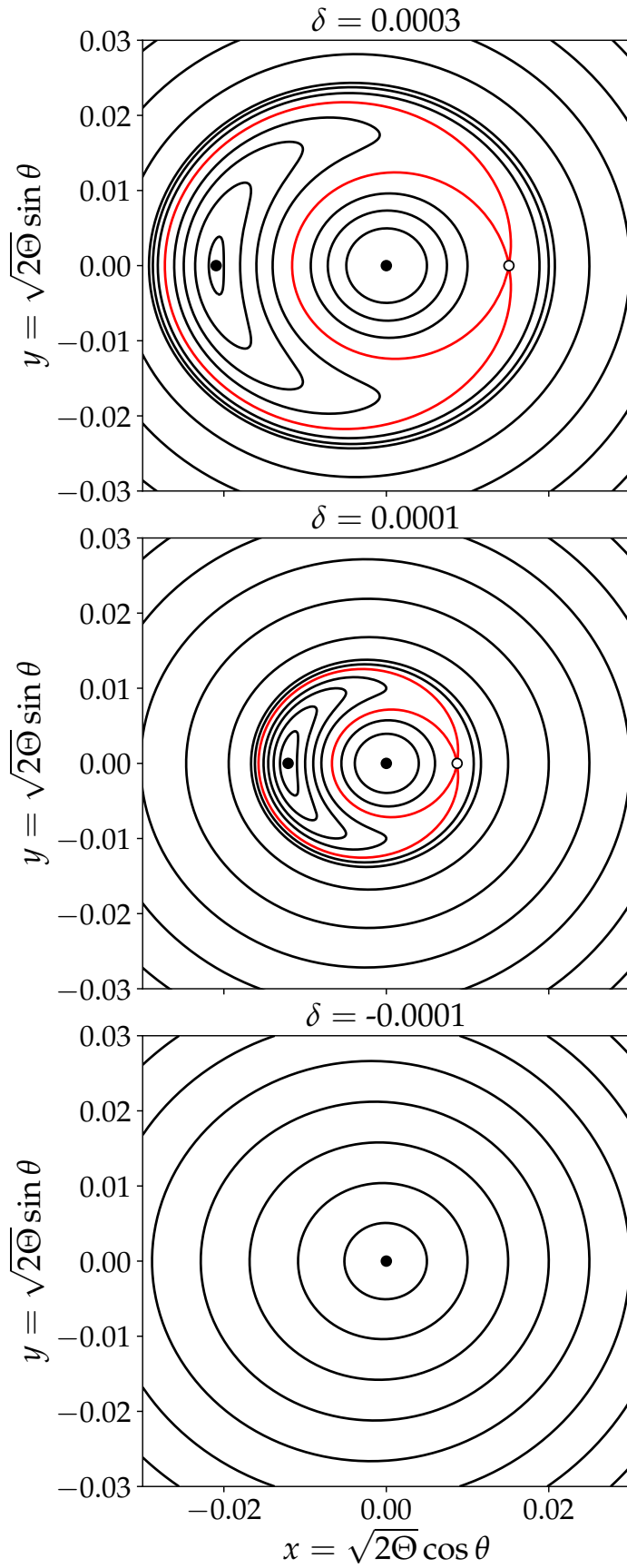


Figure 16: Phase space portraits of the Hamiltonian 140 for different values of δ . The red curve is the separatrix. Filled circles are stable fixed points and the open circle is the unstable saddle point.

space structure for positive δ . Each curve is a constant trajectory defined by a specific value of \mathcal{H} . Given specific values of δ , and c , the Hamiltonian 129 is completely defined and the system moves around on one of the level curves in fig. 16 for all time. Because $\Theta \propto \Gamma_0 \propto e_0^2$, the radial distance from the origin to a point on any given level curve is proportional to the eccentricity of the outer orbit. There are three fixed points, the leftmost one and the origin are stable and the right most one is unstable. The stability of a fixed point is easily calculated by evaluating the Hessian matrix in eq. (44), but is also apparent from the figure because there appear to be no small amplitude circulatory trajectories around the rightmost point.

The phase space of the first two panels of fig. 16 is divided into two *topologically*⁶ different regions divided by the separatrix curve (red curve). The separatrix curve passes through the unstable saddle point and consists of two ‘branches’, an inner branch (small red quasi-circle) and an outer branch (large red quasi-circle). The two branches intersect the x axis at two points, the region between them is called the resonant region. The trajectories in between the two branches are called *librations* and they do not include the origin, the trajectories outside the outer branch and inside the inner branch of the separatrix are called *circulations* and they do include the origin. The system is said to be in resonance if its trajectory is a curve within the resonant region, in which case θ does not pass through all the values in $\{0, 2\pi\}$ and is slowly varying. Depending on the distance from the resonance center (the leftmost stable fixed point), a resonant trajectory can include large excursions in eccentricity.

If we vary the δ parameter from a positive value (first panel of fig. 16), to a negative value the phase space changes. As δ decreases towards zero the two outer fixed points approach the origin (second panel in fig. 16), finally at $\delta = 0$, corresponding to an exact 6 : 1 commensurability, the three fixed points coalesce into a single fixed point at the origin. For negative δ there are only circulatory trajectories enclosing the origin and no resonant trajectories are possible.

This changing behaviour of the Hamiltonian based on the sign of δ is best illustrated using a *bifurcation diagram*, shown in fig. 17. The bifurcation diagram shows the value of the Hamiltonian at the two outer fixed points as a function of δ . The dashed curve is the value of \mathcal{H} evaluated at the saddle point, and the solid line is the value of \mathcal{H} at the left center point. The possible types of trajectories are indicated in the diagram.

While the analysis beforehand has concentrated on a particular 6 : 1 MMR, it is worth mentioning that many of the properties of the phase space (number of fixed points, shape of separatrix) look similar for

⁶ Topology is a field in mathematics which studies properties of space preserved under continuous deformations such as stretching, twisting and crumpling. For example, a circle is topologically equivalent to an ellipse, a sphere is equal to an ellipsoid, and a coffee cup is equivalent to a torus.

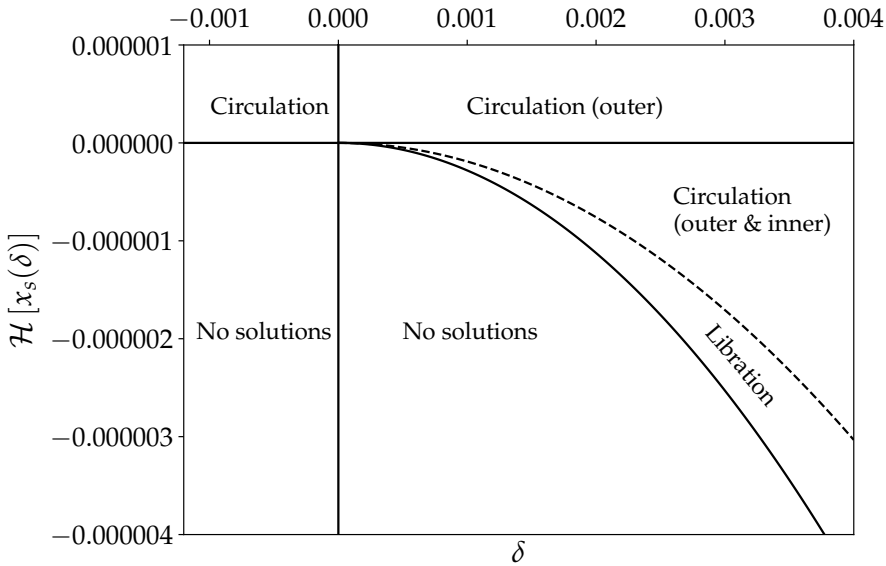


Figure 17: The bifurcation diagram of the Hamiltonian 129. The dashed curve denotes the value of \mathcal{H} evaluated at the saddle point x_s , and the solid curve the value of \mathcal{H} at the left center point.

other resonances, most major differences are in the structure of the bifurcation diagram.

3.4 RESONANCE PASSAGE

Finally, we turn to the topic of resonance passage. As mentioned previously, we can model the resonance passage as a slowly varying δ parameter in Hamiltonian 129. Looking at fig. 16, an immediate consequence of the resonant passage is apparent. If the system starts at positive delta and ends up at negative delta, the resonant angle is necessarily circulating at the end. Thus, divergent resonance passage ($\dot{\delta} < 0$) cannot result in a capture into resonance. Because the two orbits in an evolving circumbinary system are diverging away from each other, the δ parameter starts positive ($P_o/P_i < 6$), passes through zero and end up being negative ($P_o/P_i > 6$). As long as the stellar binary's orbit decays due to tidal forces, no capture will occur in such systems.

The assumption that δ varies *slowly* is crucial. As long as $\dot{\delta}/\delta$ is small compared to the libration or circulation frequency, or equivalently the characteristic time of resonance passage is large compared to the libration/circulation period, the system approximately follows the level curves in fig. 16. In other words, we require

$$\left| \frac{\dot{\delta}}{\delta} \right| \ll \frac{1}{T} \quad (141)$$

where T is the period of circulatory or libratory motion. In reality, an evolving circumbinary system is fully described only by a nonconservative Hamiltonian because the tidal decay forces acting on the stellar binary dissipate energy. Such Hamiltonians are however analytically intractable.

One can show that given a Hamiltonian $\mathcal{H}(\theta, \Theta; \delta)$ where δ is slowly varying, there exists a constant of motion called the *adiabatic invariant* (see for example Landau and Lifshitz (1976)), given by

$$\mathcal{J} = \oint \Theta d\theta \quad (142)$$

where \oint means that the integration is done over the complete range of variation of the coordinate variable, in our case, $\{0, 2\pi\}$. Along such path the Hamiltonian and δ are constant. The integral 142 is in fact the definition of the famous physical *action* from the *principle of least action*. The action in this case is thus an adiabatic invariant.

\mathcal{J} remains constant on average when δ is varied and it has a particularly simple interpretation in the case of a one dimensional Hamiltonian, namely, it is equal to the area enclosed by a level curve of the Hamiltonian in (x, y) coordinates. For a circular trajectory

$$\mathcal{J}_{\text{circ}} = 2\pi\Theta = \pi R^2 \quad (143)$$

Remember that since $\mathcal{J} \propto \Theta$, it depends on the eccentricity of the outer orbit.

For a general trajectory, the integral in eq. (142) is most easily evaluated by switching the integration variable to Θ . Using $\frac{d\theta}{dt} = \frac{\partial \mathcal{H}}{\partial \Theta}$ and $\frac{d\Theta}{dt} = -\frac{\partial \mathcal{H}}{\partial \theta}$, we have

$$\mathcal{J} = -\oint \left. \frac{\frac{\partial \mathcal{H}}{\partial \Theta}}{\frac{\partial \mathcal{H}}{\partial \theta}} \right|_{\mathcal{H}=\mathcal{H}_{\text{curve}}} \Theta d\Theta \quad (144)$$

where $\mathcal{H}_{\text{curve}}$ is the value of the Hamiltonian corresponding to a particular level curve.

There is a caveat to the conservation of \mathcal{J} however. If the trajectory approaches the separatrix, the librational period tends to infinity (remember the pendulum model). As $T \rightarrow \infty$, the adiabatic criterion in eq. (141) is no longer satisfied and \mathcal{J} is not conserved. After passing the separatrix curve however, \mathcal{J} is once again conserved. At the exact moment of separatrix crossing, the adiabatic invariant experiences a discontinuity, it is this discontinuity which is responsible for a sudden increase in eccentricity in the case of divergent resonance crossing.

Figure 18 shows the evolution of the adiabatic invariant as δ varies. Assuming the system is not in resonance to begin with, it starts on a circular trajectory with $\mathcal{J} = 2\pi\Theta_{\text{init}}$ within the inner branch of the separatrix (top left panel, grey circle). At a particular $\delta = \delta_t$ which depends on the initial area of the circle, the adiabatic invariant is equal to the area enclosed by the inner branch of the separatrix (top

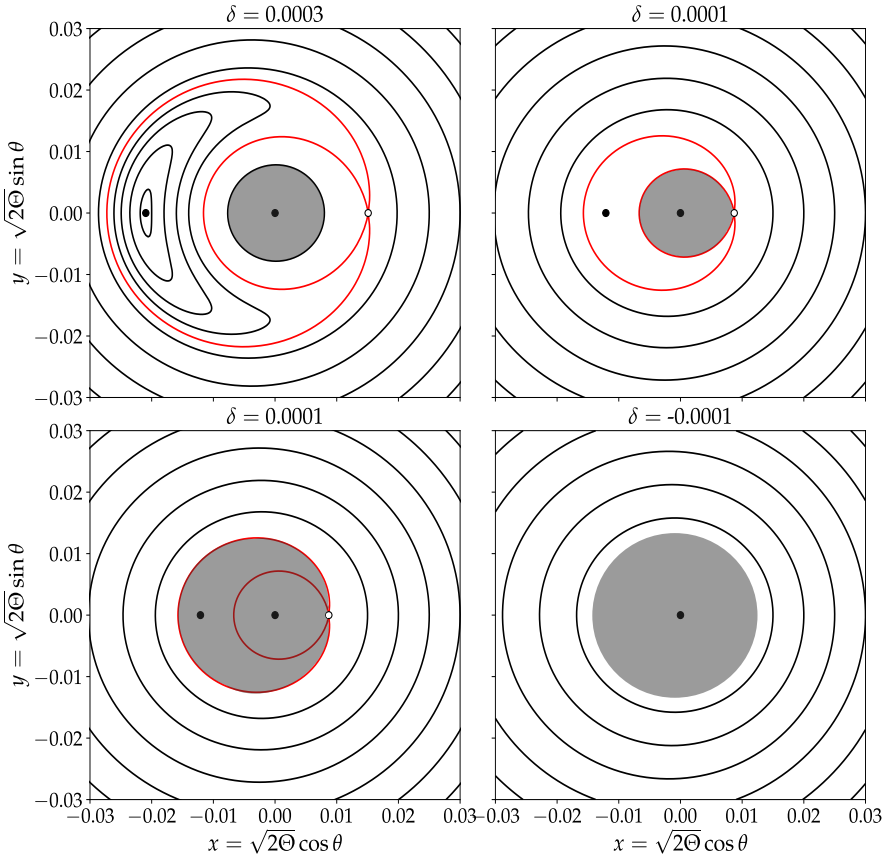


Figure 18: The evolution of the adiabatic invariant \mathcal{J} with varying δ . Dark circle denotes the adiabatic invariant, red curve is the separatrix. Top left panel - initially the trajectory is a circle. Top right panel - at $\delta = 0.0001$ the initial adiabatic invariant is equal to the area enclosed by the inner separatrix. Bottom left - the trajectory expands to the outer branch of the separatrix which corresponds to a discontinuity in \mathcal{J} . Bottom right - at $\delta = -0.0001$ the phase space has only circulatory trajectories and the adiabatic invariant is larger than initially.

right panel). The adiabatic invariant has no choice but to suddenly expand to the value equal to the area of the outer separatrix branch (bottom left panel). Finally, as δ decreases further and goes past $\delta = 0$, the separatrix disappears, the adiabatic invariant is again conserved and the system is left on a trajectory with a larger Θ (and therefore larger e_o) than it initially started with.

In order to calculate the adiabatic invariant after the discontinuous jump and therefore also the final eccentricity, we need to know the initial adiabatic invariant (the initial eccentricity) and the areas enclosed by the two branches of the separatrix for any given δ . We

start by calculating the separatrix areas, plugging in the Hamilton's equations into eq. (142), we have

$$\mathcal{J} = \oint \frac{1}{\Theta \sqrt{\Theta + c \sin(\theta)}} \left(\frac{\Theta^2 \cos(\theta)}{2\sqrt{\Theta + c}} + 2\Theta \sqrt{\Theta + c} \cos(\theta) + 2\Theta - \delta \right) d\Theta \quad (145)$$

To solve the integral, we need an expression for θ as a function of Θ on the level curve corresponding to the separatrix. Since the separatrix passes through the saddle point, it is defined by the equation

$$\mathcal{H}_s = \Theta^2 - \delta\Theta + \Theta^2 \sqrt{\Theta + c} \cos \theta \quad (146)$$

where \mathcal{H}_s is the value of the Hamiltonian at the saddle point. We can easily solve eq. (146) for $\cos \theta$ and $\sin \theta$ using the trigonometric identity $\sin^2 \theta + \cos^2 \theta = 1$. Plugging those expressions into eq. (145), we have

$$\mathcal{J} = 2 \oint_{\Theta_1}^{\Theta_2} \frac{\Theta (\Theta + c) (2\Theta - \delta) + \frac{\Theta}{2} (-\Theta^2 + \Theta\delta + \mathcal{H}_s) + 2(\Theta + c) (-\Theta^2 + \Theta\delta + \mathcal{H}_s)}{\sqrt{\frac{1}{\Theta+c} (\Theta^4 (\Theta + c) - (-\Theta^2 + \Theta\delta + \mathcal{H}_s)^2) (\Theta + c)^{\frac{3}{2}}}} d\Theta \quad (147)$$

Where we have used the symmetry of the separatrix to integrate along its upper part. The lower limit of integration is the value the location of the saddle point $\Theta_1 = \Theta_s$, the upper limit is the value of Θ at $\theta = \pi$ where the inner and the outer branch cross the separatrix.

Since it is not possible to derive an analytic solution for the location of the fixed points and hence also the points at which the separatrix crosses the x axis, we have to resort to numerical methods of finding the equation roots. To find the roots we use the Python package SciPy (Jones, Oliphant, and Peterson, 2001) and its well-tested routine `fsolve` for finding roots of nonlinear equations. The algorithm for finding the area enclosed by the separatrix is then

1. Determine the location of the saddle point by finding the root for eq. (134) with $\theta = 0$. There is only one root and the algorithm easily converges.
2. Evaluate the Hamiltonian 129 at the location of the saddle point denoting the value by \mathcal{H}_s , this determines the separatrix curve.
3. Solve eq. (146) for the two roots at $\theta = \pi$ which are the locations at which the two branches of the separatrix cross the x axis. The shape of the function is simple and the root-finding algorithm easily converges.
4. Solve the integral 147 using the SciPy module `integrate.quad`. The lower limit of integration is the location of the saddle point

and the upper is either the root of the lower separatrix branch or the upper one, depending on which area we are interested in.

Now that we have an algorithm which determines the areas enclosed by the two branches of the separatrix, the eccentricity kick can be determined as follows

1. Calculate $\mathcal{J}_{\text{init}} = 2\pi\Theta_{\text{init}}$ for given system parameters and an initial eccentricity e_o .
2. We require $\mathcal{J}_{\text{init}} = \mathcal{J}_{\text{inner}}$ where $\mathcal{J}_{\text{inner}}$ is the area enclosed by the inner branch of the separatrix. To find the value of $\delta = \delta_t$ for which this equality is true, we numerically solve for the root of $\mathcal{J}_{\text{init}} - \mathcal{J}_{\text{inner}}(\delta) = 0$.
3. The final action $\mathcal{J}_{\text{final}}$ is then equal to the area enclosed by outer branch of the separatrix evaluated at $\delta = \delta_t$, that is, $\mathcal{J}_{\text{final}} = \mathcal{J}_{\text{outer}}(\delta_t)$.
4. Once the resonance passage is over the trajectory is again circulatory and we can recover the final eccentricity by solving the equation

$$\mathcal{J}_{\text{final}} = 2\pi\Theta_{\text{final}} = \frac{\pi}{2}6^{1/3}m_3 \left(1 - \sqrt{1 - e_o^2}\right) \quad (148)$$

for e_o .

For a system with $\mu_i = 0.5 M_\odot$, $m_3 = 10^{-3} M_\odot$ and initial eccentricities $e_i = 0.2$, $e_o = 0.05$ we obtain a final outer eccentricity after resonance passage of $e_o = 0.089$. We will use the algorithms defined above to investigate the dependence of the eccentricity kick on system parameters in chapter 5.

4

N-BODY SIMULATIONS OF CIRCUMBINARY SYSTEMS UP TO THE COMMON ENVELOPE PHASE

While analytic models can give us important insight into the physics of divergent resonance passage in a circumbinary system they cannot compare to the full solution of the equations of motion. Here I describe a different approach to studying evolving circumbinary systems, by means of direct N-body simulations coupled with simulations of the stellar binary. These simulations provide a complete picture of the dynamical evolution of the system. To realistically simulate the dynamics of a stellar binary with a circumbinary planet as the stellar binary evolves, we need to know how stars evolve at each time step and how they interact with the outer planet(s). To solve this computationally we need to couple in some way a stellar evolution code with an N-body solver.

4.1 THE N-BODY PROBLEM

The *N-body problem* is a problem of N gravitationally interacting masses. The equations of motion are

$$m_i \ddot{r}_i = \sum_{j=1, j \neq i}^N G m_i m_j \frac{\dot{r}_{ij}}{|\dot{r}_{ij}|^3} \quad (149)$$

where m_i is the mass of the i -th particle, \dot{r}_i is its position vector, $\dot{r}_{ij} = \dot{r}_j - \dot{r}_i$ and $i = 1 \dots N$. Once the initial positions $r_{i,0}$ and velocities $\dot{r}_{i,0}$ are specified, there exists a unique solution which can only be obtained numerically for $N > 2$. The N -body system of equations is extremely sensitive to the initial conditions and special care must be taken to ensure numerical accuracy of the solutions. Since eq. (149) involve the force calculation between each pair of N particles, the computational complexity of the problem scales as $\mathcal{O}(N^2)$.

There are many different ways of solving eq. (149) numerically, and the choice of method depends primarily on the problem at hand. For systems with large N approximation schemes are often used which manage to reduce the complexity to order $\mathcal{O}(N \ln N)$. In celestial mechanics N is generally on the order of a few and the integration times are very long (sometimes billions of years), high precision is thus required and the complexity is $\mathcal{O}(N^2)$. Another difficulty is the fact that eq. (149) has a singularity when two particles come very close to each other which can lead to arbitrarily high particle velocities if not properly handled. For a system of N gravitationally interacting bodies the total energy and angular momentum are always conserved, however,

this need not be true for a numerical solution of the equations of motion. Often, the ‘quality’ of an integrator¹ is judged by how well it conserves the total energy.

A class of integrators called *symplectic integrators* (Vogelaere, 1956; Ruth, 1983; Feng, 1986) is often used in celestial mechanics. Instead of solving eq. (149), these integrators solve the equivalent Hamiltonian system. They preserve invariant properties such as phase space density and in many cases can have an upper bound on the energy error.

4.2 REBOUND - AN OPEN SOURCE N-BODY INTEGRATOR

Because the N-body problem occurs very often in astrophysical applications, there exist multiple numerical solvers for problems of various scales and with varying degree of accuracy. Traditionally, the code most often used for applications in celestial mechanics is MERCURY (Chambers and Migliorini, 1997; Chambers, 1999), written in the FORTRAN programming language.

For the problem of simulating a circumbinary system which involves pure N-body computations and dissipative forces, I have opted to use a different code called REBOUND (Rein and Liu, 2012). REBOUND is an open-source code freely available on GitHub², it is written in C99 and also has a Python interface, it is under active development. The reasons for choosing REBOUND over MERCURY are plenty, most important being the ease of use, the availability of integrators accurate to machine precision and the fact that REBOUND uses Jacobi coordinates by default (which matches well with the analysis in chapter 3) while MERCURY uses heliocentric coordinates which are more suitable to Solar System type of problems.

REBOUND comes with many integrators, the most important of which are the symplectic integrator WHFAST (Rein and Tamayo, 2015) and an adaptive high-order integrator called IAS15 (Rein and Spiegel, 2014). For applications which involve velocity-dependent non-conservative forces such as tidal decay of binary stars, IAS15 is a better choice because symplectic integrators are by construction designed for conservative forces.

IAS15 is designed to solve a system of differential equations of the form

$$\ddot{\mathbf{y}}(t) = \mathbf{F}(\dot{\mathbf{y}}, \mathbf{y}, t) \quad (150)$$

¹ An *integrator* is a name often given to any numerical scheme which solves a system of differential equations.

² <https://github.com/hannorein/rebound>

where $\ddot{\mathbf{y}}$ is the acceleration and F is an arbitrary force which may depend also on the velocity. Equation (150) can be expanded into a truncated series:

$$\ddot{\mathbf{y}}(t) \approx \ddot{\mathbf{y}}_0 + \mathbf{a}_0 t + \mathbf{a}_1 t^2 + \cdots + \mathbf{b}_6 t^7 \quad (151)$$

where $\ddot{\mathbf{y}}_0$ is the acceleration evaluated at $t = 0$. It can then be rewritten as

$$\ddot{\mathbf{y}}(h) \approx \ddot{\mathbf{y}}_0 + \mathbf{b}_0 h + \mathbf{b}_1 h^2 + \cdots + \mathbf{b}_6 h^7 \quad (152)$$

where dt is the *timestep*, $h = t/dt$ and $\mathbf{b}_k = \mathbf{a}_k dt^{k+1}$. Finally, we rewrite it once again as

$$\ddot{\mathbf{y}}(h) \approx \ddot{\mathbf{y}}_0 + \mathbf{g}_1 h + \mathbf{g}_2 h(h - h_1) + \mathbf{g}_3 h(h - h_1)(h - h_2) + \cdots + \mathbf{g}_8 h(h - h_1) \dots (h - h_7) \quad (153)$$

Where the timestep h is now divided into substeps h_1, \dots, h_7 in the interval $[0, 1]$. The coefficients \mathbf{g}_k can be determined from \mathbf{b}_k . When the expansion is written in this form, the coefficient \mathbf{g}_k depends only on the force evaluations at previous substeps h_n with $n \leq k$. Equation (152) can then be integrated to give the velocity

$$\dot{\mathbf{y}} \approx \dot{\mathbf{y}}_0 + h dt \left(\ddot{\mathbf{y}}_0 + \frac{h}{2} \left(\mathbf{b}_0 + \frac{2h}{3} (\mathbf{b}_1 + \dots) \right) \right) \quad (154)$$

and once again for the position

$$\mathbf{y} \approx \mathbf{y}_0 + \dot{\mathbf{y}}_0 h dt + \frac{h^2 dt^2}{2} \left(\ddot{\mathbf{y}}_0 + \frac{h}{3} \left(\mathbf{b}_0 + \frac{h}{2} (\mathbf{b}_1 + \dots) \right) \right) \quad (155)$$

To get the new positions and velocities, we need to estimate the coefficients \mathbf{g}_k (and hence also \mathbf{b}_k). These are obtained using an implicit scheme (see Rein and Spiegel, 2014, for details). To obtain the best possible accuracy for the position and the velocity, the spacing of substeps in IAS15 Rein and Spiegel (2014) chose Gauss-Radau spacing³ with $h_n = 0, 0.0562, 0.1802, 0.3526, 0.5471, 0.7342, 0.8853$ and 0.9775 . In a Gauss-Radau integration scheme where a function $F(t)$ is integrated on the domain $[0, dt]$ with m quadrature points and the absolute error term is of order $\mathcal{O}(dt^{2m})$ Rein and Spiegel (2014). For $m = 8$ the error term is $\mathcal{O}(dt^{16})$ which makes this a 15-th order scheme, hence the name IAS15. The fact that this integrator is 15th order means that by reducing the timestep by a factor of α we reduce the error by a factor of α^{16} ! Thus, to obtain an accurate solution a very small timestep is often not necessary, it is usually sufficient to take a fraction of the smallest relevant dynamical timescale in the problem.

The *total error* in for example energy or position depends not only on the error associated with the truncation of an infinite series in

³ Gauss-Radau spacing is related to the Gaussian quadrature which is a way of approximating a solution to an integral on a definite interval

a numerical scheme but also on error E_{floor} associated with the finite precision of floating-point numbers (IAS15 uses double precision numbers) also known as roundoff error, a random error E_{random} coming from an addition of two floating-point numbers and a bias error E_{bias} associated with the bias of floating-point operations. That is, the total error E is

$$E = E_{\text{floor}} + E_{\text{rand}} + E_{\text{bias}} + E_{\text{scheme}} \quad (156)$$

The total error is then dominated by the largest term.

IAS uses an adaptive timestepping scheme in which a new time step is chosen after previous timestep, since it is very high-order, the timestep can be chosen such that the error associated with the scheme E_{scheme} remains below 10^{-16} , which is less than the precision of double floating-point numbers. We say that the integrator is accurate to machine precision. Therefore, it is not possible to achieve better precision with a different integrator unless the floating-point precision is extended (to say 128 bit numbers). The total error then depends on the other errors. E_{floor} is constant, and E_{bias} in general might grow linearly with time because some floating-point operations might be biased, for example, in a series of repeated additions the error might be preferentially positive instead of either positive or negative with equal probability. To avoid these types of errors all mathematical operations in IAS15 use only the operators $+, -, \times, /$ which are guaranteed to give the same result⁴ in C99 independent of the hardware on which the code is run or the compiler differences.

Even if such biases are removed and the error in each individual calculation is completely random, the error (designated E_{rand}) grows with time. Brouwer (1937) showed that quantities such as the energy or position error grow as $\propto t^{1/2}$ and the error in angles grows as $\propto t^{3/2}$, this is known as *Brouwer's law*. Extensive test of the IAS15 integrator presented in Rein and Spiegel (2014) show that it follows Brouwer's law, that is, the error is dominated by the E_{random} term. The closest comparable integrator, RADAU in MERCURY generally has a two orders of magnitude greater error.

4.3 BINARY_C - A BINARY STELLAR EVOLUTION CODE

If we were interested in the dynamics of circumbinary system on the main sequence, an N-body integrator would be sufficient because purely gravitational forces dominate. To investigate the dynamics beyond the main sequence we need some prescription the evolution of the stellar binary.

⁴ This is in general not true for other operations such as \sqrt{x} which may give slightly different results depending on the system architecture.

I opted to use the `binary_c`⁵ stellar evolution code described in Izzard et al. (2004), Izzard et al. (2006), and Izzard et al. (2009), which is based on a binary stellar evolution code BSE (Hurley, Tout, and Pols, 2002). Both BSE and `binary_c` do not solve the equations of stellar structure directly (which is very computationally expensive) but rather uses analytical formulae fitted to the outputs of detailed models which do solve the stellar structure equations. Since analytic expressions are computationally ‘cheap’ to evaluate, the codes are very fast. `binary_c` is unfortunately not freely available for download, however it is available upon request from the author. The code is written in C and it includes an API interface for calling functions which evolve the binary system for specified initial conditions and output the physical variables for each time step. Table 5 shows the input parameters which need to be specified in order to run the code. For all

Parameter	meaning
M1	mass of primary star
M2	mass of secondary star
PER	initial orbital period of the binary in days
ECC	initial eccentricity
Z	metallicity
EVOLTIME	total evolution time

Table 5: Initial parameters for the stellar evolution code `binary_c`.

the other parameters we keep the default values specified in the code, for the metallicity we choose a fixed value of solar-like metallicity of 0.02 and evolve all systems for a duration of a Hubble time (13.7 Gyr).

In order to later on couple the `binary_c` code with REBOUND, and easily plot the output from the code, I have written a Python interface to the code. The interface is built using the Python library `ctypes` which enables one to access C functions from within Python if the C code is compiled as a *shared library*. I use `ctypes` to access `binary_c` API functions from within Python and grab the output directly into memory as a Python object.

Figure 19 shows an example output of the `binary_c` code for an eccentric short-period binary ($e = 0.3$, $P = 100$ days), consisting of a main-sequence star of mass $m_1 = 1.2 M_{\odot}$, and a red-dwarf of mass $m_2 = 0.5 M_{\odot}$. The final outcome of the stellar evolution in this case is a binary consisting of a white dwarf and a red dwarf. The top panel shows the evolution of the radius in time. It is apparent that the higher mass star ascends the red giant branch first, while the lower mass star stays at near constant radius. The stellar radius is an important parameter because tidal forces which drive the orbital evolution depend very strongly on radius. It is also important because

⁵ http://www.ast.cam.ac.uk/~rgi/binary_c.html

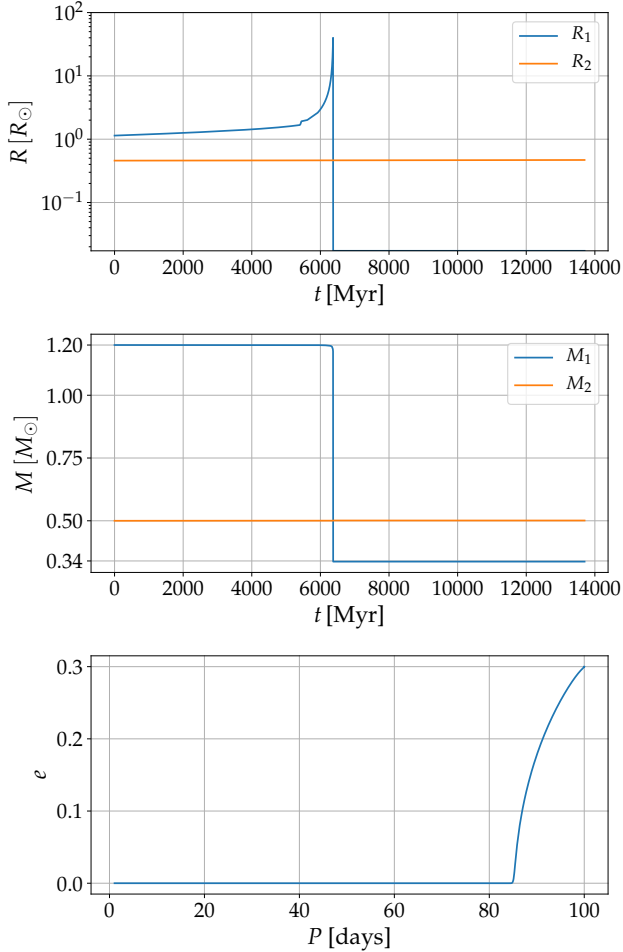


Figure 19: An example of the stellar evolution output data from the `binary_c` code for $m_1 = 1.2 M_{\odot}$, $m_2 = 0.5 M_{\odot}$, $e = 0.3$, $P = 100$ days. Top panel shows the time evolution of the stellar radii, middle panel shows the mass loss from both stars and the bottom panel shows the orbital evolution in period-eccentricity space.

for close binaries with a period shorter than about 1000 days, the stellar radius of the primary at the tip of the red giant branch (the sharp peak in the figure) reaches beyond the Roche Lobe radius of the primary which triggers the formation of a common envelope.

The middle panel shows the masses of the two stars as a function of time. The mass loss is for the purposes of dynamical modeling negligible up to the CE phase (less than 1% for the primary star and near zero for the secondary). During the CE phase a large percentage of the total mass in the system is suddenly ejected. After the ejection again nothing interesting happens because the secondary in this case is a low-mass star.

The orbital evolution of the binary in period-eccentricity space is shown in the bottom panel of fig. 19. Initially the eccentricity is $e = 0.3$ and the period is 100 days, very quickly however the orbit is circularized via tidal interactions and it continues to shrink at near zero

eccentricity until a common-envelope event is triggered. Because resonance widths tend to zero as the binary eccentricity declines, the influence of resonance passage on CB planets is most significant if the passage happens at non-zero binary eccentricity.

Figure 20 shows the evolutionary tracks in period-eccentricity space of stars in observed main sequence CB systems (see table 1). Shown are only the tracks from those stars which experience significant orbital evolution within a Hubble time. We see that only a single circumbinary planet, PH-1 A (ab) b, crosses a resonance at an appreciable eccentricity of the stellar binary, namely the 7:1 MMR. All the other planets either cross the resonances after the binary's orbit has circularized or they orbit outside of even the 9 : 1 MMR location. Thus, only a small subset of the initial parameter space results in outcomes which favor resonance crossing scenarios likely to cause significant eccentricity excitation. Nevertheless, the sample of observed circumbinary systems in table 1 is very small and there might still be a significant population of CB planets located just inside the 6 : 1 and 7 : 1 MMR locations.

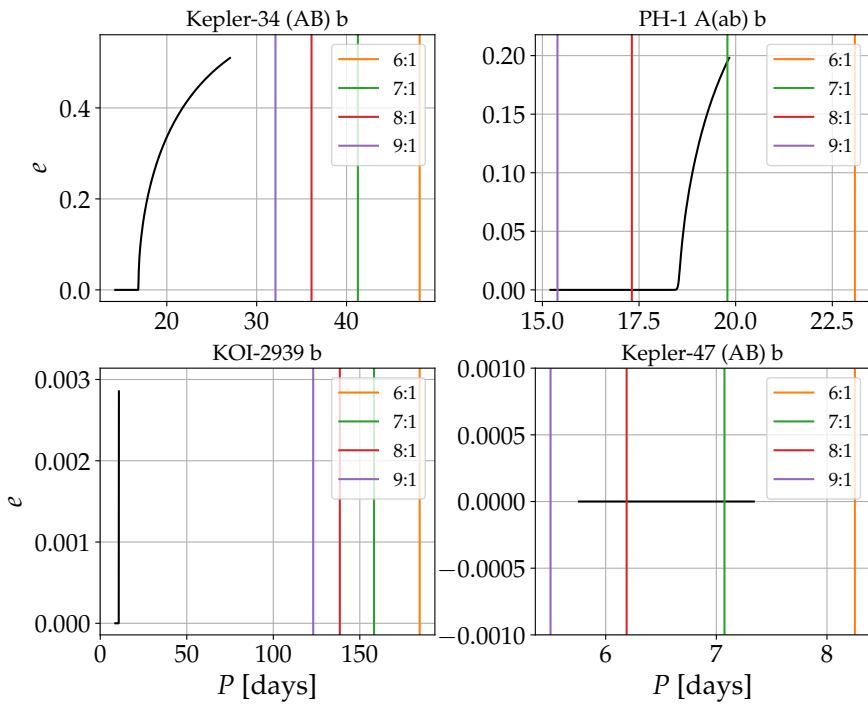


Figure 20: Evolutionary tracks of circumbinary planet hosting main-sequence binaries in period-eccentricity space. The vertical lines show the location of high-order mean motion commensurabilities up to the 9 : 1 commensurability . The title above each panel shows the name of the stellar binary and the planet.

Having covered binary evolution up to the common envelope phase, the question remains what happens during and after the common envelope. The common envelope is a very short lived and poorly un-

derstood phase of binary stellar evolution (for a recent review see Ivanova et al. (2013)). Depending on the model it lasts on the order of a few tenths to a few thousands of years, a blink of an eye when compared to typical stellar evolution timescales. As mentioned in section 1.4, it is modeled with a simple α parameter which tells us what percentage of the orbital energy went into ejection of the common envelope. By default `binary_c` uses a value of $\alpha_{CE} = 3.0$. Most stellar evolution codes, including `binary_c`, do not resolve the CE phase but just proceed to calculate the evolution after ejection, accounting for the mass loss and the possibility of a merger during the CE.

To get an idea of what the most common outcomes of common envelope evolution are, in fig. 21 we plot a density map of `binary_c` outcomes classified into four categories:

1. None - CE did not occur
2. CE - CE did occur and the final system is a binary
3. CE & merger - CE occurred and the two stars merged into a single star
4. SN - CE occurred and the two stars underwent a double-degenerate supernova

Left panel of fig. 21 shows a stellar evolution outcomes for very short period binaries with $P = 10$ days, similar to the binaries observed in circumbinary systems. It appears that all main-sequence binary stars similar to the observed circumbinary systems end up as a single star, a product of a stellar merger event during the CE phase. For the somewhat longer period binaries (right panel), the part of parameter space which does not result in a merger is slightly larger and also possible for low mass binaries. In general, these results should be taken with a grain of salt because the physics behind the CE phase is so uncertain. We can however conclude that all of the circumbinary planet hosting binaries do undergo a common envelope phase, the question is just whether they end up as a single star or a very tight binary.

4.4 STABILITY OF CIRCUMBINARY SYSTEMS ON THE MAIN SEQUENCE

Before moving to the simulations of CB planets around evolving binaries, we investigate the stability during the main sequence. A reasonable strategy is to use REBOUND and integrate systems with various initial conditions for a certain period of time, say 10 million years. There is however a useful and computationally cheaper way of assessing stability. As mentioned in chapter 2, phase space trajectories

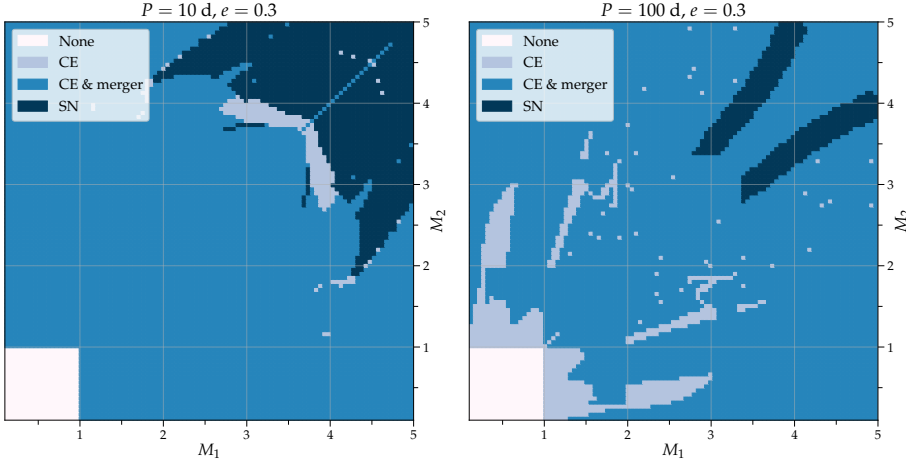


Figure 21: Final outcomes of stellar evolution generated by the `binary_c` code as a function of the two masses. Left panel: binary with an initial period of $P = 100$ days and initial eccentricity. Right panel: a binary with an initial period of $P = 10$ days. Both panels show systems with an initial eccentricity of $e = 0.3$. Various outcomes are denoted by different colors specified in the legend.

with arbitrarily small differences in their initial conditions are said to be *chaotic* if they tend to diverge from each other exponentially. Measuring the rate of this exponential divergence gives us some estimate of how 'chaotic' the trajectories are.

The system of N-body equations eq. (149) is of the form

$$\dot{\mathbf{x}} = \mathbf{f}(\mathbf{x}), \quad \mathbf{x} \in \mathbb{R}^{6N} \quad (157)$$

The solution to these equations defines a trajectory $\mathbf{x}(t)$ in phase space. Consider now a trajectory \mathbf{x}' initially close to \mathbf{x} , $\mathbf{x}'(0) = \mathbf{x}(0) + \delta\mathbf{x}(0)$. To measure their relative divergence, we cannot just study the Euclidian norm $\|\delta\mathbf{x}(t)\|$ as a function of time because in the case of bounded motion, this distance cannot grow indefinitely. What we need is a measure of *local* exponential divergence of nearby trajectories. Since local means in the vicinity of a point in phase space \mathbf{x} , we can *linearize* the equations of relative motion by expanding the function $\mathbf{f}(\delta\mathbf{x})$ around zero to first order. The linearized equations of relative motion, also called the *variational equations*, then have the form

$$\dot{\delta} = \mathbf{A}(t)\delta \quad (158)$$

where the vector $\delta(t) \equiv \delta\mathbf{x}(t)$ measures the Euclidian distance between two neighboring trajectories in phase space and \mathbf{A} is the Jacobian matrix with elements $A_{ij} = \partial f_i / \partial x_j$. For as long as $\delta\mathbf{x}(t)$ stays small, the linearized equations are a good approximation of the mo-

tion. The *Maximum Lyapunov Exponent* is then defined as (Hinse et al., 2010; Morbidelli, 2002)

$$\gamma = \lim_{t \rightarrow \infty} \frac{1}{t - t_0} \ln \left(\frac{\|\dot{\delta}(t)\|}{\|\dot{\delta}(t_0)\|} \right) = \lim_{t \rightarrow \infty} \frac{1}{t - t_0} \int_{t_0}^t \frac{\|\dot{\delta}(s)\|}{\|\delta(s)\|} ds \quad (159)$$

The ratio $\|\dot{\delta}/\delta\|$ measures the rate of change of the separation vector δ . The rate of change of δ is then $e^{\gamma t}$. If $\gamma > 0$, the initial separation grows exponentially in time and we have chaotic motion. If $\gamma = 0$ the separation does not change and we have quasi-periodic or regular motion. Finally, for $\gamma < 0$ the two trajectories approach each other at an exponential rate, this only happens for dissipative systems because it implies the existence of attractive fixed points which act as sinks in phase space. This is not possible for conservative Hamiltonian systems since it is a violation of Liouville's theorem.

In practice, calculating the limit when $t \rightarrow \infty$ is computationally not feasible and usually one takes a sufficiently long time $t = t_{\max}$. For a recent review on the calculation of maximum Lyapunov exponents see Frouard, Fouchard, and Vienne (2008). There are various ways of more efficiently computing either the MLE or so called chaos indicators closely related to the MLE. One such indicator is called the *Mean Exponential Growth of Nearby Orbits* (Cincotta, P. M. and Simó, C., 2000; Cincotta, Giordano, and Simó, 2003) or MEGNO for short. It is defined as

$$Y(t) = \frac{2}{t} \int_{t_0}^t \frac{\|\dot{\delta}(s)\|}{\|\delta(s)\|} s ds \quad (160)$$

and its time-avaraged mean value is

$$\langle Y \rangle(t) = \frac{1}{t} \int_{t_0}^t Y(s) ds \quad (161)$$

The difference between the MLE and the MEGNO indicator is that the integral in MEGNO is weighted by time during the integration, thus giving more wait to the rate of divergence of the separation vector at later times. Numerically, the MEGNO is computed by integrating the variational equations eq. (158) wit a random initial displacement vector δ_0 during the time interval $t - t_0$. Most other chaos indicators based on the MLE do not have this weighting. Generally, $\langle Y \rangle$ can be parametrized as a linear function in time $\langle Y \rangle(t) = \alpha t + \beta$. Cincotta, Giordano, and Simó (2003) show that if the motion is quasi-periodic $\alpha \approx 0$ and $\beta \approx 2$ and $\langle Y \rangle \rightarrow 2$ as $t \rightarrow \infty$. Indeed, it converges to zero than the MLE (Cincotta, Giordano, and Simó, 2003). In the case of a chaotic orbit Y and $\langle Y \rangle$ increase linearly with time ($\alpha \neq 0$).

The relationship between chaotic orbits (high MEGNO) and *stability* of a system is not straightforward. A system is deemed stable for a certain time if there are no *close encounters* between any two bodies in the system leading to hyperbolic orbits. Chaotic trajectories need

not lead to ejections because the chaos might be *bounded*. Bounded chaos means that even if at a certain point in phase space we have exponentially diverging trajectories, the trajectories are still bounded to a certain *finite* volume of phase space. Thus, high MEGNO values can only be used as a proxy for instability. We should always keep that caveat in mind when interpreting MEGNO maps (or any other chaos indicator). For a discussion about the relationship between chaos, resonance overlap and stability, see Deck, Payne, and Holman (2013).

Since MEGNO is calculated for a finite integration time, there is always a possibility that some trajectories start quasi-period and suddenly become chaotic after a time longer than the integration time. However, if an orbit has a large MEGNO value after a small interval of time, it is almost certainly chaotic for all times. MEGNO is ideal for revealing regions of phase space which are chaotic due to overlapping mean-motion resonances.

The question remains what is a suitable integration time for calculating the MEGNO values for a given system. There is no unique answer as it depends on the problem. For our purposes, the answer is - whatever time is enough to reveal the fine structure in the space of orbital parameters due to resonance overlap. If we were to calculate the MEGNO values for say the Solar System and choose an extremely long integration time on the order of billions of years, we would find that almost all initial conditions result in chaotic orbit because even though the Solar System looks stable now, it can be chaotic on a sufficiently long timescale.

The REBOUND package includes functions to calculate the MEGNO value out of the box. It does by integrating the variational equations for a specified period of time, either with the high-order IAS15 integrator or the symplectic WHFAST. Since we are interested in the stability of circumbinary systems on the main-sequence which are (to a good degree of approximation) conservative, we opt for the WHFAST integrator since it is faster than IAS15. We chose to calculate MEGNO as a function of two orbital parameters because we can then construct a density plot which is more informative than a one dimensional function.

Figure 22 shows an example of MEGNO maps for a system with $m_1 = 1 M_{\odot}$, $m_2 = 1 \times 10^{-3} M_{\odot}$ and $m_3 = m_2$, that is, a system with a single star and two Jupiter mass planets. We choose $P_i = 10$, $e_i = 0.1$, $\omega_o - \omega_i = 0$, and we vary e_o and P_o . Both planets have the same value of the argument of pericentre. We could have just as well chosen some other parameters, these are just the most useful ones to plot. The left panel shows a MEGNO map for a total integration time of 1000 years. The $n : 1$ resonances are easily noticeable, it also appears that the region up to the $2 : 1$ resonance is mostly unstable. The panel on the right shows the same MEGNO map with a longer integration time of 5000 yr. As expected, the resonances are more easily

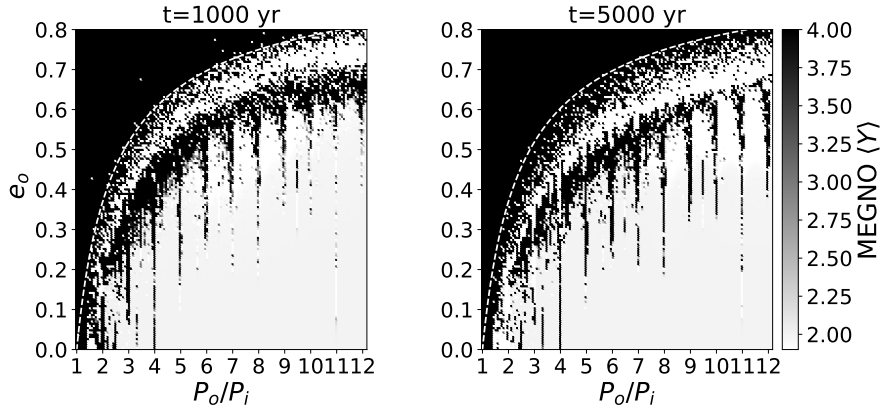


Figure 22: MEGNO maps for a system with $m_1 = 1 M_{\odot}$, $m_2 = 1 \times 10^{-3} M_{\odot}$, $m_3 = m_2$, $P_i = 10$ days, $e_i = 0.1$ and $\omega_o - \omega_i = 0$, calculated on a 150×150 grid in variables $(P_o/P_i, e_o)$. White points are regular orbits and the dark grey points are chaotic orbits. The left panel shows a MEGNO map for an integration time of 1000 years and the right one for an integration time of 5000 years. The dashed white line in the top left corner of each panel is defined by $R_p/a_i = 1$ where $R_p = a_o(1 - e_o)$ is the outer periastron distance. Every outer orbit above that line is crossing the inner orbit and is therefore guaranteed to be unstable in almost all cases.

apparent, however, the computational demands for a longer integration are considerable (an hour on a 32 core machine with a parallelized code) and we opt to use an integration time of around 1000 yr. Both plots show an unusual strip of regular orbits at very high eccentricities. This is most likely due the linear approximation of the variational equations used to calculate the MEGNO values. The variational equations are valid only in the vicinity of the point at which we expand the full equations of motion, presumably it fails in this particular region because at those high eccentricities the planets are likely to experience close encounters which significantly perturb both planets and the linear approximation breaks down. Above the strip at even higher eccentricities the orbits are again chaotic because at that point the close encounters actually result in an ejection event and an ejection event automatically assigns a maximum value of MEGNO.

After introducing the MEGNO technique on an example of a single-star system with two planets, we apply it to circumbinary systems. Figure 23 shows MEGNO maps for the observed circumbinary systems with relatively close-in planets. Plotted on top of the MEGNO results are the analytically derived resonance widths (blue ‘bubbles’ in the figure) from Mardling (2013) (see section 2.4.3.1 for derivation), the red dots are the observationally derived values for the planet eccentricity and period. The first thing one should notice when comparing the various panels in fig. 23 to fig. 22 is the much larger volume of phase space occupied by chaotic orbits. This is due to the fact that

the circumbinary systems have an inner mass ratio larger by a factor of about 1000 compared to a single-star system with Jupiter mass planets. The higher inner mass ratio, combined with the fact that the stars in a circumbinary system tend to be eccentric, leads to a formation of chaotic zone extending all past the 5 : 1 MMR for most binary eccentricities. This chaotic region is indeed unstable, Holman and Wiegert (1999) ran full N-body simulations of test particles in close orbits around binaries and later fit analytical formulae which give the size of the instability region. Later, Mudryk and Wu (2006) found that the instability region is due to resonance overlap, as is visible in fig. 23.

Looking at the analytic predictions for the resonant widths in fig. 23, we see that all regions of resonance overlap lead to chaotic trajectories. For all but one of the systems, the resonant widths roughly follow the first emerging chaotic trajectories. The exception is Kepler-34 which orbits a highly eccentric binary and is located in a region with mostly black dots. Since Kepler-34 is a confirmed exoplanet with a well determined orbit, we conclude that the chaotic region in the first pane which does not overlap with the analytical prediction is most likely reasonably stable. All the other CB planets lie comfortably outside the inner chaotic zone and none of the planets lie within the 5 : 1 MMR, which is why the 6 : 1 MMR is the first we considered in detail in chapter 3. Notice most importantly that the extent of the inner chaotic region at moderate planet eccentricities depends crucially on the binary eccentricity e_i , the higher it is, the further away an inner most planet has to be in order to be on a stable orbit. Sutherland and Fabrycky (2015) investigate the chaotic zone in detail by means of N-body simulations and find that the most likely outcome for a planet in the inner chaotic zone is ejection, and a significant fraction of planets collide with one of the stars.

4.5 COUPLING BETWEEN `binary_c` AND REBOUND

In order to realistically simulate the dynamical evolution of a circumbinary system, we need to combine a model for the orbital evolution of the stellar binary given by `binary_c` with the N-body code `REBOUND`. A best conceivable solution would be an N-body code which at each timestep on top of the gravitational forces acting on the three bodies also calculates the tidal forces acting on the binary. Since the tidal forces depend on all kinds of stellar parameters such as the luminosities of the stars, their temperatures, core masses etc.; we would also need the full output of the `binary_c` code between each N-body timestep. Actually, not only would we need to run `binary_c` between each timestep in the N-body code but also between each *substep* of a given timestep since the IAS15 integrator requires several force evaluations in an interval $[0, dt]$.

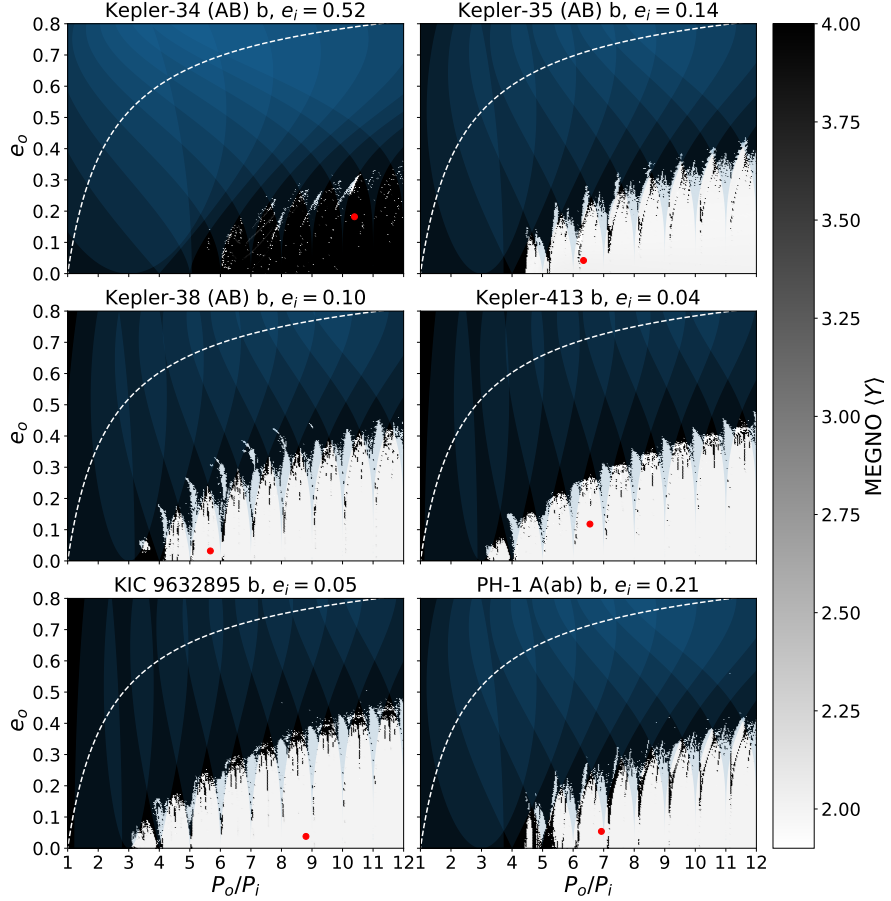


Figure 23: MEGNO maps for the observed circumbinary systems with relatively close-in planets. Red dots show observationally derived values for the orbital parameters of the planets. The color coding shows the MEGNO value, darker shades corresponding to chaotic orbits with high MEGNO and lighter ones to regular orbits. Plotted on top of the MEGNO maps is the analytical prediction for the resonance widths of $n : 1$ mean-motion resonances, starting with $n = 2$ (see section 2.4.3.1). The dashed white line in the top left corner of each panel is defined by $R_p/a_i = 1$ where $R_p = a_o(1 - e_o)$ is the outer periastron distance. Every outer orbit above that line is crossing the inner orbit and is therefore guaranteed to be unstable in almost all cases.

While not impossible, such approach would require a lot of work and we would need to make sure that `binary_c` is able to work with timesteps of a fraction of the dynamical time in the system (on the order of days), when it normally works with timesteps comparable to stellar evolution timescales (millions of years). This would almost certainly be challenging and would most likely require some sort of interpolation scheme for the `binary_c` output variables.

There is however an easier solution to the problem. We could ignore the gravitational influence of the circumbinary planet on the stellar binary and in the N-body code force the binary to move in a way

consistent with the output of `binary_c` generated beforehand. This would mean that we are in a regime of a *restricted three body problem* where the inner two masses do not experience the force of the third mass⁶, a reasonable approximation because the mass ratio between the total mass of the stellar binary in a circumbinary system and the outer planet is $m_3/m_{12} \approx 10^{-3}$.

The question remaining then is how to ‘force’ the stellar binary in REBOUND to move in the (a, e) such that its trajectory matches the output from `binary_c`. There are two options, the first one is to directly change the orbital elements a_i and e_i after each internal `binary_c` timestep (long compared to IAS15 timestep). The other approach is to construct a force which acts on the stellar binary such that the values of (a_i, e_i) after specified time match the `binary_c` values at that time; such force is necessarily velocity-dependent. Both approaches are implemented in REBOUNDx, a library for incorporating additional effects in REBOUND simulations (<https://github.com/dtamayo/reboundx>), as functions `modify_orbits_direct` and `modify_orbits_forces`. We opt to use the second approach because it is more physically motivated than directly changing the orbital elements ‘by hand’. Indeed, a velocity-dependent force is exactly how the tidal decay of the binary happens in the first place.

In REBOUNDx, the force is constructed such that when orbit-averaged it gives an *exponential* growth/decay of the semi-major axis and the eccentricity. The approach is based on Papaloizou and Larwood (2000); the force governing the eccentricity evolution is given by

$$\mathbf{a}_{\text{damp}} = -2 \frac{(\mathbf{v} \cdot \mathbf{r}) \mathbf{r}}{r^2 \tau_e} \quad (162)$$

and for the semi-major axis evolution

$$\mathbf{a}_{\text{damp}} = -\frac{\mathbf{v}}{\tau_a} \quad (163)$$

where \mathbf{a} is the acceleration vector. These two forces act in a way such that the eccentricity/semi-major axis exponentially increase/decrease by a factor of $e = 2.71\dots$ over a timescale τ_e/τ_a . The eccentricity damping keeps the angular momentum constant which means that some semi-major axis evolution is always induced. It also induces some pericentre precession. Both effects are physical.

The problem of changing the orbital elements of the stellar binary then reduces to a suitable choice of two damping timescales, between

⁶ Actually, this is not strictly true for the implementation in the code. The calculation of the forces on the stars at each IAS15 timestep does include the influence of the planet. However, since the stars are ‘forced’ to move according to a trajectory previously generated beforehand with `binary_c`, which was derived assuming an isolated system of two stars, it is still effectively a restricted problem over sufficiently long timescales (at least one `binary_c` period).

each `binary_c` timesteps. An exponential decay in the semi-major axis is described by the differential equation

$$\left(\frac{\dot{a}}{a}\right) = \frac{1}{\tau_a} \quad (164)$$

which can be easily solved with the method of the separation of variables, giving

$$\ln a_{k+1} - \ln a_k = \frac{t_{k+1} - t_k}{\tau_a} \quad (165)$$

where we have discretized the solution with a_k designating the value of the semi-major axis at timestep k and a_{k+1} the value at timestep $k + 1$. The damping timescale is then

$$\tau_a = \frac{t_{k+1} - t_k}{\ln \frac{a_{k+1}}{a_k}} \quad (166)$$

Therefore, given the values of a_k and a_{k+1} (which are pre calculated with `binary_c`), we can determine the exponential decay timescale and pass it to REBOUND such that at time t_{k+1} the value of a in REBOUND matches the one in `binary_c`. The algorithm for running a simulation of a circumbinary system is then

1. Choose stellar parameters, evolve binary system using `binary_c` from a point at which significant changes in (a, e) start occurring (RGB branch) up to the start of the common envelope phase. Save output data to file.
2. Load orbital parameters from `binary_c`, calculate array of damping timescales τ_a and τ_e for each `binary_c` timestep.
3. Integrate system using REBOUND with the IAS15 integrator from the zeroth to the final value of time in `binary_c` output, at each time t for which there is data from `binary_c` change damping timescales with a new value from array

Figure 24 shows the result of an N-body integration of a system with masses $M_1 = 1.4M_\odot$, $M_2 = 0.7M_\odot$, initial eccentricity $e = 0.3$ and initial period $P = 200$ days. The integration time in REBOUND has been rescaled by a factor of 10^3 compared to the output in `binary_c` in order to reduce runtime; in the simulations which include an outer planet the integration runs for the complete duration. The left panel shows the relative error of the orbital elements calculated by REBOUND compared to those from `binary_c`. The right panel shows a small portion of the total integration time between two `binary_c` timesteps (orange stars). The errors are negligible. Even though this is a two-body system, the energy is not conserved because of the presence of a velocity-dependent force (or equivalently, dissipative processes).

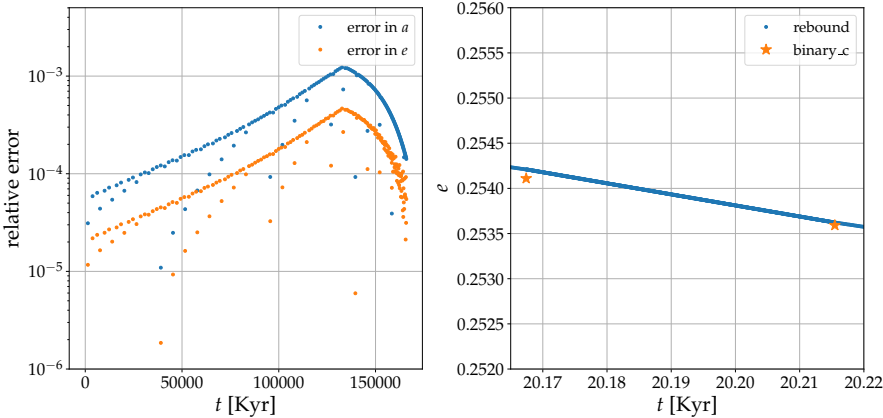


Figure 24: Results of a REBOUND integration of a two-body system representing a stellar binary. The left panel shows the relative error in the orbital elements a and e between REBOUND and `binary_c`. The right panel shows the output of REBOUND (blue dots) between two `binary_c` timesteps (orange stars). The integration time in REBOUND has been rescaled by a factor of 10^3 for reasons of computational efficiency.

4.6 INTIAL CONDITIONS

Before running full N-body simulations of circumbinary systems, a suitable choice of initial conditions needs to be made. Since N-body simulations are in general very computationally costly, we need to run simulations which explore the various parts of the parameter space and which can be done in reasonable time on the available computer architecture. Unfortunately the N-body problem with small N is not parallelizable and is therefore largely limited by the CPU clock speed which has not progressed significantly in the past decade. Having access to large clusters of CPUs is therefore only useful for running many simulations with different initial conditions.

We are most interested in the binary systems which could be the progenitors of the observed post common-envelope CB planets. We restrict ourselves to a single binary period of 200 days which usually leads to binary systems at the end of the common envelope instead of a merger. The *shape* of evolutionary tracks of binary stars in semi-major axis-eccentricity space only weakly depends on the initial period (much more important are the masses) and as long as the adiabatic criterion for resonant passage is satisfied in both cases, its outcome will stay the same. Nevertheless, we do run a few simulations with shorter period to check this is indeed the case. We also restrict the simulations to only systems which reach the common-envelope phase on the red giant branch, systems which reach the CE phase on the asymptotic giant branch (higher mass and longer period binaries) have post MS evolution times prior to the CE phase on the order of

hundreds of millions of years which would take too long to simulate with the IAS15 integrator.

The initial conditions are presented in table 6. For the primary mass we choose three values, ranging from $1.2 M_{\odot}$ to $2.0 M_{\odot}$. Lower primary masses are not interesting because such binary stars take too long to evolve past the common envelope phase and as a consequence we cannot observe their final post common-envelope configurations. On the higher end, we don't go higher than primary mass of $2 M_{\odot}$ because stars more massive than $2 M_{\odot}$ do not ignite Helium in their cores violently, in the form of a helium flash. Primaries which do not undergo the Helium flash reach a smaller RGB tip radius and are more likely to experience a CE event on the AGB. We specify the secondary mass with a mass ratio $q = m_1/m_2$ for three different values. The case of binaries with mass fraction near unity is not considered because such systems undergo two common-envelope events in a short time span.

For the inner eccentricity, perhaps the most important parameter for the global dynamics, we choose a circular value of $e = 0.0$, a slightly eccentric value of $e = 0.1$, and a highly eccentric value of $e = 0.3$. The outer eccentricity is set to a value in the range $0 - 0.2$. The outer period, planet, is chosen such that initially, the planet is outside the inner chaotic zone and inside the $6 : 1$ MMR. Finally, the

Parameter	Value
$m_1 [M_{\odot}]$	1.2, 1.6
q	0.3, 0.6, 0.8
P_i [days]	200
e_i	0.0, 0.1, 0.3
P_o/P_i	5.8-5.9
e_o	0-0.2
$\omega_i - \omega_o$	0

Table 6: The initial choice of parameters for the N-body simulations.

difference of pericentres is kept at a fixed value of zero, that is, the orbits are aligned. Starting at a different value of $\omega_i - \omega_o$ would not change the results considerably because the relative orientations of the two orbits become either randomized, aligned or anti-aligned on a short timescale.

RESULTS

Finally, having established the main aspects of the dynamics of CB planets on the main sequence, we move on to the results of both the analytical model and the full N-body simulations.

5.1 ECCENTRICITY KICK PREDICTED BY THE ANALYTICAL MODEL

Following the results presented in section 3.4, we can calculate the eccentricity kick experienced by a circumbinary planet during divergent resonance passage of the 6 : 1 MMR. The kick depends only on the inner mass ratio $\mu_i = m_1 m_2$, the outer mass ratio $\mu_o = m_3$ (both in units of m_{12}), the inner eccentricity e_i , and the initial outer eccentricity. While the eccentricity kick depends on the dimensionless inner mass ratio $\mu_i = m_1 m_2$, this quantity is difficult to grasp intuitively. There is another more intuitive dimensionless parameter, the inner mass ratio $q = m_2/m_1$. It is related to μ_i by

$$\mu_i = \frac{q}{(1+q)^2} \quad (167)$$

We choose to plot the results in the form of a density map showing the percentage increase over the initial outer eccentricity, as a function of the inner mass ratio q and the inner eccentricity. This is shown in fig. 25 for two values of initial outer eccentricity e_o . The density map shows $e_{o,\text{final}}/e_{o,\text{initial}}$.

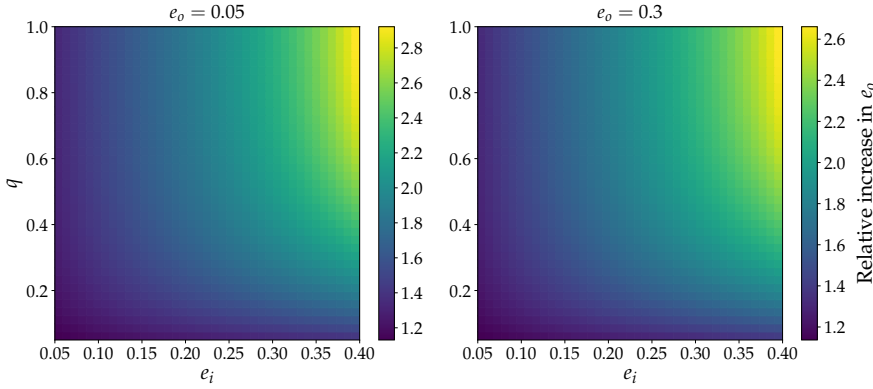


Figure 25: The color coding shows the relative increase in the CB planet eccentricity $e_{o,\text{final}}/e_{o,\text{initial}}$ after the passage of the 6 : 1 MMR, calculated using the algorithm described in section 3.4.

The increase in eccentricity scales with the parameters as we expected; it increases with increasing mass ratio q , and inner eccentricity e_i . As e_i approaches zero the eccentricity kick goes to zero

as well, this makes sense since the resonance widths approach zero (eq. (99)). The effect of varying the outer mass ratio $\mu_o = m_3$ is negligible for sensible values of the mass (earth masses to Jupiter masses). Comparing the left and right panel of fig. 25, we see that the relative increase in eccentricity is practically independent of the initial eccentricity. Thus, the outcome of the kick depends primarily on the stellar orbital parameters and only weakly depends on the planet parameters.

As was already apparent in the conclusion of section 3.4, the kick is very small when starting at small eccentricities, which is the case for most observed CB planets. This result could have perhaps been expected considering that high order resonances studied in the context of the solar system were known to be weak; there was however no *a priori* reason to assume that would be the case for CB planets because of both the much higher inner mass ratios and the higher inner eccentricities when compared to a system such as a single star with two planets. Intuitively it does make sense that is the case because of the large powers of eccentricities involved in the relevant disturbing function terms.

Even though the 6 : 1 resonance, and hence also resonances of higher order, might not be important for the global dynamics of evolving circumbinary systems, it is not a useless result. One thing we can obtain as a sort of by product of the analysis presented in section 3.4 are the resonance *capture* probabilities. After developing a procedure to calculate the areas enclosed by the two branches of the Hamiltonian separatrix, it is straightforward to calculate the corresponding capture probability (Murray and Dermott, 1999). We do not do it here, but without listing any numbers we can conclude that these probabilities are low because a small eccentricity kick corresponds to a small capture probability in the inverse scenario of convergent orbital evolution. Since all planets form in protoplanetary disks and then (in the majority of cases) migrate inwards, they can end up getting captured into resonance. This is how the planets around single stars end up in resonance. The possible explanation for the fact that none of the observed CB planets are in a 6 : 1, 7 : 1 or higher order resonance is that they did not end up getting captured because of the small capture probabilities. This is an important result in itself.

One might wonder if there are other cases where else could we apply the derived Hamiltonian model. Circumbinary planets were the main motivation for this work but the results are equally valid for any hierarchical triple systems with large inner mass ratios and in the vicinity of the 6 : 1 MMR.

5.2 N-BODY SIMULATIONS

Following the specification of the initial conditions for the N-body simulations (table 6), in this section we present the results. We plot the orbital parameters of a few representative cases.

Table 7 and table 8 show the results for two values of primary mass and three values of mass ratio. We see that whether or not there is a visible eccentricity kick depends primarily on the eccentricity of the stellar binary. If the orbit of the binary is circular there is no kick. This is what is expected based on the results from the analytical model (fig. 25). The fact that the mass ratio is not very important is again consistent with the analytical prediction.

	$q = 0.3$	$q = 0.6$	$q = 0.8$
$e_i = 0.0$	N	N	N
$e_i = 0.1$	K	K	K
$e_i = 0.3$	K	K	K

Table 7: N-body simulation results for $m_1 = 1.2$ and various values of q . All planets initially start just inside the $6 : 1$ MMR. The letter 'N' means that no significant events happened and the planet survived the evolution prior to the CE. 'K' means that the planet experienced a visible eccentricity kick due to the $6 : 1$ MMR. The letters 'K&E' means that the planet experienced an eccentricity kick and as a result was ejected out of the system. Finally, 'E' means that the planet was ejected as a result of a close encounter not due to the eccentricity kick.

	$q = 0.3$	$q = 0.6$	$q = 0.8$
$e_i = 0.0$	N	N	N
$e_i = 0.1$	K	K	K
$e_i = 0.3$	K&E	K	K

Table 8: Same as table 7 except with $m_1 = 1.6$.

Figure 26 shows the time evolution of the orbital elements for a system with $m_1 = 1.6$, $q = 0.3$ and $e_i = 0.1$. The resonance is crossed when the inner eccentricity is still significant and there is a small noticeable kick in the eccentricity. After the kick the secular effects start to dominate and the eccentricity decreases towards a value lower than the initial value at $t = 0$. This decrease in eccentricity is likely a result of the forced eccentricity going to zero due to the circularization of the binary's orbit. The relative orientation of the arguments of pericentres (bottom left panel) is randomized until the secular decline in the eccentricity during which the orbits become aligned. The arguments of pericentre then again become randomized.

Figure 27 shows the evolution of the same system as in fig. 26 except with a higher initial value of binary eccentricity $e_i = 0.3$. The onset of the eccentricity kick is visible at around $t = 6$ Myr at which point the planet is quickly ejected from the system. The arguments of pericentres are initially anti-aligned.

In fig. 28 we again integrate the system with the same binary masses as in fig. 26, but this time starting the planet at a higher initial eccentricity of $e_o = 0.2$ instead of starting it at the forced eccentricity. A strong secular decline in the eccentricity is visible from the beginning and the eccentricity kick is stronger than for the system with $e_i = 0.1$, reaching a value above $e_o = 0.2$. One can also clearly see the gap in the relevant harmonic angle Φ_{216} (see table 4) which librates around π during the resonant passage. Interestingly, even though the planet in this example starts at a higher initial eccentricity of $e_o = 0.2$, it does not get ejected at the start of the kick, most likely due to a lower spread in e_o (lower amplitude of the secular variations). The arguments of pericentre are anti-aligned up to the onset of the kick at which point they become randomized and then the pericentre evolution proceeds as in fig. 26. In all cases where we see a kick, its magnitude is roughly consistent with the analytic predictions from fig. 25, given the approximations involved. More importantly, the kick scales with the system parameters in a way one would expect (in particular, it vanishes for a circular binary).

To get a sense of the timescale of the secular changes, we integrate the system plotted in fig. 27 for a time of 1000 years and plot the eccentricities and arguments of pericentres, this is shown in fig. 29. Secular variation in the eccentricity due to angular momentum exchange with the binary with a period of around 300 years is clearly visible. The difference in the arguments of pericentres also exhibits secular variations.

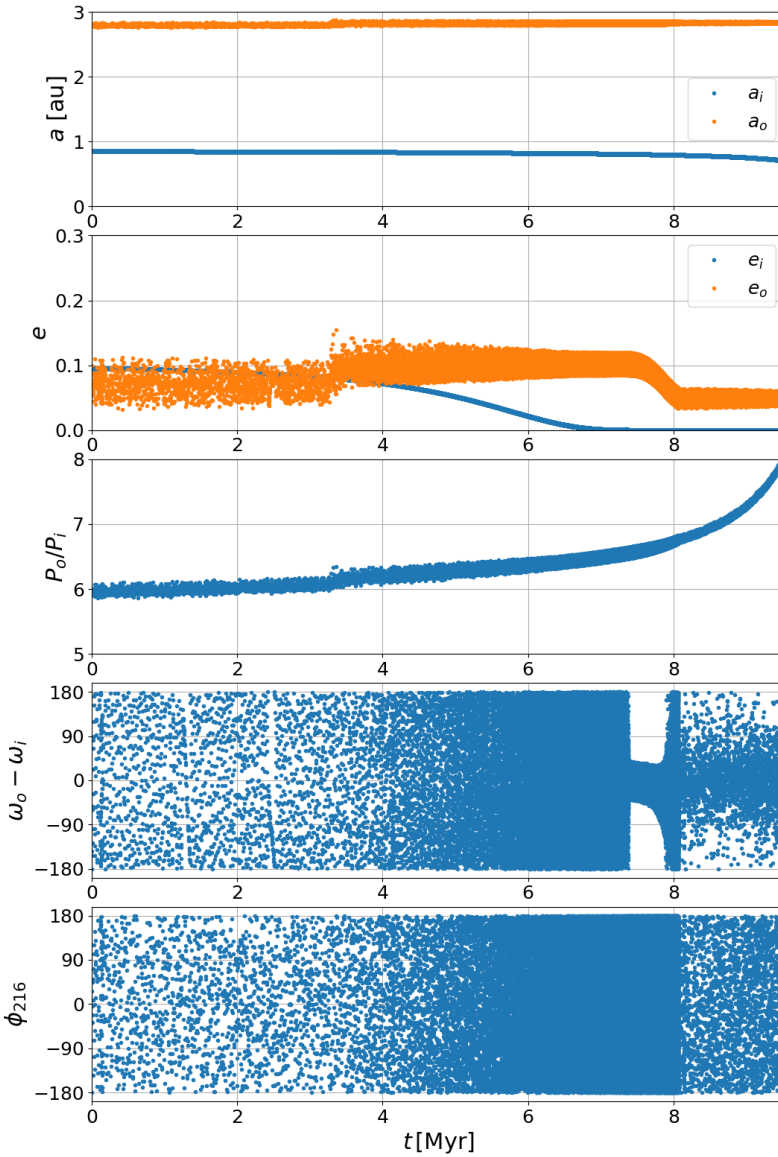


Figure 26: The N-body evolution of a circumbinary system with $m_1 = 1.6$, $q = 0.3$, $P_i = 200$ days, $e_i = 0.1$. The outer eccentricity is initially set to a value corresponding to the forced eccentricity of the planet when the binary is on the main sequence. In order from top to bottom, the plots show the time evolution of: a) semi-major axes, b) eccentricities, c) Difference in arguments of pericentre, d) The resonant angle for the 6 : 1 MMR (see table 4). For this system a resonance kick can be seen around $t = 3.5$ Myr. A secular decline in the eccentricity is also visible.

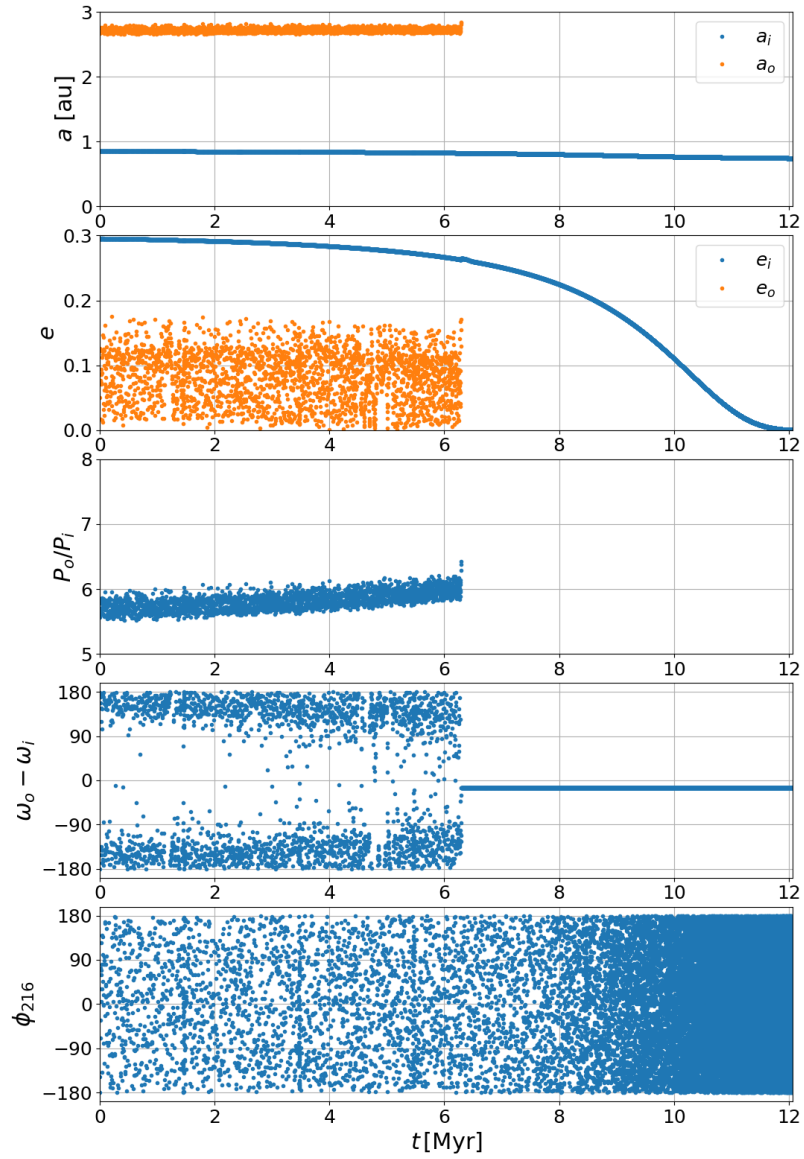


Figure 27: Same as fig. 26 except with the binary eccentricity increased to $e_i = 0.3$. In this case the resonance kick leads to the ejection of the planet.

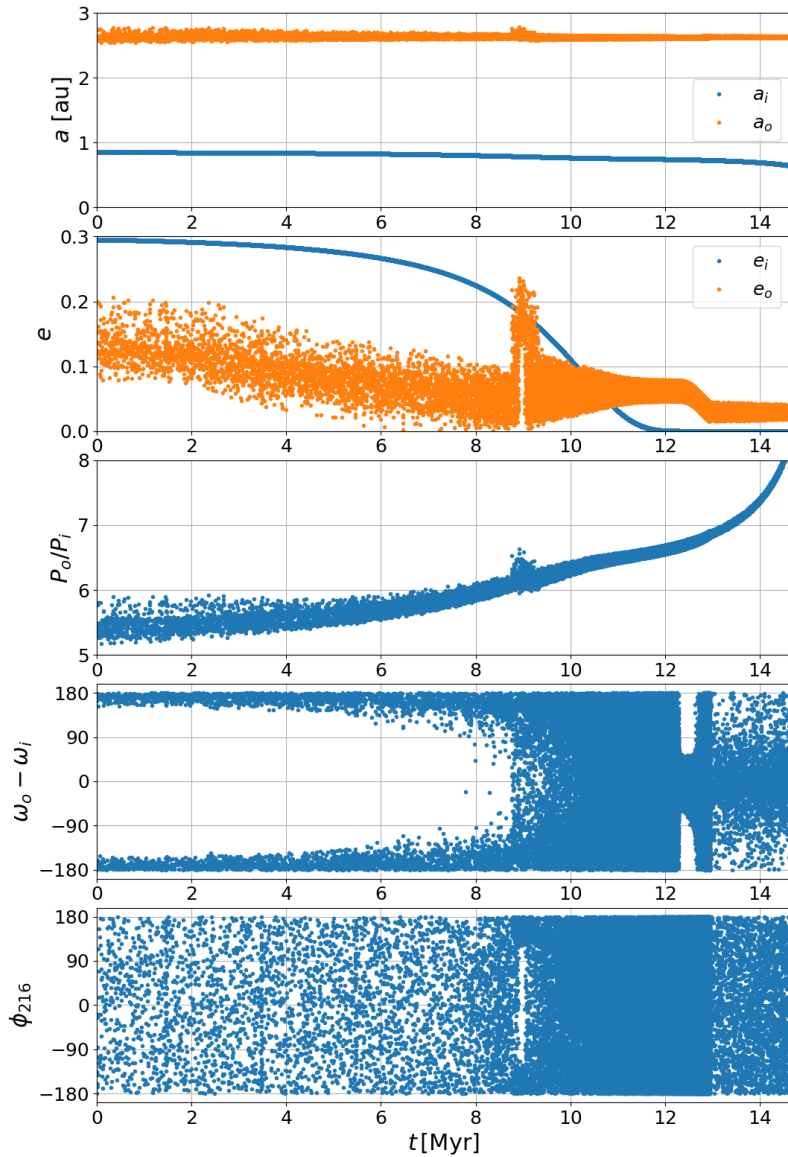


Figure 28: Same as fig. 27 except with a higher initial planet eccentricity of $e_o = 0.2$.

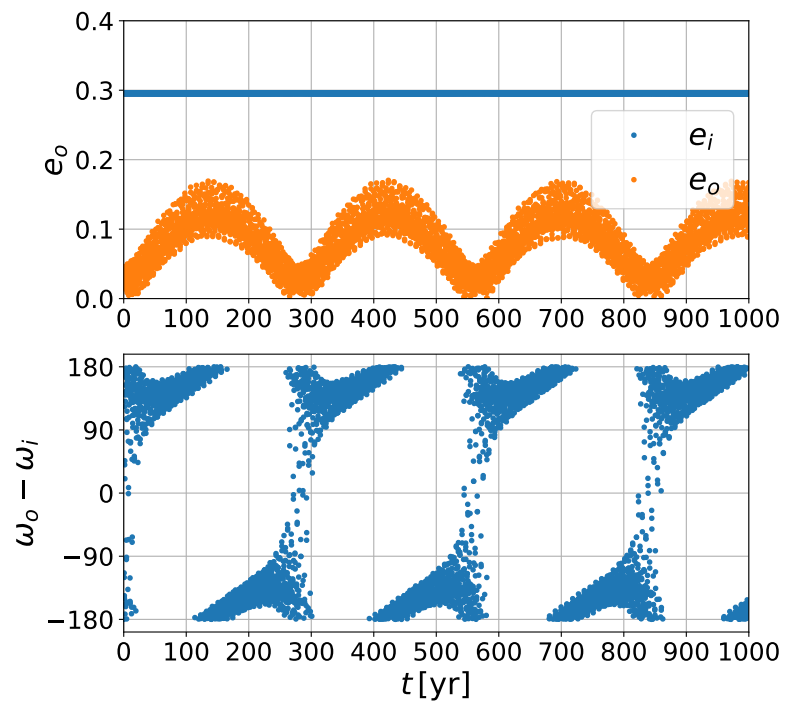


Figure 29: A close up view on the secular interactions for the system in fig. 27. The integration time is 1000 years, a fraction of the red giant branch timescale.

6

CONCLUSIONS

The goal of this thesis was to evaluate the stability of CB planets during the red giant branch part of binary evolution and prior to the beginning of the CE phase. In particular, a major goal was to investigate the effect of high order mean motion resonances such as the 6 : 1 MMR. In chapter 3 we have developed a Hamiltonian model of the 6 : 1 MMR applicable to arbitrary choices of all three masses in the problem. This model is not only significant for this particular case of CB system but can also be used in any other appropriate scenario, including studying resonant capture in the case of convergent orbital evolution. The procedure outlined in chapter 3 can be used to derive similar models of higher order resonances such as 7 : 1 and 8 : 1, however, in that case one has to be careful to expand the Keplerian part of the Hamiltonian to higher order than second order.

In chapter 4, we have developed a computational framework which uses well tested and open-source (or in the case of `binary_c`, easily available upon request) astrophysical codes in order to consistently simulate an evolving binary system with an outer planet in an N-body simulation. This procedure can be easily extended to any number of planets and any prescription for the orbital evolution of the stellar binary.

Both the analytic results and the numerical simulations gave similar results when the assumptions going into the analytical model were satisfied. We found that resonant effects are important only for appreciable eccentricity of the binary. Since even the eccentric binaries circularize on a short timescale, resonant passage which happens at significant binary eccentricity is an event with relatively small probability. On the other hand, secular effects were found to be important with the secular decline in the planet eccentricity happening in all cases. In light of these results, the conclusions of Kostov et al. (2016) should not change significantly if one includes the red-giant phase prior to the start of the common envelope. Therefore, the puzzle of first vs second generation planet formation in post common envelope CB systems remains unsolved. Given better observations of individual post common envelope systems, one should definitely take into account the orbital changes happening during the red giant branch. Although they might not be important for the majority of systems, a single observed post common envelope system whose progenitor configuration is determined to be unstable during the red giant branch would be an important result, similar to what Mustill et al. (2013) has done with a study of progenitors on the main sequence.

In retrospect, I found that the choice of initial conditions presented in section 4.6 is not ideal. To maximize science goals it would have been more useful to do a detailed study of possible progenitors of the observed post common envelope systems. This is left as a possibility for a future study.

6.1 FUTURE WORK

Based on the work done in this thesis, I could imagine several different topics which could be studied in detail, perhaps in a dedicated journal paper. First, it would be useful to extend the analysis done in chapter 3 to similar resonances such as the 5 : 1 (which is not well studied), 7 : 1 and even higher order. One could then also derive probabilities of capture into such resonances and publish such work on its own, without a focus on a particular application. Second, one could extend the N-body simulations presented in chapter 4 and include two planets, mass-loss and the CE phase¹ to gain a full consistent picture of the post main sequence evolution. Third, although we initially expected that resonant effect would be most important, it turned out that secular effects were more important. These can also be studied analytically, by working with the secular disturbing function listed in eq. (79). Fourth, one could look at the effects of close encounters between CB planets and the two stars and their effect on White Dwarf pollution with heavy elements (from collisions or tidal disruption of the planets), although this is likely to be less important in CB systems than in single star system because Smullen, Kratter, and Shannon (2016) finds that in CB system, the outcome of close encounters is an ejection of the planet in the majority of cases, rather than collision with one of the stars. Finally, we completely neglected the possibility that the planet is inclined relative to the plane of the binary, one could then study inclination resonances and the Kozai-Lidov effect (Naoz, 2016). However, this would require an extension of the disturbing function derived by Mardling (2013) and inclusion of two additional orbital angles, Ω and I .

¹ In fact, I wrote a test code which does exactly that, but I was not able to present the results here due to time limitations.

BIBLIOGRAPHY

- [1] S. J. Aarseth, C. A. Tout, and R. A. Mardling, eds. *The Cambridge N-Body Lectures*. Vol. 760. Lecture Notes in Physics, Berlin Springer Verlag. 2008. doi: [10.1007/978-1-4020-8431-7](https://doi.org/10.1007/978-1-4020-8431-7).
- [2] Eric Agol and Daniel C Fabrycky. “Transit Timing and Duration Variations for the Discovery and Characterization of Exoplanets.” In: (), pp. 1–19. arXiv: [arXiv:1706.09849v1](https://arxiv.org/abs/1706.09849v1).
- [3] J. H. Applegate. “A mechanism for orbital period modulation in close binaries.” In: *ApJ* 385 (Feb. 1992), pp. 621–629. doi: [10.1086/170967](https://doi.org/10.1086/170967).
- [4] P.J. Armitage. *Astrophysics of Planet Formation*. Cambridge University Press, 2010. ISBN: 9780521887458. URL: <https://books.google.se/books?id=zjlZQnFfMs8C>.
- [5] D. J. Armstrong, H. P. Osborn, D. J A Brown, F. Faedi, Y. G??mez Maqueo Chew, D. V. Martin, D. Pollacco, and S. Udry. “On the abundance of circumbinary planets.” In: *Mon. Not. R. Astron. Soc.* 444.2 (2014), pp. 1873–1883. ISSN: 13652966. doi: [10.1093/mnras/stu1570](https://doi.org/10.1093/mnras/stu1570). arXiv: [arXiv:1404.5617v1](https://arxiv.org/abs/1404.5617v1).
- [6] D. P. Bennett et al. “The First Circumbinary Planet Found by Microlensing: OGLE-2007-BLG-349L(AB)c.” In: *AJ* 152, 125 (Nov. 2016), p. 125. doi: [10.3847/0004-6256/152/5/125](https://doi.org/10.3847/0004-6256/152/5/125). arXiv: [1609.06720 \[astro-ph.EP\]](https://arxiv.org/abs/1609.06720).
- [7] D. Brouwer. “On the accumulation of errors in numerical integration.” In: *AJ* 46 (Oct. 1937), pp. 149–153. doi: [10.1086/105423](https://doi.org/10.1086/105423).
- [8] D. Brouwer and G.M. Clemence. *Methods of celestial mechanics*. Academic Press, 1961. URL: <https://books.google.se/books?id=eKgNAQAAIAAJ>.
- [9] B. Campbell, G. A. H. Walker, and S. Yang. “A search for sub-stellar companions to solar-type stars.” In: *ApJ* 331 (Aug. 1988), pp. 902–921. doi: [10.1086/166608](https://doi.org/10.1086/166608).
- [10] J. E. Chambers. “A hybrid symplectic integrator that permits close encounters between massive bodies.” In: *MNRAS* 304 (Apr. 1999), pp. 793–799. doi: [10.1046/j.1365-8711.1999.02379.x](https://doi.org/10.1046/j.1365-8711.1999.02379.x).
- [11] J. E. Chambers and F. Migliorini. “Mercury - A New Software Package for Orbital Integrations.” In: *AAS/Division for Planetary Sciences Meeting Abstracts #29*. Vol. 29. Bulletin of the American Astronomical Society. July 1997, p. 1024.

- [12] Cincotta, P. M. and Simó, C. "Simple tools to study global dynamics in non-axisymmetric galactic potentials – I." In: *Astron. Astrophys. Suppl. Ser.* 147.2 (2000), pp. 205–228. DOI: [10.1051/aas:2000108](https://doi.org/10.1051/aas:2000108). URL: <https://doi.org/10.1051/aas:2000108>.
- [13] P M Cincotta, C M Giordano, and C Simó. "Phase space structure of multi-dimensional systems by means of the mean exponential growth factor of nearby orbits." In: *Phys. D Nonlinear Phenom.* 182.3 (2003), pp. 151–178. ISSN: 0167-2789. DOI: [http://dx.doi.org/10.1016/S0167-2789\(03\)00103-9](http://dx.doi.org/10.1016/S0167-2789(03)00103-9). URL: <http://www.sciencedirect.com/science/article/pii/S0167278903001039>.
- [14] Katherine M. Deck, Matthew Payne, and Matthew J. Holman. "First-Order Resonance Overlap and the Stability of Close Two-Planet Systems." In: *Astrophys. J.* 774.2 (2013), p. 129. ISSN: 0004-637X. DOI: [10.1088/0004-637X/774/2/129](https://doi.org/10.1088/0004-637X/774/2/129). URL: <http://stacks.iop.org/0004-637X/774/i=2/a=129?key=crossref.59b4a2d4b6a0b24bcd46e279541efc56>.
- [15] A. Duquennoy and M. Mayor. "Multiplicity among solar-type stars in the solar neighbourhood. II - Distribution of the orbital elements in an unbiased sample." In: *A&A* 248 (Aug. 1991), pp. 485–524.
- [16] Kang Feng. "Difference Schemes for Hamiltonian Formalism and Symplectic Geometry." In: *J. Comput. Math.* 4.3 (July 1986), pp. 279–289. ISSN: 0254-9409. URL: <http://dl.acm.org/citation.cfm?id=8528.8538>.
- [17] S. Ferraz-Mello. *Canonical Perturbation Theories: Degenerate Systems and Resonance*. Astrophysics and Space Science Library. Springer New York, 2007. ISBN: 9780387389059. URL: <https://books.google.se/books?id=TYVCAAAQBAJ>.
- [18] J. Frouard, M. Fouchard, and A. Vienne. "Comparison of fast Lyapunov chaos indicators for Celestial Mechanics." In: *SF2A-2008*. Ed. by C. Charbonnel, F. Combes, and R. Samadi. Nov. 2008, p. 121.
- [19] A. P. Hatzes, W. D. Cochran, M. Endl, B. McArthur, D. B. Paulson, G. A. H. Walker, B. Campbell, and S. Yang. "A Planetary Companion to γ Cephei A." In: *ApJ* 599 (Dec. 2003), pp. 1383–1394. DOI: [10.1086/379281](https://doi.org/10.1086/379281). eprint: [astro-ph/0305110](https://arxiv.org/abs/astro-ph/0305110).
- [20] J. Henrard and A. Lemaitre. "A second fundamental model for resonance." In: *Celest. Mech.* 30.2 (1983), pp. 197–218. ISSN: 00088714. DOI: [10.1007/BF01234306](https://doi.org/10.1007/BF01234306).
- [21] T. C. Hinse, A. A. Christou, J. L.A. Alvarellos, and K. Goździewski. "Application of the MEGNO technique to the dynamics of Jovian irregular satellites." In: *Mon. Not. R. Astron. Soc.* 404.2 (2010), pp. 837–857. ISSN: 00358711. DOI: [10.1111/j.1365-2966.2010.16307.x](https://doi.org/10.1111/j.1365-2966.2010.16307.x). arXiv: [0907.4886](https://arxiv.org/abs/0907.4886).

- [22] T. C. Hinse, J. W. Lee, K. Goździewski, N. Haghighipour, C.-U. Lee, and E. M. Scullion. "New light-travel time models and orbital stability study of the proposed planetary system HU Aquarii." In: *MNRAS* 420 (Mar. 2012), pp. 3609–3620. DOI: [10.1111/j.1365-2966.2011.20283.x](https://doi.org/10.1111/j.1365-2966.2011.20283.x). arXiv: [1112.0066 \[astro-ph.EP\]](https://arxiv.org/abs/1112.0066).
- [23] Matthew J Holman and Paul A Wiegert. "Long-Term Stability of Planets in Binary Systems." In: *Astron. J.* 117.1 (1999), pp. 621–628. ISSN: 00046256. DOI: [10.1086/300695](https://doi.org/10.1086/300695). arXiv: [9809315 \[astro-ph\]](https://arxiv.org/abs/9809315). URL: <http://stacks.iop.org/1538-3881/117/i=1/a=621>.
- [24] J. R. Hurley, C. A. Tout, and O. R. Pols. "Evolution of binary stars and the effect of tides on binary populations." In: *MNRAS* 329 (Feb. 2002), pp. 897–928. DOI: [10.1046/j.1365-8711.2002.05038.x](https://doi.org/10.1046/j.1365-8711.2002.05038.x). eprint: [astro-ph/0201220](https://arxiv.org/abs/astro-ph/0201220).
- [25] Wolfram Research, Inc. *Mathematica, Version 11.1*. Champaign, IL, 2017.
- [26] Amplitude Instability and Conservative Nonlinear Oscillator. "Amplitude Instability and Ergodic Behavior for Conservative Nonlinear Oscillator Systems." In: (1969).
- [27] N Ivanova et al. "Common envelope evolution: where we stand and how we can move forward." In: *Astron. Astrophys. Rev.* 21.1 (2013), p. 59. ISSN: 1432-0754. DOI: [10.1007/s00159-013-0059-2](https://doi.org/10.1007/s00159-013-0059-2). URL: <https://doi.org/10.1007/s00159-013-0059-2>.
- [28] R. G. Izzard, C. A. Tout, A. I. Karakas, and O. R. Pols. "A new synthetic model for asymptotic giant branch stars." In: *MNRAS* 350 (May 2004), pp. 407–426. DOI: [10.1111/j.1365-2966.2004.07446.x](https://doi.org/10.1111/j.1365-2966.2004.07446.x). eprint: [astro-ph/0402403](https://arxiv.org/abs/astro-ph/0402403).
- [29] R. G. Izzard, L. M. Dray, A. I. Karakas, M. Lugaro, and C. A. Tout. "Population nucleosynthesis in single and binary stars. I. Model." In: *A&A* 460 (Dec. 2006), pp. 565–572. DOI: [10.1051/0004-6361:20066129](https://doi.org/10.1051/0004-6361:20066129).
- [30] R. G. Izzard, E. Glebbeek, R. J. Stancliffe, and O. R. Pols. "Population synthesis of binary carbon-enhanced metal-poor stars." In: *A&A* 508 (Dec. 2009), pp. 1359–1374. DOI: [10.1051/0004-6361/200912827](https://doi.org/10.1051/0004-6361/200912827). arXiv: [0910.2158 \[astro-ph.SR\]](https://arxiv.org/abs/0910.2158).
- [31] J.D. Jackson. *Classical Electrodynamics*. Wiley, 2007. ISBN: 9788126510948. URL: <https://books.google.se/books?id=2hZ0CgAAQBAJ>.
- [32] Eric Jones, Travis Oliphant, Pearu Peterson, et al. *SciPy: Open source scientific tools for Python*. 2001–. URL: <http://www.scipy.org/>.

- [33] Veselin B. Kostov, Keavin Moore, Daniel Tamayo, Ray Jayawardhana, and Stephen A. Rinehart. "TATOOINE'S FUTURE: THE ECCENTRIC RESPONSE OF <i>KEPLER</i> 'S CIRCUMBINARY PLANETS TO COMMON-ENVELOPE EVOLUTION OF THEIR HOST STARS." In: *Astrophys. J.* 832.2 (2016), p. 183. ISSN: 1538-4357. DOI: [10.3847/0004-637X/832/2/183](https://doi.org/10.3847/0004-637X/832/2/183). URL: <http://stacks.iop.org/0004-637X/832/i=2/a=183?key=crossref.0b599d472f25add91b68af43fc4e428e>.
- [34] L.D. Landau and E.M. Lifshitz. *Mechanics*. Butterworth-Heinemann. Butterworth-Heinemann, 1976. ISBN: 9780750628969. URL: <https://books.google.se/books?id=e-xASAehg1sC>.
- [35] J. Laskar. "Large scale chaos and the spacing of the inner planets." In: *A&A* 317 (Jan. 1997), pp. L75–L78.
- [36] J. J. Lissauer. "Planet formation." In: *ARA&A* 31 (1993), pp. 129–174. DOI: [10.1146/annurev.aa.31.090193.001021](https://doi.org/10.1146/annurev.aa.31.090193.001021).
- [37] Rosemary A. Mardling. "New developments for modern celestial mechanics - I. General coplanar three-body systems. Application to exoplanets." In: *Mon. Not. R. Astron. Soc.* 435.3 (2013), pp. 2187–2226. ISSN: 00358711. DOI: [10.1093/mnras/stt1438](https://doi.org/10.1093/mnras/stt1438). arXiv: [arXiv:1308.0607](https://arxiv.org/abs/1308.0607).
- [38] T. R. Marsh, S. G. Parsons, M. C P Bours, S. P. Littlefair, C. M. Copperwheat, V. S. Dhillon, E. Breedt, C. Caceres, and M. R. Schreiber. "The planets around NN serpentis: Still there." In: *Mon. Not. R. Astron. Soc.* 437.1 (2013), pp. 475–488. ISSN: 00358711. DOI: [10.1093/mnras/stt1903](https://doi.org/10.1093/mnras/stt1903). arXiv: [1310.1391](https://arxiv.org/abs/1310.1391).
- [39] R. G. Martin, P. J. Armitage, and R. D. Alexander. "Formation of Circumbinary Planets in a Dead Zone." In: *ApJ* 773, 74 (Aug. 2013), p. 74. DOI: [10.1088/0004-637X/773/1/74](https://doi.org/10.1088/0004-637X/773/1/74). arXiv: [1306.5241 \[astro-ph.EP\]](https://arxiv.org/abs/1306.5241).
- [40] M. Mayor and D. Queloz. "A Jupiter-mass companion to a solar-type star." In: *Nature* 378 (Nov. 1995), pp. 355–359. DOI: [10.1038/378355a0](https://doi.org/10.1038/378355a0).
- [41] S. Meschiari. "Planet Formation in Circumbinary Configurations: Turbulence Inhibits Planetesimal Accretion." In: *ApJ* 761, L7 (Dec. 2012), p. L7. DOI: [10.1088/2041-8205/761/1/L7](https://doi.org/10.1088/2041-8205/761/1/L7). arXiv: [1210.7757 \[astro-ph.EP\]](https://arxiv.org/abs/1210.7757).
- [42] A. Morbidelli. *Modern celestial mechanics: aspects of solar system dynamics*. Advances in astronomy and astrophysics. Taylor & Francis, 2002. ISBN: 9780415279390. URL: <https://books.google.se/books?id=xpU0AQAAIAAJ>.

- [43] Lawrence R. Mudryk and Yanqin Wu. "Resonance Overlap Is Responsible for Ejecting Planets in Binary Systems." In: *Astrophys. J.* 639.1 (2006), pp. 423–431. ISSN: 0004-637X. DOI: [10.1086/499347](https://doi.org/10.1086/499347). arXiv: [0511710 \[astro-ph\]](https://arxiv.org/abs/0511710). URL: <http://stacks.iop.org/0004-637X/639/i=1/a=423>.
- [44] C.D. Murray and S.F. Dermott. *Solar System Dynamics*. Cambridge University Press, 1999. ISBN: 9780521575973. URL: <https://books.google.se/books?id=aU6vcy5L8GAC>.
- [45] Alexander J. Mustill, Jonathan P. Marshal, Eva Villaver, Dimitri Veras, Philip J. Davis, Jonathan Horner, and Robert A. Wittenmyer. "Main-sequence progenitor configurations of the NN ser candidate circumbinary planetary system are dynamically unstable." In: *Mon. Not. R. Astron. Soc.* 436.3 (2013), pp. 2515–2521. ISSN: 00358711. DOI: [10.1093/mnras/stt1754](https://doi.org/10.1093/mnras/stt1754). arXiv: [1309.3881 \[astro-ph.EP\]](https://arxiv.org/abs/1309.3881).
- [46] S. Naoz. "The Eccentric Kozai-Lidov Effect and Its Applications." In: *ARA&A* 54 (Sept. 2016), pp. 441–489. DOI: [10.1146/annurev-astro-081915-023315](https://doi.org/10.1146/annurev-astro-081915-023315). arXiv: [1601.07175 \[astro-ph.EP\]](https://arxiv.org/abs/1601.07175).
- [47] J. C. B. Papaloizou and J. D. Larwood. "On the orbital evolution and growth of protoplanets embedded in a gaseous disc." In: *MNRAS* 315 (July 2000), pp. 823–833. DOI: [10.1046/j.1365-8711.2000.03466.x](https://doi.org/10.1046/j.1365-8711.2000.03466.x). eprint: [astro-ph/9911431](https://arxiv.org/abs/astro-ph/9911431).
- [48] Hagai B Perets. "Second generation planets." In: *eprint arXiv* 1001 (2010), p. 581. arXiv: [1001.0581](https://arxiv.org/abs/1001.0581). URL: http://adsabs.harvard.edu/cgi-bin/nph-data{_}query?bibcode=2010arXiv1001.0581P{\&}link{_}type=ABSTRACT.
- [49] M. Perryman. *The Exoplanet Handbook*. May 2011.
- [50] B. Pichardo, L. S. Sparke, and L. A. Aguilar. "Circumstellar and circumbinary discs in eccentric stellar binaries." In: *MNRAS* 359 (May 2005), pp. 521–530. DOI: [10.1111/j.1365-2966.2005.08905.x](https://doi.org/10.1111/j.1365-2966.2005.08905.x). eprint: [astro-ph/0501244](https://arxiv.org/abs/astro-ph/0501244).
- [51] A. Pierens and R. P. Nelson. "On the migration of protoplanets embedded in circumbinary disks." In: *A&A* 472 (Sept. 2007), pp. 993–1001. DOI: [10.1051/0004-6361:20077659](https://doi.org/10.1051/0004-6361:20077659). arXiv: [0707.2677](https://arxiv.org/abs/0707.2677).
- [52] D. Prialnik. *An Introduction to the Theory of Stellar Structure and Evolution*. Cambridge University Press, 2009. ISBN: 9781316284308. URL: <https://books.google.se/books?id=oSZbBgAAQBAJ>.
- [53] Roman R. Rafikov. "BUILDING TATOOINE: SUPPRESSION OF THE DIRECT SECULAR EXCITATION IN <i>KEPLER</i> CIRCUMBINARY PLANET FORMATION." In: *Astrophys. J.* 764.1 (2013), p. L16. ISSN: 2041-8205. DOI: [10.1088/2041-8205/764/1/L16](https://doi.org/10.1088/2041-8205/764/1/L16). URL: <http://stacks.iop.org/2041-8205/764/i=1/a=L16?key=crossref.26019c5f59fc44a501d3a3a256807b2c>.

- [54] H. Rein. "A proposal for community driven and decentralized astronomical databases and the Open Exoplanet Catalogue." In: *ArXiv e-prints* (Nov. 2012). arXiv: [1211.7121 \[astro-ph.EP\]](#).
- [55] H Rein and S Liu. "REBOUND: an open-source multi-purpose N-body code for collisional dynamics." In: *Astron. Astrophys.* 537 (2012), A128. ISSN: 1432-0746. DOI: [10.1051/0004-6361/201118085](#). arXiv: [arXiv:1110.4876v2](#). URL: http://adsabs.harvard.edu/cgi-bin/nph-data{_}query?bibcode=2012A{\%}2526A...537A.128R{\&}link{_}type=ABSTRACT{\%}5Cnpapers://0be24a46-325a-4116-a3c6-fd8a3b614472/Paper/p14436.
- [56] Hanno Rein and David S. Spiegel. "IAS15: A fast, adaptive, high-order integrator for gravitational dynamics, accurate to machine precision over a billion orbits." In: *Mon. Not. R. Astron. Soc.* 446.2 (2014), pp. 1424–1437. ISSN: 13652966. DOI: [10.1093/mnras/stu2164](#). arXiv: [1409.4779 \[astro-ph.EP\]](#).
- [57] Hanno Rein and Daniel Tamayo. "WHFAST: A fast and unbiased implementation of a symplectic Wisdom-Holman integrator for long-term gravitational simulations." In: *Mon. Not. R. Astron. Soc.* 452.1 (2015), pp. 376–388. ISSN: 13652966. DOI: [10.1093/mnras/stv1257](#). arXiv: [1506.01084 \[astro-ph.EP\]](#).
- [58] Ronald D Ruth. "A canonical integration technique." In: *IEEE Trans. Nucl. Sci.* 30.CERN-LEP-TH-83-14 (1983), pp. 2669–2671.
- [59] Dominik R. G. Schleicher and Stefan Dreizler. "Planet formation from the ejecta of common envelopes." In: *Astron. Astrophys.* 563 (2014), A61. ISSN: 0004-6361. DOI: [10.1051/0004-6361/201322860](#). arXiv: [1312.3479](#). URL: http://adslabs.org/adsabs/abs/2014A{_}A...563A..61S/.
- [60] Rachel A. Smullen, Kaitlin M. Kratter, and Andrew Shannon. "Planet scattering around binaries: Ejections, not collisions." In: *Mon. Not. R. Astron. Soc.* 461.2 (2016), pp. 1288–1301. ISSN: 13652966. DOI: [10.1093/mnras/stw1347](#). arXiv: [1604.03121](#).
- [61] Adam P Sutherland and Daniel C Fabrycky. "On the Fate of Unstable Circumbinary Planets: Tatooine's Close Encounters with a Death Star." In: *Astrophys. J.* 818.1 (2015), p. 6. ISSN: 1538-4357. DOI: [10.3847/0004-637X/818/1/6](#). arXiv: [1511.03274](#). URL: <http://arxiv.org/abs/1511.03274{\%}7B{\%}25{\%}7D0Ahttp://dx.doi.org/10.3847/0004-637X/818/1/6>.
- [62] S. E. Thorsett, Z. Arzoumanian, and J. H. Taylor. "PSR B1620-26 - A binary radio pulsar with a planetary companion?" In: *ApJ* 412 (July 1993), pp. L33–L36. DOI: [10.1086/186933](#).
- [63] Rene de Vogelaere. "Methods of integration which preserve the contact transformation property of the Hamiltonian equations." In: *Department of Mathematics, University of Notre Dame, Report 4* (1956), p. 30.

- [64] M Völschow, Robi Banerjee, and Frederic V Hessman. "Second generation planet formation in NN Serpentis?" In: *Astron. Astrophys.* 562 (2014), A19. ISSN: 0004-6361. DOI: [10.1051/0004-6361/201322111](https://doi.org/10.1051/0004-6361/201322111). arXiv: [1312.7512](https://arxiv.org/abs/1312.7512). URL: <http://www.aanda.org/10.1051/0004-6361/201322111>.
- [65] J. N. Winn and D. C. Fabrycky. "The Occurrence and Architecture of Exoplanetary Systems." In: *ARA&A* 53 (Aug. 2015), pp. 409–447. DOI: [10.1146/annurev-astro-082214-122246](https://doi.org/10.1146/annurev-astro-082214-122246). arXiv: [1410.4199 \[astro-ph.EP\]](https://arxiv.org/abs/1410.4199).
- [66] A. Wolszczan and D. A. Frail. "A planetary system around the millisecond pulsar PSR1257 + 12." In: *Nature* 355 (Jan. 1992), pp. 145–147. DOI: [10.1038/355145a0](https://doi.org/10.1038/355145a0).
- [67] J.-P. Zahn. "Tidal evolution of close binary stars. I - Revisiting the theory of the equilibrium tide." In: *A&A* 220 (Aug. 1989), pp. 112–116.
- [68] J.-P. Zahn and L. Bouchet. "Tidal evolution of close binary stars. II - Orbital circularization of late-type binaries." In: *A&A* 223 (Oct. 1989), pp. 112–118.
- [69] M Zorotovic and M R Schreiber. "Origin of apparent period variations in eclipsing post-common-envelope binaries." In: 95 (2013), pp. 1–16.
- [70] S. de Ruyter, H. van Winckel, T. Maas, T. Lloyd Evans, L. B. F. M. Waters, and H. Dejonghe. "Keplerian discs around post-AGB stars: a common phenomenon?" In: *A&A* 448 (Mar. 2006), pp. 641–653. DOI: [10.1051/0004-6361:20054062](https://doi.org/10.1051/0004-6361:20054062). eprint: [astro-ph/0601578](https://arxiv.org/abs/astro-ph/0601578).
- [71] H. van Winckel et al. "Post-AGB stars with hot circumstellar dust: binarity of the low-amplitude pulsators." In: *A&A* 505 (Oct. 2009), pp. 1221–1232. DOI: [10.1051/0004-6361/200912332](https://doi.org/10.1051/0004-6361/200912332). arXiv: [0906.4482 \[astro-ph.SR\]](https://arxiv.org/abs/0906.4482).